Summer 9-1-2014

The Regulation of Glucose Metabolism during Osteoblast Differentiation

Emel Esen
Washington University in St. Louis

WASHINGTON UNIVERSITY IN ST. LOUIS

Division of Biology and Biomedical Sciences

Developmental Regenerative and Stem Cell Biology

Dissertation Examination Committee:
Fanxin Long, Chair
Thomas Baranski
Roberto Civitelli
Kelle Moley
Michael Mueckler
Clay Semenkovich

The Regulation of Glucose Metabolism during Osteoblast Differentiation

By

Emel Esen

A dissertation presented to the
Graduate School of Arts and Sciences
of Washington University in
partial fulfillment of the
requirements for the degree
of Doctor of Philosophy

August 2014

Saint Louis, Missouri

TABLE OF CONTENTS

LIST of FIGURES and TABLES

Chapter 1. Introduction

Chapter 2. WNT-LRP5 Signaling Induces Warburg Effect through mTORC2 Activation during Osteoblast Differentiation

Chapter 3: Aerobic glycolysis is required for bone anabolism in the mouse

Chapter 4: Intermittent PTH promotes bone anabolism by stimulating glycolysis via IGF-SGK1 signaling

LIST of ABBREVIATIONS

^{14}C1 -glc: glucose specifically labeled at C1 (carbon 1)

^{14}C6 -glc: glucose specifically labeled at C6 (carbon 6)

APC: adenomatous polyposis coli

BFR: bone formation rate

BMD: bone mineral densities.

BMD: Bone mineral density

BMP: Bone morphogenetic protein

CamK2: Calcium–calmodulin-dependent protein kinase II

cAMP: Cyclic adenosine monophosphate

CBP/p300: CREB-binding Protein/p300

CRE: cAMP responsive elements

DCA: dichloroacetate

Dkk1: dickkopf

DM1: type one diabetes

DM2: type two diabetes

Dox: doxycycline

DPM: disintegration per minute

ECM: Extracellular matrix

FGF: Fibroblast growth factor

Fra1: fos-related antigen 1

FZD: Frizzled

G6P: glucose-6-phosphate

G6PD: glucose 6-phosphate dehydrogenase

GFPT1 (known as GFAT): Glutamine fructose-6-phosphate aminotransferase

GIP: glucose dependent insulinotropic peptide

GIPR: GIP receptors

GLUT: glucose transporter

GSK2β: glycogen synthase kinase 3β

GSSG: oxidized glutathione

HBP: Hexosamine biosynthesis pathway

HH: hedgehog

hMSC: Human mesenchymal stem cells.

IDH: isocitrate dehydrogenase

IGF: Insulin-Like Growth Factor

IGF1R: Insulin-Like Growth Factor 1 Receptor

iPTH: intermittent PTH

IR: insulin receptor

JNK2: c-Jun N-terminal kinase 2

LEF: lymphoid-enhancer-factor

LRP: lipoprotein receptor-related protein

MCT: monocarbocylate transporters

mtDNA: mitochondrial DNA

mTORC1: mammalian target of rapamycin complex 1

mTORC2: mammalian target of rapamycin complex 2

OAA: Oxaloacetate

OPG: Osteoprotegerin

Osx: Osterix.

OXPHO: Oxidative phosphorylation

PDC: Pyruvate dehydrogenase complex

PDK: pyruvate dehydrogenase kinases.

PHD: prolyl hydroxylase enzymes

PI3K: Phosphoinositide 3-kinase

PKA: protein kinase A

PKC: protein kinase C

PPP: pentose phosphate pathway

PTH: Parathyroid hormone

PTHR1: PTH receptor 1

R5P: ribose-5-phosphate.

RANKL: Receptor activator of nuclear factor kappa-B ligand

Runx2: runt-domain transcription factor 2

sFRP-1: Secreted frizzled-related protein 1

SOST: Sclerostin

TCA cycle: tricarboxylic acid cycle

TCF: T cell-factor

TSC2: tuberous sclerosis 2

UDP-GlcNAc: uridine diphospho-N-acetylglucosamine

VEGF: vascular endothelial growth factor

α-KG: α-ketoglutarate

β-TrCP: β-transducin repeat-containing protein

BPs: Bisphosphonates

ACKNOWLEDGEMENT

First of all, I want to thank my thesis advisor for his training over the past years. He taught me how to become a scientist, how to think critically and conduct research. He always encouraged me to present my data and helped me to develop my skills.

Current and past members of Long Lab, ia olin Tu, Kyu Sang oeng, ena Regan, Courtney Karner, ian ua n Chen, oohyun Lim, Wen-Chih Lee, hepeng Wang, u Shi, Seung-on Lee helped me with the techniques and provided useful feedbacks.

All of the members of my thesis committee; Thomas Baranski, Kelle Moley, Roberto Civitelli, Michael Mueckler, Clay Semenkovich have been instrumental and supportive during my training. Especially I want to thank Semenkovich lab for their various technical inputs and sharing reagents; Maggie Chi from Moley lab for her technical help; Michael Mueckler for sharing Glut1 antibody, Tom Baranski for all the helpful discussions and Leila Denise Revello from Civitelli Lab for helpful suggestions with PTH protocols.

I appreciate the musculoskeletal core providing all the instruments, Crystal for her expertise with various techniques.

Finally, I want to thank my family and friends who supported me all this time. My family supported me to follow my passion and move so far away from them. My friends in St. Louis made life easier to live abroad. The biggest support for me was always from my husband, who is also a dear friend and colleague who made my PhD life a lot easier and more fun. I appreciate his constant patience, support and help while putting my thesis together.

ABSTRACT OF THE DISSERTATION

Regulation of Cellular Glucose Metabolism during Osteoblast Differentiation

by

Emel Esen

Doctor of Philosophy in Biology and Biomedical Sciences

Developmental, Regenerative and Stem Cell Biology

Washington University in St. Louis, August 2014

Professor Fanxin Long, Chair

Differentiation and cell-specific functions are coupled with metabolic alterations to meet the needs of the cell. In this thesis, I have investigated the alterations of cellular metabolism in osteoblast-lineage cells in response to two different bone anabolic signals, WNT and PTH. I have further elucidated the mechanism underlying the metabolic changes, and have explored the functional importance of such changes for bone anabolism.

Osteoblasts, the principal bone-forming cells, are differentiated from mesenchymal progenitor cells through sequential stages. These stages are identifiable by molecular markers, cell morphology and location. Transcription factors and developmental signals important for osteoblast differentiation have been studied in detail. One such developmental signal is the WNT family of proteins. WNTs are a large family of glycoproteins that activate β-catenin-dependent or -independent intracellular pathways, both of which are involved in bone formation. However, the mechanism through which WNT signaling stimulates osteoblast differentiation is not well understood.

Early studies demonstrated that bone cells consume a large amount of glucose, producing lactate as the major end product even in aerobic conditions, a phenomenon known as aerobic

glycolysis. However, the significance of increased aerobic glycolysis for bone formation was not known. Based on the link between metabolic abnormalities and the genetic mutations in WNT pathway components, I hypothesized that WNT regulates cellular metabolism and that such regulation contributes to osteoblast differentiation. I tested this hypothesis *in vitro* by using ST2 cells, and showed that WNT signaling increased glucose utilization, stimulated aerobic glycolysis via induction of glycolytic enzymes, and suppressed glucose entry to TCA cycle. This process was mostly regulated by a signaling cascade dependent on Lrp5-Rac1-mTORC2 and independent of β-catenin. Increased glycolysis was important for *in vitro* osteoblast differentiation and correlated with increased bone formation in WNT hyperactivation mouse models. I tested the functional importance of enhanced aerobic glycolysis *in vivo* by two different models. First, I showed that pharmacological enhancement of pyruvate entering the TCA cycle attenuated the high-bone mass phenotype caused by hyperactive WNT signaling in the mouse. Second, I showed that genetic deletion of LDHA, the enzyme catalyzing the last step of glycolysis, from osteoblast-lineage cells suppressed normal postnatal bone accrual due to reduced osteoblast number and function. Thus, WNT signaling reprograms glucose metabolism, and WNT-induced metabolic reprogramming contributes to osteoblast differentiation both *in vitro* and *in vivo*. Moreover, LDHA is required for optimal bone formation in postnatal mice.

Parathyroid hormone (PTH) has been an effective bone anabolic drug in the clinic by targeting osteoblasts and stimulating bone formation. However, it is not well understood how PTH signaling stimulates bone formation. In early studies, PTH was shown to alter cellular metabolism towards lactate production. In light of the role of metabolic regulation in WNT-induced bone formation, I examined the potential role of metabolic alterations in mediating the anabolic effect of PTH. In MC3T3-E1 cells and neonatal calvarial cells, I showed that PTH

enhanced glucose uptake and aerobic glycolysis, activated pentose phosphate pathway but reduced contribution of glucose to TCA cycle. PTH-induced glucose utilization required IGF-PI3K-SGK1 signaling. Importantly, pharmacological enhancement of pyruvate entering the TCA cycle attenuated the bone anabolic effect by PTH. Thus, changes in cellular glucose metabolism may be an important mechanism mediating the anabolic effect of PTH.

This thesis confirms the earlier findings that lactate-producing glycolysis is an important feature of osteoblasts, and further characterizes the alterations of cellular metabolism during osteoblast differentiation in response to both WNT and PTH pathways. More importantly, this thesis shows for the first time that metabolic alterations are functionally important for the differentiation process.

CHAPTER 1

Introduction

1. General Functions of Bone

Bones constitute the skeleton, which is the framework of the body that protects and supports the internal organs. The mammalian skeleton houses the bone marrow, which functions to produce blood cells. Bones are also the reservoir for important minerals such as calcium and phosphate, and thus affect the homeostasis of these minerals in the circulation.

Bone formation, known as ossification, is a process that starts early in embryos and continues throughout life. There are two different processes for bone formation in mammals, which are endochondral and intramembranous ossification. Endochondral ossification, which occurs in long bones like the humerus and femur, starts with condensation of committed mesenchymal cells that differentiate into chondrocytes producing cartilage extracellular matrix (ECM). Chondrocytes proliferate to drive the cartilage growth and undergo several steps of maturation. Finally, these cells exit the cell cycle and undergo hypertrophy (enlargement of cell) and form pre-hypertrophic and hypertrophic chondrocytes. Hypertrophic chondrocytes secrete type X collagen, and these cells mostly undergo apoptosis. During endochondral bone formation, mesenchymal cells on the outer edge of cartilage matrix form perichondrium. These perichondrial cells later form the bone collar. Blood vessels together with the cells forming perichondrium and hematopoietic origin cells invade the cartilage. Mesenchymal cells start to differentiate into osteoblast establishing the primary ossification center, while cartilage membrane is replaced by bone matrix and marrow cavity (Long and Ornitz, 2013). Osteoblasts deposit extracellular matrix, rich in type I collagen, that later gets mineralized with accumulation of calcium phosphate. The 2nd type of ossification is known as intramembranous ossification and occurs in flat bones like the skull and parts of scapula. In intramembranous ossification, there is no intermediate step of cartilage formation before ossification. Mesenchymal progenitors directly

condense into osteoblasts. The origin of cells is different in two ossifications. Mesenchymal cells in endochondral bone are mostly derived from lateral and paraxial mesoderm, whereas, mesenchymal cells in intramembranous ossifications are mostly derived from neural crest cells (Olsen et al., 2000).

Ossified bone consists of three major cells types; osteoblasts, osteoclasts and osteocytes. Osteoblasts are the bone forming cells derived from the mesenchyme whose function is to synthesize the ECM and also produce enzymes that function to mineralize the ECM. Osteocytes represent approximately 95% of the cells in mature bone. Osteocytes work as the mechanotransducer of bone to regulate osteoblastic and osteoclastic activities (Bonewald, 2011; Feng et al., 2006; Roberts et al., 2013). In contrast to osteoblasts, the main function of the osteoclasts, multinuclear cells of hematopoietic origin, is bone resorption. Osteoblasts control osteoclasts through regulation of the pro-osteoclastogenic receptor activator of nuclear factor kappa-B ligand (RANKL) and the anti-osteoclastogenic osteoprotegerin. Osteoblasts and osteoclasts work in balance to achieve bone homeostasis. Bone undergoes continuous remodeling during development and adult life. To maintain bone mass over time, bone formation and bone resorption should occur at the same rate.

An unbalanced increase in bone resorption relative to formation results in bone loss and ultimately osteoporosis. Osteoporosis is a disease characterized by reduced bone mass and increased risk of fractures. The prevalence increases by age and the presence of other metabolic diseases such as diabetes, although the reason is not well understood. Current osteoporosis treatment relies primarily on antiresorptive medicine that prevents bone loss via blocking osteoclast activity (Sambrook et al., 2012). Anabolic therapy, such as intermittent treatment of parathyroid hormone (PTH), is mostly used for patients at a higher risk of fracture with severe

osteoporosis. Teriparatide, a bioactive fragment of PTH, stimulates bone formation on the surface of cancellous and cortical bone, and improves the microarchitecture. However, prolonged usage of teriparatide has diminished effects (Hodsman et al., 2005). The anabolic function of teriparatide treatment is suggested to be bi-phasic. In the early phase, PTH stimulates bone modeling (bone formation in new space) whereas extended PTH administration stimulates bone remodeling with a positive balance (Dobnig et al., 2005; Hodsman and Steer, 1993; Lindsay et al., 2006). The exact mechanism of the anabolic action of PTH is not known, but requires IGF signaling (Wang et al., 2007). A greater understanding of the anabolic signals on osteoblast differentiation and homeostasis can provide new insights for alternative treatments and potential preventative measures for osteoporosis.

1.1. Osteoblast Differentiation

Osteoblasts form from mesenchymal progenitor cells through sequential stages of differentiation, referred as the osteoprogenitor, the preosteoblast and the mature osteoblast stage (Figure 1). These different-stages are defined by the *in vivo* morphology and localization as well as different gene expression. The osteoprogenitors have a more fibroblast-like morphology and are located within periosteal layers. During maturation, these cells obtain a more cuboidal morphology and are localized on the bone surface (Owen, 1963). At the molecular level, all progenitor cells express the transcription factor, SOX9. Osteoprogenitors start to express the runt-domain transcription factor 2 (Runx2) and preosteoblasts express Osterix (Osx), a zinc-finger transcription factor, along with Runx2. Finally, mature osteoblasts express osteocalcin. After differentiation, mature osteoblasts have three different fates; embedding in bone matrix to form osteocytes, becoming bone lining cells or undergoing apoptosis (Figure 2). The regulation

Figure 1. Different stages of osteoblast differentiation.

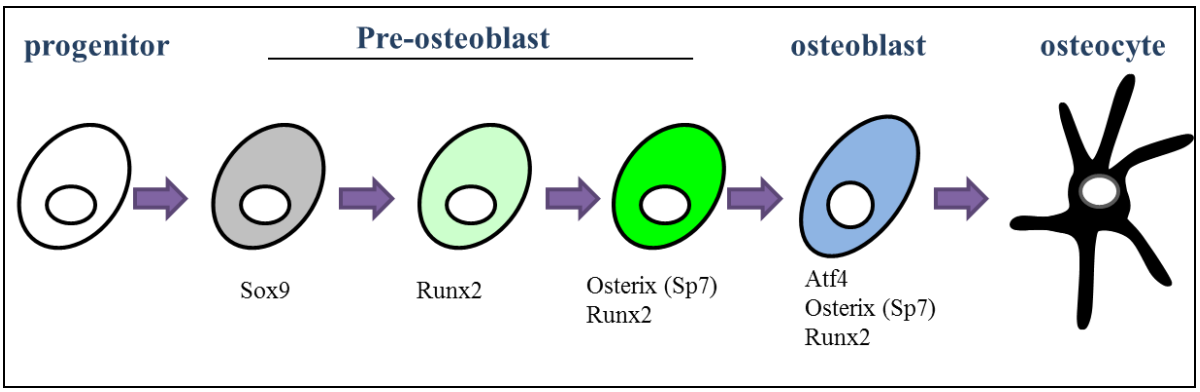

of these mature osteoblast fates are not understood. The various regulatory factors (e.g, developmental signals and transcription factors) that regulate osteoblast differentiation from progenitors will be discussed below.

Figure 2. Fates of mature osteoblasts.

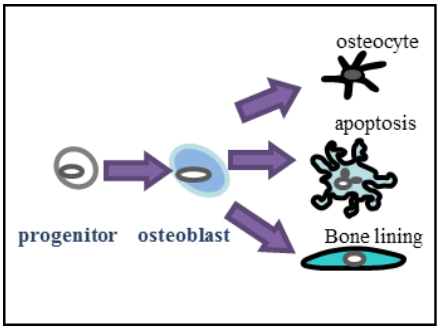

1.1.1. Transcription Factors

The SOX (SRY-related HMG-box) transcription factors are key regulators of skeletal development. Mutations in Sox9 cause the human disease, campomelic dysplasia, in which endochondral bone development is disrupted. However, the role of Sox9 in osteoblast lineage cells is not clear due to its crucial role in chondrogenesis. There is no chondrocytes or osteoblasts

in Sox9 ablated limb bunds, but it is not clear if the later depends on the first (Akiyama et al., 2002).

Runx2 and Osx are the main transcription factors that regulate osteoblast differentiation. Osx or Runx2 deficient mice lack mature osteoblasts and hence calcified bones (Ducy et al., 1997; Komori et al., 1997; Nakashima et al., 2002). Runx2 haploinsufficiency causes a skeletal dysplasia (Mundlos et al., 1997), but there is no known human disease associated with Osx mutations**.** Developmentally, Runx2 is expressed as early as E10.5 in osteochondro progenitors, which are the cells with the capacity to differentiate into osteoblasts or chondrocytes. Chondrocytes lose Runx2 expression during differentiation while osteoblasts maintain Runx2 throughout differentiation. Osx is expressed at a later stage than Runx2 and functions downstream of Runx2 as Runx2 is expressed normally in Osx null mice, whereas, Osx is not expressed in the Runx2 null animals. Overall, both Runx2 and Osx are indispensable for osteoblast differentiation and are both used to define differentiation stages.

ATF4 is a CREB family transcription factor that is active in mature osteoblasts. It is necessary for bone formation via regulating different processes. First, ATF4 directly regulates osteocalcin expression, which is a matrix protein specific for mature osteoblasts. Second, it regulates collagen 1 processing and secretion without affecting its expression. Third, ATF4 affects osteoclasts via regulating RANKL expression. Lastly, it favors amino acid import by regulating genes involved in amino acid import, metabolism and assimilation. Atf4 deficient mice have reduced trabecular bone and size due to defect in osteoblast function and size respectively (Dobreva et al., 2006; Natarajan et al., 2001; Sambrook et al., 2012; Yang et al., 2004). Thus, ATF4 affects different aspects of osteoblast biology at a later stage compared to Runx2 and Osx.

Activator protein 1 (AP1) transcription factors are members of the Jun and Fos family of basic leucine zipper proteins. Although they are not osteoblast lineage specific, they play specific roles in osteoblast differentiation and function, as demonstrated by several loss- or gain-of-function studies in mice. In mice, overexpression of either fos-related antigen 1 (Fra1) or a splice variant of FosB results in increased osteoblast differentiation and function (Jochum et al., 2000; Sabatakos et al., 2000). Conversely, mice lacking Fra1 or JunB in the mouse embryo develop osteopenia associated with reduced bone formation (Eferl et al., 2004; Kenner et al., 2004).

The role of these transcription factors has been shown mostly by genetic studies, however how these transcription factors are regulated both transcriptionally and post-transcriptionally and how they affect different features of osteoblasts is not fully understood.

1.1.2. Developmental Signals

All the major developmental signaling pathways, such as Hedgehog (HH), Notch, WNT, BMP and FGF affect osteoblast differentiation at different stages.

1.1.2.1. WNT Signaling

WNTs are a large family of glycoproteins that activate both β-catenin dependent or independent intracellular pathways upon binding to their membrane receptor, Frizzled (FZD) and a co-receptor usually from the low density lipoprotein receptor-related protein (LRP) family. WNTs bind to the FZD family of seven-pass transmembrane receptors on the plasma membrane causing the receptors to activate the Dishevelled family proteins. Normally, β-catenin is complexed with adenomatous polyposis coli (APC) and Axin in the absence of WNT. This complex facilitates phosphorylation of β-catenin by glycogen synthase kinase 3β (GSK3β),

which subsequently leads to degradation of β-catenin via the β-TrCP mediated ubiquitin/proteasome pathway. In the absence of β-catenin, Groucho proteins suppress transcription of WNT target genes by binding to T cell factor (TCF) and lymphoid enhancer factor (LEF) proteins that occupy the promoters and enhancers of WNT target genes in the nucleus (Komiya and Habas, 2008; MacDonald et al., 2009; Zeng et al., 2005). However, interaction of WNT proteins with its receptor FZD and the co-receptors LRP5/6 leads to disassembly of the destruction complex. As a consequence, proteosomal degradation of β-catenin is disrupted (Bilic et al., 2007; Davidson et al., 2005; Wu et al., 2008). Stabilized β-catenin accumulates in the nucleus and activates WNT target genes by displacing transcription inhibitors and recruiting histone acetylase CBP/p300 (Figure 3). In addition to preventing β-catenin degradation, WNT activates JNK2 (c-Jun N-terminal kinase 2) through a $G\alpha_{q/11}\beta\gamma$-PI3K-Rac1 signaling cascade. JNK2 activation leads to phosphorylation of β-catenin at a specific site; this phosphorylation is important for the translocation of stabilized β-catenin to the nucleus (Wu et al., 2008). Overall, effectors for β-catenin dependent WNT signaling are well characterized.

β-catenin independent WNT signaling is less characterized and can be classified according to the cascades it initiates, such as WNT/PCP signaling and WNT/calcium signaling, both of which are downstream of Dishevelled. WNT/PCP signaling regulates cytoskeletal rearrangement by JNK and small GTPases such as, Rac and Rho. In WNT/calcium signaling, intracellular Ca^{2+} level is elevated, which in turn activates several kinases, such as protein kinase C (PKC), Calcium–calmodulin-dependent protein kinase II (CamK2) (James et al., 2008). Another target of β-catenin independent WNT signaling is the mTOR complex 1 (mTORC1) pathway, which controls the protein translation machinery. In this model, without WNT ligand, GSK3β activates TSC2 that is the inhibitor of mTORC1. Upon ligand binding, GSK3β gets

Figure 3. WNT/β-catenin Pathway

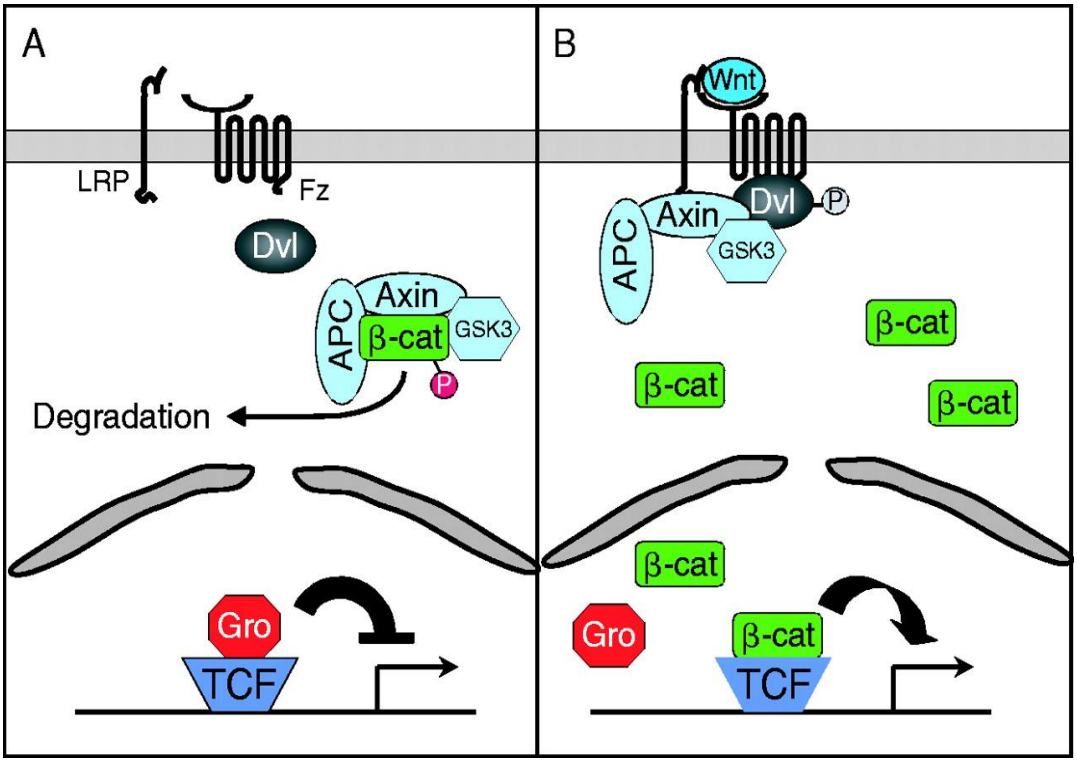

Cadigan K M , and Liu Y I J Cell Sci 2006;119:395-402 ©2006 by Tht Company of Biologists Ltd

inactivated; TSC2 activation is reduced, which leads to activation of mTORC1 (Inoki et al., 2006). Alternatively, WNT can regulate mTORC1 independent of GSK3β, but through PI3K-AKT signaling (Chen et al., 2014). Overall, β-catenin independent WNT signaling pathway has multiple branches, most of which are not well characterized.

WNT signaling has been studied as an important player in bone formation. The first evidence came from the co-receptor Lrp5 loss- and gain-of-function mutations that are linked to low and high bone mass diseases, respectively (Babij et al., 2003; Gong et al., 2001). Genetic studies in mice supported these Lrp5 phenotypes although there are conflicting reports regarding whether Lrp5 acts directly or indirectly on osteoblasts (Cui et al., 2011; Kato et al., 2002). It is noteworthy that Lrp5 mutations usually cause a postnatal phenotype, without having a major

embryonic phenotype. Removal of negative regulators of WNT signaling, such as Secreted frizzled-related protein 1 (sFRP-1), Sclerostin (SOST), Dickkopf-related protein 1 (DKK1), (Bodine et al., 2004; Li et al., 2006; Li et al., 2008; Li et al., 2005) or overexpression of WNT ligands, WNT10b (Bennett et al., 2005) and WNT7b (Chen et al., 2014), leads to a high bone-mass phenotype in mice. Conversely, WNT10b null mice have reduced bone mass postnatally and are resistant to age-related bone loss. Several groups removed β-catenin at different stages during osteoblast differentiation. β-catenin is indispensable for osteoblast differentiation in the mouse embryo. Conditional ablation of β-catenin from the progenitor cells disrupted osteoblast differentiation prior to the Osx positive stage in the embryo. Deletion of β-catenin in Osx-positive cells prevents subsequent differentiation to mature osteoblasts (Hu et al., 2005; Rodda and McMahon, 2006). β-catenin is also important for chondrocyte-osteoblast fate decision; β-catenin removal leads to ectopic cartilage formation (Day et al., 2005; Hill et al., 2005). Removal of β-catenin at more mature osteoblasts did not show a clear osteoblast defect (Glass et al., 2005). By taking advantage of an inducible system, a recent paper showed that deletion of β-catenin postnatally from the Osx-lineage cells has a direct effect on osteoblasts. This effect is followed by increase in bone resorption and marrow adiposity (Chen and Long, 2013). Overall, genetic studies indicate that WNT signaling is essential for bone formation, however, how WNT directs cell-fate decision and which downstream effector is more critical at different stages is not understood.

Although less well studied, β-catenin independent WNT signaling also plays a role in osteoblast differentiation. WNT induced activation of Protein kinase C delta (PKCδ) in mesenchymal progenitors promotes osteoblast differentiation (Tu et al., 2007) and WNT-induced activation of mTORC1 is partially involved in the high-bone mass phenotype of WNT7b

overexpression mice (Chen et al., 2014). Moreover, another WNT ligand, WNT5A suppresses the transcription factor PPARγ and shifts mesenchymal differentiation from adipocytes to osteoblasts (Albers et al., 2011). The discrepancy between the osteoblast phenotypes obtained by alteration of Lrp5 and β-catenin postnatally suggests that there might be β-catenin-independent WNT pathways important for osteoblast differentiation and function (Cui et al., 2011; Glass et al., 2005).

1.1.2.2. Other Extracellular Signals

Indian Hedgehog (IHH) is the only HH expressed in the mammalian endochondral skeleton. Embryos lacking IHH display severe defects in chondrocyte development and lack mature osteoblasts in the endochondral skeleton (Long et al., 2001; St-Jacques et al., 1999). Further studies demonstrate that HH has a direct role in osteoblast specification in the perichondrial region (Long et al., 2004). In the absence of HH, osteoblast differentiation is arrested at a very early stage even before expression of Runx2 in the lineage (Hu et al., 2005). Thus, HH is critical for both chondrocyte and osteoblast formation.

The BMPs, which belong to the transforming growth factor-β (TGF-β) family of secreted growth factors, play a critical role in bone formation. Although it is difficult to study the function of BMPs due to their redundant functions, it has been shown that BMP2/4 regulates osteoblast differentiation and is specifically important for the progression from the Runx2 to Osx-positive stage (Bandyopadhyay et al., 2006). In contrast, BMP3 null mice are characterized by increased bone mass (Daluiski et al., 2001). This unexpected result was explained by recent studies showing that BMP3 inhibits BMP2 and BMP4 signaling via engaging the BMP type II receptor (Kokabu et al., 2012). In addition to their role in osteoblast differentiation, BMPs also regulate

the function of mature osteoblasts (Mishina et al., 2004). In brief, BMPs are important for both differentiation and function of osteoblasts.

FGFs, operating through cell surface tyrosine kinase FGF receptors (FGFRs), have different functions in bone formation depending on the ligand and/or ligand-receptor combinations. While there is some controversy over the role of different FGF receptors/ligands in bone development, overall, FGF signaling likely promotes osteoblast differentiation, proliferation and mature osteoblast mineralization. (Jacob et al., 2006; Mayahara et al., 1993; Ohbayashi et al., 2002).

Notch signaling, which mediates communication between neighboring cells through single-pass transmembrane proteins, restricts osteoblast differentiation from mesenchymal stem cell (MSCs). Genetic removal of Notch signaling components in the limb mesenchyme gives rise to increased bone mass in adolescent mice. Increased bone mass is accompanied with a loss of mesenchymal progenitor population (Hilton et al., 2008). This model is consistent with the gain of function mutation in Notch2 that is associated with a syndrome displaying bone loss among other characteristics (Isidor et al., 2011).

The effect of different developmental signals on osteoblast differentiation has been documented extensively based on the phenotypic studies. However, how the signals drive the cell-fate decision in a very stage dependent manner and how they affect the activity of transcription factors is not understood. Moreover, the potential of posttranscriptional regulations associated with osteoblast cell specifications has not been explored.

1.1.3. Metabolic Signals in Osteoblast Differentiation/Function

The insulin and insulin-like growth factor (IGF) family of ligands and receptors are two well-established metabolic pathways (Nakae et al., 2001). These receptors are tyrosine kinases and can form either homodimers or heterodimers on the cell surface. The receptors undergo a conformational change and get auto-phosphorylated upon ligand binding (Hubbard, 1997).

Both of these receptors, insulin receptors (IR) and insulin like growth hormone 1 receptor (IGF1R), are expressed highly by osteoblasts (Pun et al., 1989; Thomas et al., 1996a) indicating the responsiveness of skeleton to these metabolic signals.

The direct role of insulin as a bone anabolic agent was first suggested by early *in vitro* studies showing that physiological insulin can enhance bone anabolic markers such as collagen and alkaline phosphatase (Kream et al., 1985; Pun et al., 1989; Rosen and Luben, 1983). This direct role is further supported by mouse genetics data indicating that osteoblast specific removal of IR cause reduced trabecular bone due to decreased bone formation and reduced mature osteoblast number (Fulzele et al., 2010). This result was in contrast with the normal bone mass phenotype from a different genetic model in which IR was removed from all the tissues but was transgenically re-expressed in the pancreas, liver, and brain to avoid ketoacidosis induced lethality (Irwin et al., 2006). This discrepancy was explained by the difference in the age of the analyzed mice. It is possible that osteoblasts require more insulin during development and might become less dependent on insulin signaling by aging. Recent studies revealed that insulin signaling in osteoblasts could even regulate whole body glucose metabolism through secretion of an osteoblast specific hormone, osteocalcin (Clemens and Karsenty, 2011). Overall, insulin directly targets osteoblasts and regulates bone formation by affecting both osteoblast function

and number. It remains to be investigated whether aging osteoblasts have a diminished response to insulin.

IGF1 has an anabolic role in bone development. Initial work was done in cultured osteoblastic cells where IGF1 stimulated survival (Hill et al., 1997), proliferation, differentiation, and matrix production (Hock et al., 1988). *In vitro* studies were confirmed by animal experiments using genetically altered mice. For instance, IGF1R null mice demonstrate delayed skeletal calcification along with severe growth retardation. However, these mice die postnatally due to organ hypoplasia and other complications. In contrast, IGF1 null mice show a relatively normal skeletal calcification but are also smaller than wild-type mice and have increased postnatal lethality (Liu et al., 1993). Osteoblast specific manipulations of IGF signaling have clarified the role of IGF in osteoblast function. Animals with overexpression of IGF1 in mature osteoblasts exhibit higher bone formation rate (BFR), higher bone volume and bone mineral density (BMD) without any change in total osteoblast or osteoclast numbers (Zhao et al., 2000). On the other hand, osteoblast-specific IGF1R knockout mice have reduced trabecular bone as a result of reduced osteoblast number and BFR at 3 weeks of age. At 6 weeks of age, there is no significant difference at osteoblast number but there is impairment of mineralization and trabecular structure (Zhang et al., 2002). Osteoblast-specific IGF1R knockout mice ablated PTH-induced bone formation in the mouse (Wang et al., 2007), which indicates that IGF signaling can be required for other anabolic signals. In summary, IGF signaling is essential for proper osteoblast function and further research is necessary to understand why it is required for the anabolic action of PTH.

Although both insulin and IGF signaling are important for bone formation, their role showed significant differences. First, mice lacking IR in osteoblasts have reduced mature

osteoblast number, which was only observed transiently in animals lacking IGF1R. Second, IGF1 does not regulate osteocalcin; hence IGF1R knockout mice lack a systemic metabolic phenotype. Third, insulin was able to partially rescue IGF1R deletion in primary osteoblasts; however IGF1 cannot rescue IR deletion. IGF1R knock out primary osteoblasts showed enhanced insulin sensitivity, which might potentially compensate for the lack of IGF1R (Fulzele et al., 2007). Despite these differences, papers published in the last decade strengthened the critical role of both IGF and insulin signaling in osteoblast function, differentiation and homeostasis, which is consistent with bone being a metabolically active organ.

Apart from insulin and IGF, glucose dependent insulinotropic peptide (GIP), an intestinally secreted hormone that stimulates insulin secretion from pancreatic beta-cells following food ingestion and nutrient, also regulates bone formation by both acting on osteoblasts and osteoclasts. Osteoblasts express GIP receptors (GIPR) and GIP increases collagen type I synthesis and alkaline phosphatase activity in isolated osteoblasts (Bollag et al., 2000). GIPR1 null mice show low bone mass phenotype (Tsukiyama et al., 2006; Xie et al., 2005) due to both reduced osteoblast activity, and increased osteoclast number, without affecting osteoblast number. Conversely, transgenic mice with GIP overexpression have a significant increase in bone mass resulted by reduced bone resorption and enhanced bone formation (Xie et al., 2007). It is important to note that both GIPR null and GIP transgenic mice have normal baseline blood glucose level, weight, and food intake as control mice. These studies suggest that nutrient ingestion is also linked to bone formation.

Systemic metabolic pathways directly affect osteoblast function, which might explain the correlation of osteoporosis with metabolic diseases. However, how those metabolic signals affect transcription factors, how they cross talk with developmental signals and how they affect the

cellular energy metabolism remains to be investigated.

2. Cellular Glucose Metabolism

Glucose is one of the major carbon sources in the cell and is an efficient fuel source for ATP production. Moreover, glucose is unique since its metabolism can furnish ATP even in the absence of oxygen.

2.1. Cellular Fates of Glucose

Glucose has several cellular metabolic fates. It first gets transported into the cells via facilitative glucose carriers (glucose transporters (GLUTs). Glucose diffusion does not require energy, it is considered as a passive transport (Bell et al., 1993)**.** Once glucose is transported into the cell, it gets phosphorylated to glucose-6-phosphate (G6P) by hexokinases and gets trapped within the cell. G6P can be stored as glycogen or can be metabolized. If metabolized, the cellular fates are as: 1) oxidation to pyruvate which either undergoes further oxidation in Tricarboxylic acid cycle (TCA cycle), or gets converted to lactate; 2) oxidation via PPP (Pentose Phosphate Pathway); 3) fueling into Hexosamine biosynthetic pathway (HBP) from fructose-6-phosphate (F6P) during glycolysis (Bouche et al., 2004) (Figure 4)**.** Thus, intracellular glucose can be used for both anabolic and catabolic pathways.

Glycolysis is the predominant route of cellular glucose utilization, in which one molecule of glucose breaks down into two molecules of pyruvate. The last step of glycolysis is catalyzed by lactate dehydrogenase enzyme (LDH) that converts pyruvate to lactate and regenerates NAD^+ that is needed as an electron acceptor to maintain further glycolysis. LDH is a tetrameric enzyme consisting of subunits A, B or C expressed from different genes. Different combinations of A

Figure 4. Cellular Fates of Glucose

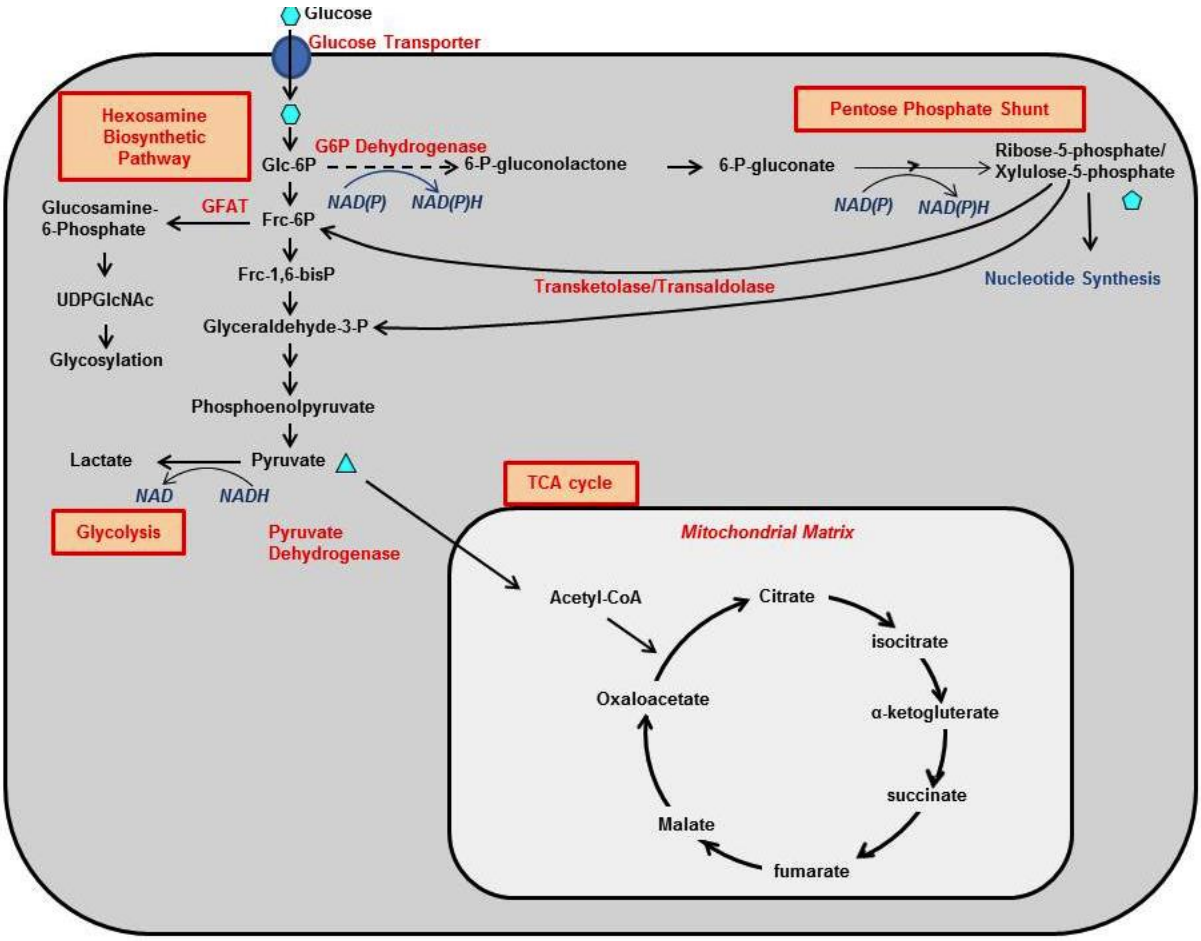

and B subunits constitute 5 different enzyme forms LDH1-5, which are expressed ubiquitously, while the C subunit is specific to the testis and sperms (Kopperschlager and Kirchberger, 1996). Intermediates can exit glycolysis before pyruvate formation to enter biosynthetic pathways, such as HBP and PPP. Thus, glycolysis generates intermediates necessary for energy production, redox regulation or anabolic reactions.

Pyruvate is at the crossroad of central metabolic fates. In addition to conversion to lactate, alternatively, it can be transaminated into alanine in the cytoplasm, decarboxylated into acetyl-coA or carboxylated into oxaloacetate (OAA) in the mitochondria. The predominant route for mitochondrial pyruvate is the decarboxylation into acetyl-coA via pyruvate dehydrogenase

complex (PDC). Elevated levels of ATP and phosphorylation inactivate PDC by pyruvate dehydrogenase kinases (PDKs). Oxidative phosphorylation (OXPHO) in TCA cycle starts with condensation of acetyl-coA with oxaloacetate to form citrate and follows a sequence of reactions to regenerate oxaloacetate and produce CO_2 molecules. During oxidation, there is constant carbon flux in and out of the cycle. For example, malate can be transported to cytosol where it is decarboxylated into pyruvate by malic enzyme producing NAD(P)H and pyruvate. Pyruvate can then be transported back to mitochondria. Citrate can also be transported across mitochondrial membranes and can get converted into oxaloacetate and acetyl-coA in the cytoplasm (Owen et al., 2002) (Figure 5).

Figure 5. Carbons can exit TCA cycle as malate and citrate.

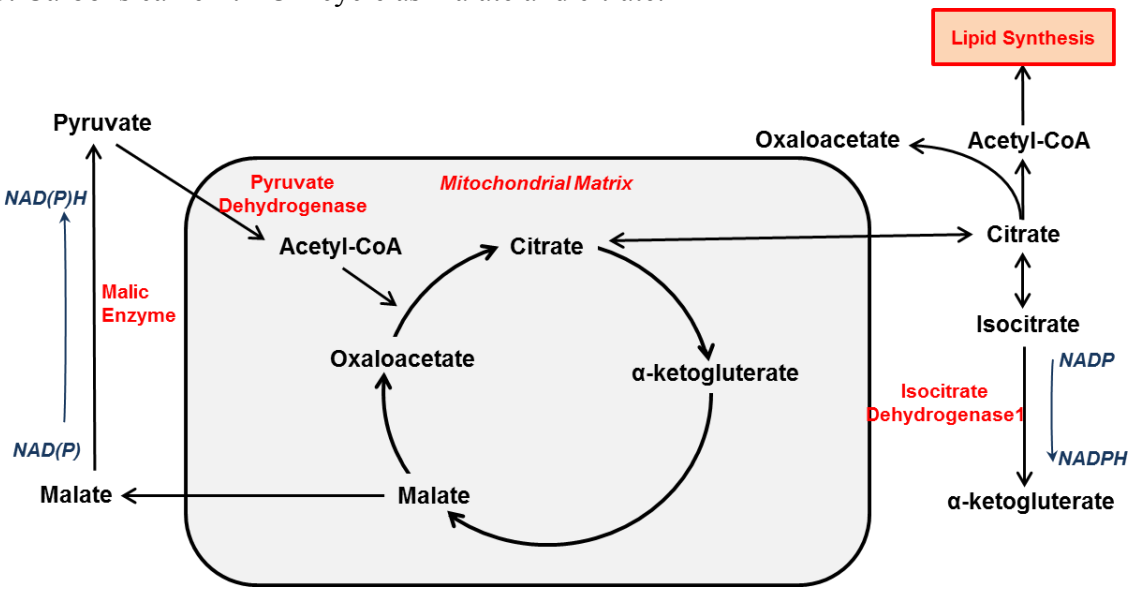

There are 12 transporters identified in the inner membranes of mammalian mitochondria (Schoolwerth and LaNoue, 1985), facilitating the flux of metabolites in-and-out of mitochondria. Loss of cycle intermediates due to removal of carbons from the TCA cycle other than CO_2 causes the need for replenishing the intermediates. The flux of carbon into the TCA cycle to replenish intermediates can be through transamination of aspartate into oxaloacetate, conversion

of glutamine into α- ketoglutarate, conversion of valine, isoleucine or methionine into succinly-coA and carboxylation of pyruvate into oxaloacetate (Lee and Davis, 1979) (Figure 6)**.** In

Figure 6. Anaplerotic reactions in the TCA cycle.

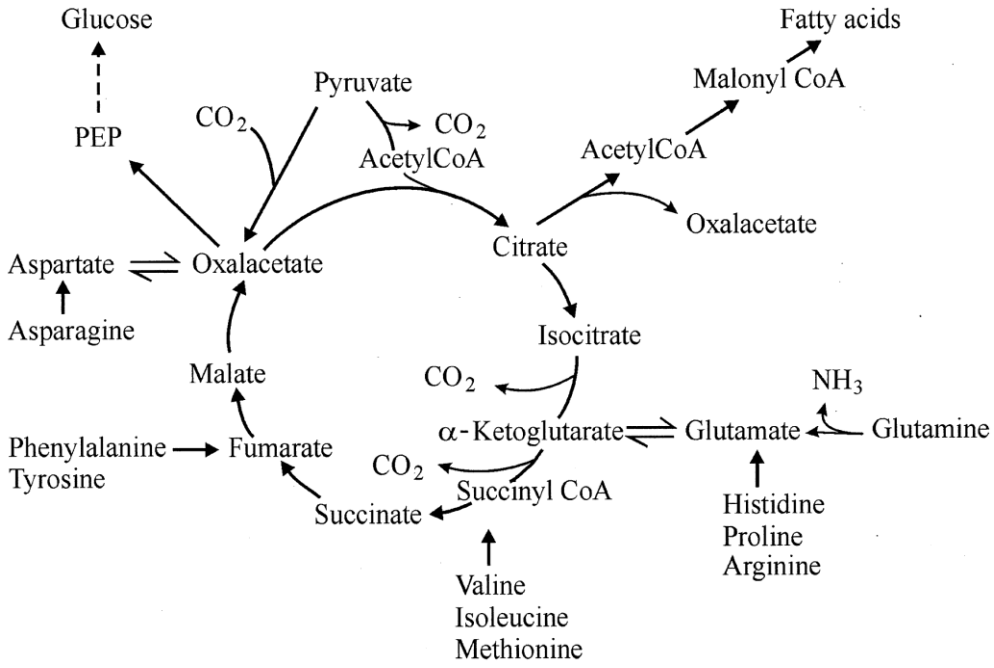

Owen O E et al. J. Biol. Chem. 2002;277:30409-30412 ©2002 by American Society for Biochemistry and Molecular Biology

summary, majority of mitochondrial pyruvate is converted to acetyl-coA to enter the TCA cycle, in which there is constant carbon flux to meet the needs of the cell.

During glycolysis, a small portion of glucose intermediates is diverted into HBP and PPP. 5 to 30% of glucose, varying in a tissue-dependent manner, is utilized in PPP that is the source of NAPDH and ribose-5-phosphate (R5P). PPP consists of oxidative and non-oxidative braches with the activity of the former being higher than the activity of the latter. Oxidative PPP starts with the rate-limiting irreversible reaction of dehydrogenation of G6P by glucose 6-phosphate dehydrogenase (G6PD). This is followed by further oxidation and decarboxylation into ribose-5 phosphate (R5P), the precursor for nucleotide synthesis. Oxidative PPP produce almost 60 percent of NADPH in the cell. NADPH provides the reducing equivalents for biosynthetic

processes such as fatty acid or cholesterol synthesis and protects against oxidative stress by reducing oxidized glutathione (GSSG). In the non-oxidative branch, PPP yields fructose 6-phosphate and glyceraldehyde 3-phosphate, both of which can enter the glycolytic pathway (Perl et al., 2011; Wamelink et al., 2008). Fructose-6-phosphate together with glutamine can be catalyzed by GFPT1 (known as GFAT) to form glucosamine-6-phosphate in the very first and rate limiting step of HBP in which approximately 2-5% of cellular glucose is used. Glucosamine-6-phosphate is further used to generate uridine diphospho-N-acetylglucosamine (UDP-GlcNAc), which is a precursor for a variety of glycosylation reactions (Teo et al., 2010). Overall, PPP and HBP take a small percentage of cellular glucose but are important anabolic pathways.

2.2. Alteration of Cellular Metabolism

Biological processes such as differentiation, proliferation, secretion, and division are linked to appropriate alterations in cellular metabolism to meet the new bioenergetic, synthetic, catabolic requirements of the cell (Rolland et al., 2001). The physiological maintenance of metabolite homeostasis is crucial for cell function since metabolic intermediates are the building blocks of the body that are required to synthesize nucleic acids, nonessential amino acids, glycogen and other biomolecules. Although it is not the focus of this thesis, cancer cells, prostate epithelial cells and differentiating embryonic stem cells provide well-characterized models to understand how cellular metabolic alterations can affect cell fate and specification. We can benefit what we learn from these models to understand potential links between cellular metabolism and osteoblast differentiation; therefore, below I describe these processes briefly.

2.2.1. Metabolic Alterations Associated with Diseases

Cancer cells manifest a unique metabolic feature by using excessive amounts of glucose and producing large amounts of lactate regardless of oxygen availability, referred as "aerobic glycolysis" (Vander Heiden et al., 2009). Aerobic glycolysis is less efficient for ATP production per glucose, but it can produce ATP at a rapid rate in the presence of excess glucose (Guppy et al., 1993) and can produce glycolytic intermediates, which are important for anabolic reactions (Gatenby and Gillies, 2004). Moreover, switching the main energy source to oxidative phosphorylation via removing LDHA reduces tumor formation in most cancer cells, suggesting that the altered metabolism is indeed important for tumor formation (Fantin et al., 2006; Le et al., 2010).

In addition to increased aerobic glycolysis, cancer cells go through a series of other metabolic alterations. Glucose flux towards PPP is increased to meet the elevated need for pentose phosphates for nucleic acid synthesis (Riganti et al., 2012)**.** Glutamine is used as an alternative carbon source for energy production by entering the TCA cycle via glutaminolysis (DeBerardinis et al., 2007; Portais et al., 1996) in some type of cancers. Glutamine depletion in these cells causes growth failure and apoptosis (Wise et al., 2008; Yuneva et al., 2007). In addition to the altered carbon metabolism, enhanced zinc import is associated with tumorigenesis of pancreatic cancer (Li et al., 2007). Overall, cancer is a good model to describe a sequence of metabolic alterations that are associated with the cell identity change.

2.2.2. Metabolic Alterations Associated with Differentiation and Cell Homeostasis

Metabolic changes accompany differentiation of stem cells. Embryonic stem cells (ESC) have a unique feature of unsaturated metabolites that are more susceptible to oxygenation and

hydrogenation reactions. This metabolite pool gets diminished during differentiation. Supplying the ESCs with metabolites involved in oxidative metabolism enhances differentiation (Yanes et al., 2010). Other studies pointed to the link between differentiation and metabolic changes as well (Folmes et al., 2011; Panopoulos et al., 2012; Zhang et al., 2013). These studies indicate that specialized cell types have a unique metabolic signature and modulations of metabolic intermediates might be important for differentiation.

Prostate epithelial cells are specialized citrate-secreting cells with a unique metabolic feature. These cells have high expression of ZIP1 zinc transporter (Franklin et al., 2003) that leads to increased zinc uptake. Zinc then gets transported to mitochondria where it attenuates aconidase activity, the enzyme required to isomerize citrate to isocitrate for the continuation of the TCA cycle (Costello et al., 1997). Due to this blockage, citrate exits mitochondria and gets secreted. To compensate for this loss of ATP production due to aborted TCA cycle and to continue to produce pyruvate, the citrate-producing prostate cells exhibit increased aerobic glycolysis. Furthermore, exit of citrate out of mitochondria requires an alternative carbon source for the continuation of the TCA cycle and for the production of more citrate. Aspartate fulfills this carbon source by forming oxaloacetate via transamination with glutamate by mitochondrial aspartate aminotransferase reaction (mAAT). High-affinity L-aspartate transporter (EAAC1) is highly expressed in prostate cells (Franklin et al., 2006). Briefly, prostate epithelial cells re-arrange their carbon metabolism to meet the needs of a specialized cell function, citrate-secretion.

Prostate epithelial cells and ESC differentiation serve as good examples of the metabolic changes for a specialized process or function. However it is not clear whether these changes are the result of different needs for the cell feature or is one of the driving forces for reprogramming cell function and fate. Moreover, the mechanistic regulation for the metabolic changes at the

molecular level has not been explored. Nonetheless, these metabolic changes can serve as models to study differentiation-related metabolic alterations in osteoblasts.

3. Metabolism of Bone

The skeleton is a highly metabolic tissue with constant remodeling driven by breaking down bones and making new bones. It is gaining more attention with the recent findings suggesting that skeleton can be a player in whole-body energy utilization through its hormonal interactions with other tissues (Clemens and Karsenty, 2011).

3.1. Bone and Metabolic Diseases

Type 1 diabetes mellitus (DM1), a disease of insulin deficiency due to the autoimmune-mediated destruction of pancreatic beta cells, is associated with bone related problems. These problems include decreased bone density, increased risk as well as early onset for osteoporosis (Kemink et al., 2000). Moreover, diabetic patients have increased fracture risk (Nicodemus and Folsom, 2001) and experience poor healing after fractures (Loder, 1988). Consistently, diabetic animal models reveal defects in osteoblast function (Lu et al., 2003; Verhaeghe et al., 1990). Functionally, delayed fracture healing in diabetic rats could be ameliorated by insulin delivery at the fracture site without affecting the systemic blood glucose (Gandhi et al., 2005).

While the association between bone and DM1 is well established as discussed above, the association between osteoporosis and type two diabetes (DM2) is less clear. There is a discrepancy in the literature such that bone mineral densities (BMDs) of DM2 patients were diminished (Isaia et al., 1987), enhanced (van Daele et al., 1995), or not changed (Wakasugi et al., 1993). This discrepancy might be associated with the bone sites studied, the heterogeneity,

severity or duration of the disease and obesity related complications in the patient populations studied. Regardless of this discrepancy, the tight link between DM1 and bone related problems, most of which are associated with osteoblast physiology, suggest that osteoblasts are the direct target cell for systemic metabolic diseases. Further research is needed to understand how these systemic diseases affect intracellular metabolism, signaling and transcriptional regulation.

3.2. Cellular Metabolism of Bone

3.2.1. Citrate Secreting Cells in the Bone

Bone metabolism is poorly understood due to lack of interest in this field. Early studies indicate that bone contains uniquely high citrate levels such that 1.6% of bone consists of citrate, and about 80% of the total body citrate resides in the bone (Dixon and Perkins, 1952). Although the high citrate concentration of bone has been known for decades, it has recently been discovered that citrate is critical for the structure of the apatite nanocrystal providing more carboxylate for calcium binding (Hu et al., 2010; Kenny et al., 1959; Taylor, 1960). Citrate is crucial for bone properties such as stability, strength, and resistance to fracture. It is not clear how bone cells accumulate citrate in the ECM, however, isocitrate dehydrogenase (IDH) activity is very low in bone (Dixon and Perkins, 1952) compared to other tissues. IDH catalyzes the oxidative decarboxylation of isocitrate producing α-KG; therefore reduced IDH activity could result in disruption of the TCA cycle and accumulation of citrate. The identity of citrate-secreting cells in the bone; the necessary metabolic alterations associated with increased citrate-secretion and the underlying mechanism is not discovered.

3.2.2. Aerobic Glycolysis in the Bone

In the early 1960's many studies using bone slices or calvarial cells showed that bone cells consume a large amount of glucose and produce lactate as the major end product while consuming oxygen very slowly even in aerobic conditions (Borle et al., 1960a; Cohn and Forscher, 1962; Peck et al., 1964). Besides lactate and CO_2, glucose carbons are also detected in amino acids; hence glucose might be the carbon source for amino acid synthesis in osteoblasts. Providing excess amino acid had no effect on the cellular CO_2 or lactate labeling from glucose, indicating that glucose is the main energy source (Flanagan and Nichols, 1964). Only in the absence of glucose, proline decarboxylation is increased to provide alternative energy source (Flanagan and Nichols, 1962). Hence, osteoblasts rely on aerobic glycolysis, similar to cancer cells.

In addition to the basal metabolic characteristics of bone, investigators studied the effect of hormones on bone metabolism. Metaphyseal bones prepared from PTH injected mice exhibited increased lactate production by 34% even in aerobic condition in the presence of glucose as a substrate. In the absence of glucose, lactate production was reduced by 7 fold and was not increased in response to PTH, confirming that glucose is the major source of lactate. On the other hand, another hormone, estradiol did not enhance lactate production in the same experiment. PTH effect on oxygen consumption was under debate (Borle et al., 1960b; Laskin and Engel, 1960). Similarly, PTH treatment increased lactate production in calvarial cells (Neuman et al., 1978; Rodan et al., 1978). PTH treatment also elevated citrate accumulation from pyruvate (Laskin and Engel, 1960). The mechanism of citrate accumulation was not clear (Cohn, 1964; Vaes and Nichols, 1961; Wolinsky and Cohn, 1969). In rat osteoblastic cells (PyMS)**,** not only PTH but also IGF, another anabolic agent, induced glucose uptake linking the

coupling of bone anabolism to increased glucose uptake (Zoidis et al., 2011). Overall, PTH favors lactate-producing glycolysis in osteoblasts.

These studies established that aerobic glycolysis is a unique characteristic of metabolism of bone cells. However, the mechanism under the regulation of glycolysis and its importance for osteoblast features and for PTH's action in the bone has not been studied.

3.2.3. The Expression of Glucose Transporters in Bone

Although it is known that bone cells rely mostly on glucose as an energy and carbon source, there is very little evidence about the specific expression of GLUTs in the bone. GLUT1 and GLUT3 were detected in an osteosarcoma cell line, UMR 106-01(Thomas et al., 1996b; Thomas et al., 1996c). Later, in growth plate chondrocytes GLUTs 1-5 were detected (Ohara et al., 2001). GLUT4 expression was shown in murine models of endochondral bone formation (Maor and Karnieli, 1999). There is also evidence for the expression of Glut1 in rodent osteoblastic cells (PyMS) (Rolland et al., 2001). Further investigation is needed to characterize the cellular location, function and necessity of specific GLUTs in the bone as well as *in vivo* expression patterns. Regardless, high expression of GLUTs is an indication of increased need for glucose in bone cells.

3.2.4. Cellular Metabolism of Osteoblast

Osteoblasts are expected to increase energy demand upon differentiation to accommodate the need for increased protein synthesis, an energetically costly process (Buttgereit and Brand, 1995). In recent years, the cellular metabolism of osteoblasts has been revisited with the advances of isolated purified cell preparations, the availability of cell lines, and availability of

metabolic techniques. Human MSC showed increased mitochondrial DNA (mtDNA) copy number, respiratory enzymes, oxygen consumption rate, mitochondrial biogenesis-associated genes, and intracellular ATP content after two weeks of osteogenic differentiation (Chen et al., 2008). However, ATP content as well as mtDNA copy number were suppressed significantly in the first three days of differentiation and other metabolic parameters were not analyzed other than two weeks of differentiation. Therefore, it was not clear how quickly MSC switched to oxidative phosphorylation and why the ATP content was suppressed in the early phase of differentiation. A recent study showed that differentiating osteoblasts increased both glycolysis and oxidative phosphorylation and mature osteoblasts relied mostly on glycolysis (Guntur et al., 2014). Thus, osteoblasts alter the cellular metabolism during differentiation in a stage-specific manner, but the global view of cellular metabolism and the necessity of these alterations are not known.

In addition to mitochondrial and glycolytic changes, the expression of Nampt, the NAD^+ biosynthetic enzyme, is increased during osteogenic differentiation (Li et al., 2013). NAD^+ dependent lysine deacetylase Sirt1 accelerates osteoblast differentiation from MSCs *in vitro* (Backesjo et al., 2006), while preventing adipocyte differentiation (Picard et al., 2004). Further studies are required to characterize the alterations in the redox-state of osteoblasts during differentiation in response to anabolic signals.

3.3. Aging Related Metabolic Dysfunction and Osteoporosis

Aging is associated with osteoporosis. In a healthy subject, bone mass increases along with growth, reaches the peak in adolescence and then starts to decline with aging after staying constant for several years. Failure to reach optimal bone mass during growth or unbalanced bone

formation and resorption can lead to age-related osteoporosis (Raisz, 2005). Increased apoptosis is a proposed mechanism in age-related decrease in bone mass (Zhou et al., 2008), although there are some discrepancies between different studies about the causal role. The responsiveness of osteoblasts to proliferative signals is reduced with age while senescence markers are increased (Kassem and Marie, 2011). In aging rats, there is a reduction in the number of mature osteoblasts with a concomitant accumulation of pre-osteoblasts, suggesting an impairment of osteoblast differentiation by aging (Roholl et al., 1994). Osteoblasts and adipocytes come from same mesenchymal progenitor cells. Interestingly, there is an induction of bone marrow adipocytes by aging (Bethel et al., 2013). This inverse relationship between osteoblast and adipocyte numbers during aging, led to the hypothesis that enhanced adipocyte differentiation by aging from mesenchymal progenitor cells results a reduced pool of available progenitor cells for osteoblast differentiation. Although studies in aging mice showed increased capacity of differentiation of mesenchymal progenitor cells to adipocytes along with a reduced osteoblastic capacity, a human study failed to show a reduced adipocyte-forming capacity of MSC with donor age (Kassem and Marie, 2011). Thus, this hypothesis remains to be further explored. In summary, aging leads to a variety of defects that could result attenuated osteoblast number and function, but the causative reason behind these defects in not understood.

IGFs are important regulators of skeletal remodeling. Although there is high variation among healthy people, serum IGF levels are usually low at birth and increase during adolescence, and then decrease progressively with age (Brabant et al., 2003). In addition to serum IGF levels, matrix IGF1 also decreases with aging (Seck et al., 1998). This decrease correlates with the decrease in bone mineral density. Osteoblasts lose their responsiveness to IGF during aging (Cao et al., 2007). Injecting IGF1 together with one of the IGF binding proteins ameliorates aging

related bone loss in rats (Xian et al., 2012). Therefore, it is possible that aging related risk of osteoporosis could be due to reduced IGFs in bone matrix and circulation.

Aging is associated with other changes in whole body metabolism and is linked with higher prevalence of DM2. Although it is more straightforward for DM1, both type 1 and type 2-diabetes manifest changes in serum IGF and IGF binding protein levels (Frystyk et al., 1999; Maes et al., 1986; Sandhu, 2005). Administration of IGF1 improves insulin sensitivity in DM1 (Carroll et al., 2000; Quattrin et al., 2001) and DM2, although increasing free IGF levels in the circulation cause other complications (Clemmons, 2012). Thus, diabetes is associated with altered IGF levels.

The onset of metabolic diseases and osteoporosis are correlated in elderly. Age related changes in systemic metabolism might contribute to osteoblast dysfunction by both affecting the differentiation capacity and function of osteoblast, and changing the fate of mesenchymal progenitor cells. IGF1 is a good candidate in that it is critical for osteoblast function; its level correlates with aging and metabolic diseases. Therefore, alterations of IGF signaling due to aging or diabetes can be the causative role of aging or diabetes-induced osteoporosis.

4. Summary

Understanding the osteoblast biology is the key to treat osteoporosis. Transcriptional changes driving osteoblast differentiation as well as developmental and metabolic signals required for the differentiation process has been documented in detail. A common mechanism downstream of different osteoblastic signals to coordinate transcriptional as well as non-transcriptional changes associated with differentiation has been lacking. Certain metabolic features of osteoblasts have been investigated decades ago, but it has never been explored how the cells alter their metabolism and whether this alteration could

be important for the differentiation process.

Based on both human genetics and mouse genetic models, the indispensable role of WNT signaling for bone formation is well established. However, these studies were mostly based on genetic removal of different pathway components and a global view of cellular changes in response to WNT signaling has not been the focus. Moreover, the contribution from β-catenin independent pathway is not clear. The first part of this thesis focuses on the changes in cellular glucose metabolism in response to WNT signaling. It describes the signaling cascades activated downstream of WNT that are required for enhanced glycolysis and emphasizes a potential role of these metabolic changes in osteoblast differentiation. Next, the requirement of glycolysis for *in vivo* osteoblast differentiation and function has been studied by removing LDHA, an enzyme upregulated by WNT, in osteoblast progenitor cells. Finally, I focus on how PTH stimulates glycolysis, how PTH regulates different glucose fates and the effect of enhanced glycolysis for PTH stimulated bone formation *in vivo*. Understanding the cellular metabolic alteration associated with osteoblast differentiation and function can help us to explore the association between aging, metabolic diseases and osteoblast biology.

References

Akiyama, H., Chaboissier, M.C., Martin, J.F., Schedl, A., and de Crombrugghe, B. (2002). The transcription factor Sox9 has essential roles in successive steps of the chondrocyte differentiation pathway and is required for expression of Sox5 and Sox6. Genes Dev *16*, 2813-2828.

Albers, J., Schulze, J., Beil, F.T., Gebauer, M., Baranowsky, A., Keller, J., Marshall, R.P., Wintges, K., Friedrich, F.W., Priemel, M.*, et al.* (2011). Control of bone formation by the serpentine receptor Frizzled-9. J Cell Biol *192*, 1057-1072.

Babij, P., Zhao, W., Small, C., Kharode, Y., Yaworsky, P.J., Bouxsein, M.L., Reddy, P.S., Bodine, P.V., Robinson, J.A., Bhat, B.*, et al.* (2003). High bone mass in mice expressing a mutant LRP5 gene. J Bone Miner Res *18*, 960-974.

Backesjo, C.M., Li, Y., Lindgren, U., and Haldosen, L.A. (2006). Activation of Sirt1 decreases adipocyte formation during osteoblast differentiation of mesenchymal stem cells. J Bone Miner Res *21*, 993-1002.

Bandyopadhyay, A., Tsuji, K., Cox, K., Harfe, B.D., Rosen, V., and Tabin, C.J. (2006). Genetic analysis of the roles of BMP2, BMP4, and BMP7 in limb patterning and skeletogenesis. PLoS Genet *2*, e216.

Bell, G.I., Burant, C.F., Takeda, J., and Gould, G.W. (1993). Structure and function of mammalian facilitative sugar transporters. J Biol Chem *268*, 19161-19164.

Bennett, C.N., Longo, K.A., Wright, W.S., Suva, L.J., Lane, T.F., Hankenson, K.D., and MacDougald, O.A. (2005). Regulation of osteoblastogenesis and bone mass by Wnt10b. Proc Natl Acad Sci U S A *102*, 3324-3329.

Bethel, M., Chitteti, B.R., Srour, E.F., and Kacena, M.A. (2013). The changing balance between osteoblastogenesis and adipogenesis in aging and its impact on hematopoiesis. Curr Osteoporos Rep *11*, 99-106.

Bilic, J., Huang, Y.L., Davidson, G., Zimmermann, T., Cruciat, C.M., Bienz, M., and Niehrs, C. (2007). Wnt induces LRP6 signalosomes and promotes dishevelled-dependent LRP6 phosphorylation. Science *316*, 1619-1622.

Bodine, P.V., Zhao, W., Kharode, Y.P., Bex, F.J., Lambert, A.J., Goad, M.B., Gaur, T., Stein, G.S., Lian, J.B., and Komm, B.S. (2004). The Wnt antagonist secreted frizzled-related protein-1 is a negative regulator of trabecular bone formation in adult mice. Mol Endocrinol *18*, 1222-1237.
Bollag, R.J., Zhong, Q., Phillips, P., Min, L., Zhong, L., Cameron, R., Mulloy, A.L., Rasmussen, H., Qin, F., Ding, K.H.*, et al.* (2000). Osteoblast-derived cells express functional glucose-dependent insulinotropic peptide receptors. Endocrinology *141*, 1228-1235.

Bonewald, L.F. (2011). The amazing osteocyte. J Bone Miner Res *26*, 229-238.

Borle, A.B., Nichols, N., and Nichols, G., Jr. (1960a). Metabolic studies of bone in vitro. I. Normal bone. J Biol Chem *235*, 1206-1210.

Borle, A.B., Nichols, N., and Nichols, G., Jr. (1960b). Metabolic studies of bone in vitro. II. The metabolic patterns of accretion and resorption. J Biol Chem *235*, 1211-1214.

Bouche, C., Serdy, S., Kahn, C.R., and Goldfine, A.B. (2004). The cellular fate of glucose and its relevance in type 2 diabetes. Endocr Rev *25*, 807-830.

Brabant, G., von zur Muhlen, A., Wuster, C., Ranke, M.B., Kratzsch, J., Kiess, W., Ketelslegers, J.M., Wilhelmsen, L., Hulthen, L., Saller, B.*, et al.* (2003). Serum insulin-like growth factor I reference values for an automated chemiluminescence immunoassay system: results from a multicenter study. Horm Res *60*, 53-60.

Buttgereit, F., and Brand, M.D. (1995). A hierarchy of ATP-consuming processes in mammalian cells. Biochem J *312 (Pt 1)*, 163-167.

Cao, J.J., Kurimoto, P., Boudignon, B., Rosen, C., Lima, F., and Halloran, B.P. (2007). Aging impairs IGF-I receptor activation and induces skeletal resistance to IGF-I. J Bone Miner Res *22*, 1271-1279.

Carroll, P.V., Christ, E.R., Umpleby, A.M., Gowrie, I., Jackson, N., Bowes, S.B., Hovorka, R., Croos, P., Sonksen, P.H., and Russell-Jones, D.L. (2000). IGF-I treatment in adults with type 1 diabetes: effects on glucose and protein metabolism in the fasting state and during a hyperinsulinemic-euglycemic amino acid clamp. Diabetes *49*, 789-796.

Chen, C.T., Shih, Y.R., Kuo, T.K., Lee, O.K., and Wei, Y.H. (2008). Coordinated changes of mitochondrial biogenesis and antioxidant enzymes during osteogenic differentiation of human mesenchymal stem cells. Stem Cells *26*, 960-968.

Chen, J., and Long, F. (2013). beta-catenin promotes bone formation and suppresses bone resorption in postnatal growing mice. J Bone Miner Res *28*, 1160-1169.

Chen, J., Tu, X., Esen, E., Joeng, K.S., Lin, C., Arbeit, J.M., Ruegg, M.A., Hall, M.N., Ma, L., and Long, F. (2014). WNT7B promotes bone formation in part through mTORC1. PLoS Genet *10*, e1004145.

Clemens, T.L., and Karsenty, G. (2011). The osteoblast: an insulin target cell controlling glucose homeostasis. J Bone Miner Res *26*, 677-680.

Clemmons, D.R. (2012). Metabolic actions of insulin-like growth factor-I in normal physiology and diabetes. Endocrinol Metab Clin North Am *41*, 425-443, vii-viii.

Cohn, D.V. (1964). Influence of Parathyroid Extract on the Metabolism of Organic Acids by Bone Slices. Endocrinology *74*, 133-137.

Cohn, D.V., and Forscher, B.K. (1962). Aerobic metabolism of glucose by bone. J Biol Chem *237*, 615-618.

Costello, L.C., Liu, Y., Franklin, R.B., and Kennedy, M.C. (1997). Zinc inhibition of mitochondrial aconitase and its importance in citrate metabolism of prostate epithelial cells. J Biol Chem *272*, 28875-28881.

Cui, Y., Niziolek, P.J., MacDonald, B.T., Zylstra, C.R., Alenina, N., Robinson, D.R., Zhong, Z., Matthes, S., Jacobsen, C.M., Conlon, R.A.*, et al.* (2011). Lrp5 functions in bone to regulate bone mass. Nat Med *17*, 684-691.

Daluiski, A., Engstrand, T., Bahamonde, M.E., Gamer, L.W., Agius, E., Stevenson, S.L., Cox, K., Rosen, V., and Lyons, K.M. (2001). Bone morphogenetic protein-3 is a negative regulator of bone density. Nat Genet *27*, 84-88.

Davidson, G., Wu, W., Shen, J., Bilic, J., Fenger, U., Stannek, P., Glinka, A., and Niehrs, C. (2005). Casein kinase 1 gamma couples Wnt receptor activation to cytoplasmic signal transduction. Nature *438*, 867-872.

Day, T.F., Guo, X., Garrett-Beal, L., and Yang, Y. (2005). Wnt/beta-catenin signaling in mesenchymal progenitors controls osteoblast and chondrocyte differentiation during vertebrate skeletogenesis. Dev Cell *8*, 739-750.

DeBerardinis, R.J., Mancuso, A., Daikhin, E., Nissim, I., Yudkoff, M., Wehrli, S., and Thompson, C.B. (2007). Beyond aerobic glycolysis: transformed cells can engage in glutamine metabolism that exceeds the requirement for protein and nucleotide synthesis. Proc Natl Acad Sci U S A *104*, 19345-19350.

Dixon, T.F., and Perkins, H.R. (1952). Citric acid and bone metabolism. Biochem J *52*, 260-265.
Dobnig, H., Sipos, A., Jiang, Y., Fahrleitner-Pammer, A., Ste-Marie, L.G., Gallagher, J.C., Pavo, I., Wang, J., and Eriksen, E.F. (2005). Early changes in biochemical markers of bone formation correlate with improvements in bone structure during teriparatide therapy. J Clin Endocrinol Metab *90*, 3970-3977.

Dobreva, G., Chahrour, M., Dautzenberg, M., Chirivella, L., Kanzler, B., Farinas, I., Karsenty, G., and Grosschedl, R. (2006). SATB2 is a multifunctional determinant of craniofacial patterning and osteoblast differentiation. Cell *125*, 971-986.

Ducy, P., Zhang, R., Geoffroy, V., Ridall, A.L., and Karsenty, G. (1997). Osf2/Cbfa1: a transcriptional activator of osteoblast differentiation. Cell *89*, 747-754.

Eferl, R., Hoebertz, A., Schilling, A.F., Rath, M., Karreth, F., Kenner, L., Amling, M., and Wagner, E.F. (2004). The Fos-related antigen Fra-1 is an activator of bone matrix formation. Embo J *23*, 2789-2799.

Fantin, V.R., St-Pierre, J., and Leder, P. (2006). Attenuation of LDH-A expression uncovers a link between glycolysis, mitochondrial physiology, and tumor maintenance. Cancer Cell *9*, 425-434.

Feng, J.Q., Ward, L.M., Liu, S., Lu, Y., Xie, Y., Yuan, B., Yu, X., Rauch, F., Davis, S.I., Zhang, S.*, et al.* (2006). Loss of DMP1 causes rickets and osteomalacia and identifies a role for osteocytes in mineral metabolism. Nat Genet *38*, 1310-1315.

Flanagan, B., and Nichols, G., Jr. (1962). Metabolic studies of bone in vitro. IV. Collagen biosynthesis by surviving bone fragments in vitro. J Biol Chem *237*, 3686-3692.

Flanagan, B., and Nichols, G., Jr. (1964). Metabolic Studies of Bone in Vitro. V. Glucose Metabolism and Collagen Biosynthesis. J Biol Chem *239*, 1261-1265.

Folmes, C.D., Nelson, T.J., Martinez-Fernandez, A., Arrell, D.K., Lindor, J.Z., Dzeja, P.P., Ikeda, Y., Perez-Terzic, C., and Terzic, A. (2011). Somatic oxidative bioenergetics transitions into pluripotency-dependent glycolysis to facilitate nuclear reprogramming. Cell Metab *14*, 264-271.

Franklin, R.B., Ma, J., Zou, J., Guan, Z., Kukoyi, B.I., Feng, P., and Costello, L.C. (2003). Human ZIP1 is a major zinc uptake transporter for the accumulation of zinc in prostate cells. J Inorg Biochem *96*, 435-442.

Franklin, R.B., Zou, J., Yu, Z., and Costello, L.C. (2006). EAAC1 is expressed in rat and human prostate epithelial cells; functions as a high-affinity L-aspartate transporter; and is regulated by prolactin and testosterone. BMC Biochem *7*, 10.

Frystyk, J., Skjaerbaek, C., Vestbo, E., Fisker, S., and Orskov, H. (1999). Circulating levels of free insulin-like growth factors in obese subjects: the impact of type 2 diabetes. Diabetes Metab Res Rev *15*, 314-322.

Fulzele, K., DiGirolamo, D.J., Liu, Z., Xu, J., Messina, J.L., and Clemens, T.L. (2007). Disruption of the insulin-like growth factor type 1 receptor in osteoblasts enhances insulin signaling and action. J Biol Chem *282*, 25649-25658.

Fulzele, K., Riddle, R.C., DiGirolamo, D.J., Cao, X., Wan, C., Chen, D., Faugere, M.C., Aja, S., Hussain, M.A., Bruning, J.C.*, et al.* (2010). Insulin receptor signaling in osteoblasts regulates postnatal bone acquisition and body composition. Cell *142*, 309-319.

Gandhi, A., Beam, H.A., O'Connor, J.P., Parsons, J.R., and Lin, S.S. (2005). The effects of local insulin delivery on diabetic fracture healing. Bone *37*, 482-490.

Gatenby, R.A., and Gillies, R.J. (2004). Why do cancers have high aerobic glycolysis? Nat Rev Cancer *4*, 891-899.

Glass, D.A., 2nd, Bialek, P., Ahn, J.D., Starbuck, M., Patel, M.S., Clevers, H., Taketo, M.M., Long, F., McMahon, A.P., Lang, R.A.*, et al.* (2005). Canonical Wnt signaling in differentiated osteoblasts controls osteoclast differentiation. Dev Cell *8*, 751-764.

Gong, Y., Slee, R.B., Fukai, N., Rawadi, G., Roman-Roman, S., Reginato, A.M., Wang, H., Cundy, T., Glorieux, F.H., Lev, D.*, et al.* (2001). LDL receptor-related protein 5 (LRP5) affects bone accrual and eye development. Cell *107*, 513-523.

Guntur, A.R., Le, P.T., Farber, C.R., and Rosen, C.J. (2014). Bioenergetics during calvarial osteoblast differentiation reflect strain differences in bone mass. Endocrinology, en20131974.

Guppy, M., Greiner, E., and Brand, K. (1993). The role of the Crabtree effect and an endogenous fuel in the energy metabolism of resting and proliferating thymocytes. Eur J Biochem *212*, 95-99.

Hill, P.A., Tumber, A., and Meikle, M.C. (1997). Multiple extracellular signals promote osteoblast survival and apoptosis. Endocrinology *138*, 3849-3858.

Hill, T.P., Spater, D., Taketo, M.M., Birchmeier, W., and Hartmann, C. (2005). Canonical Wnt/beta-catenin signaling prevents osteoblasts from differentiating into chondrocytes. Dev Cell *8*, 727-738.

Hilton, M.J., Tu, X., Wu, X., Bai, S., Zhao, H., Kobayashi, T., Kronenberg, H.M., Teitelbaum, S.L., Ross, F.P., Kopan, R.*, et al.* (2008). Notch signaling maintains bone marrow mesenchymal progenitors by suppressing osteoblast differentiation. Nat Med *14*, 306-314.

Hock, J.M., Centrella, M., and Canalis, E. (1988). Insulin-like growth factor I has independent effects on bone matrix formation and cell replication. Endocrinology *122*, 254-260.

Hodsman, A.B., Bauer, D.C., Dempster, D.W., Dian, L., Hanley, D.A., Harris, S.T., Kendler, D.L., McClung, M.R., Miller, P.D., Olszynski, W.P.*, et al.* (2005). Parathyroid hormone and teriparatide for the treatment of osteoporosis: a review of the evidence and suggested guidelines for its use. Endocr Rev *26*, 688-703.

Hodsman, A.B., and Steer, B.M. (1993). Early histomorphometric changes in response to parathyroid hormone therapy in osteoporosis: evidence for de novo bone formation on quiescent cancellous surfaces. Bone *14*, 523-527.

Hu, H., Hilton, M.J., Tu, X., Yu, K., Ornitz, D.M., and Long, F. (2005). Sequential roles of Hedgehog and Wnt signaling in osteoblast development. Development *132*, 49-60.

Hu, Y.Y., Rawal, A., and Schmidt-Rohr, K. (2010). Strongly bound citrate stabilizes the apatite nanocrystals in bone. Proc Natl Acad Sci U S A *107*, 22425-22429.

Hubbard, S.R. (1997). Crystal structure of the activated insulin receptor tyrosine kinase in complex with peptide substrate and ATP analog. Embo J *16*, 5572-5581.

Inoki, K., Ouyang, H., Zhu, T., Lindvall, C., Wang, Y., Zhang, X., Yang, Q., Bennett, C., Harada, Y., Stankunas, K.*, et al.* (2006). TSC2 integrates Wnt and energy signals via a coordinated phosphorylation by AMPK and GSK3 to regulate cell growth. Cell *126*, 955-968.

Irwin, R., Lin, H.V., Motyl, K.J., and McCabe, L.R. (2006). Normal bone density obtained in the absence of insulin receptor expression in bone. Endocrinology *147*, 5760-5767.

Isaia, G., Bodrato, L., Carlevatto, V., Mussetta, M., Salamano, G., and Molinatti, G.M. (1987). Osteoporosis in type II diabetes. Acta Diabetol Lat *24*, 305-310.

Isidor, B., Lindenbaum, P., Pichon, O., Bezieau, S., Dina, C., Jacquemont, S., Martin-Coignard, D., Thauvin-Robinet, C., Le Merrer, M., Mandel, J.L.*, et al.* (2011). Truncating mutations in the last exon of NOTCH2 cause a rare skeletal disorder with osteoporosis. Nat Genet *43*, 306-308.

Jacob, A.L., Smith, C., Partanen, J., and Ornitz, D.M. (2006). Fibroblast growth factor receptor 1 signaling in the osteo-chondrogenic cell lineage regulates sequential steps of osteoblast maturation. Dev Biol *296*, 315-328.

James, R.G., Conrad, W.H., and Moon, R.T. (2008). Beta-catenin-independent Wnt pathways: signals, core proteins, and effectors. Methods Mol Biol *468*, 131-144.

Jochum, W., David, J.P., Elliott, C., Wutz, A., Plenk, H., Jr., Matsuo, K., and Wagner, E.F. (2000). Increased bone formation and osteosclerosis in mice overexpressing the transcription factor Fra-1. Nat Med *6*, 980-984.

Kassem, M., and Marie, P.J. (2011). Senescence-associated intrinsic mechanisms of osteoblast dysfunctions. Aging Cell *10*, 191-197.

Kato, M., Patel, M.S., Levasseur, R., Lobov, I., Chang, B.H., Glass, D.A., 2nd, Hartmann, C., Li, L., Hwang, T.H., Brayton, C.F.*, et al.* (2002). Cbfa1-independent decrease in osteoblast proliferation, osteopenia, and persistent embryonic eye vascularization in mice deficient in Lrp5, a Wnt coreceptor. J Cell Biol *157*, 303-314.

Kemink, S.A., Hermus, A.R., Swinkels, L.M., Lutterman, J.A., and Smals, A.G. (2000). Osteopenia in insulin-dependent diabetes mellitus; prevalence and aspects of pathophysiology. J Endocrinol Invest *23*, 295-303.

Kenner, L., Hoebertz, A., Beil, F.T., Keon, N., Karreth, F., Eferl, R., Scheuch, H., Szremska, A., Amling, M., Schorpp-Kistner, M.*, et al.* (2004). Mice lacking JunB are osteopenic due to cell-autonomous osteoblast and osteoclast defects. J Cell Biol *164*, 613-623.

Kenny, A.D., Draskoczy, P.R., and Goldhaber, P. (1959). Citric acid production by resorbing bone in tissue culture. Am J Physiol *197*, 502-504.

Kokabu, S., Gamer, L., Cox, K., Lowery, J., Tsuji, K., Raz, R., Economides, A., Katagiri, T., and Rosen, V. (2012). BMP3 suppresses osteoblast differentiation of bone marrow stromal cells via interaction with Acvr2b. Mol Endocrinol *26*, 87-94.

Komiya, Y., and Habas, R. (2008). Wnt signal transduction pathways. Organogenesis *4*, 68-75.

Komori, T., Yagi, H., Nomura, S., Yamaguchi, A., Sasaki, K., Deguchi, K., Shimizu, Y., Bronson, R.T., Gao, Y.H., Inada, M.*, et al.* (1997). Targeted disruption of Cbfa1 results in a complete lack of bone formation owing to maturational arrest of osteoblasts. Cell *89*, 755-764.

Kopperschlager, G., and Kirchberger, J. (1996). Methods for the separation of lactate dehydrogenases and clinical significance of the enzyme. J Chromatogr B Biomed Appl *684*, 25-49.

Kream, B.E., Smith, M.D., Canalis, E., and Raisz, L.G. (1985). Characterization of the effect of insulin on collagen synthesis in fetal rat bone. Endocrinology *116*, 296-302.

Laskin, D.M., and Engel, M.B. (1960). Relations between the metabolism and structure of bone. Ann N Y Acad Sci *85*, 421-430.

Le, A., Cooper, C.R., Gouw, A.M., Dinavahi, R., Maitra, A., Deck, L.M., Royer, R.E., Vander Jagt, D.L., Semenza, G.L., and Dang, C.V. (2010). Inhibition of lactate dehydrogenase A induces oxidative stress and inhibits tumor progression. Proc Natl Acad Sci U S A *107*, 2037-2042.

Lee, S.H., and Davis, E.J. (1979). Carboxylation and decarboxylation reactions. Anaplerotic flux and removal of citrate cycle intermediates in skeletal muscle. J Biol Chem *254*, 420-430.

Li, J., Sarosi, I., Cattley, R.C., Pretorius, J., Asuncion, F., Grisanti, M., Morony, S., Adamu, S., Geng, Z., Qiu, W.*, et al.* (2006). Dkk1-mediated inhibition of Wnt signaling in bone results in osteopenia. Bone *39*, 754-766.

Li, M., Zhang, Y., Liu, Z., Bharadwaj, U., Wang, H., Wang, X., Zhang, S., Liuzzi, J.P., Chang, S.M., Cousins, R.J.*, et al.* (2007). Aberrant expression of zinc transporter ZIP4 (SLC39A4) significantly contributes to human pancreatic cancer pathogenesis and progression. Proc Natl Acad Sci U S A *104*, 18636-18641.

Li, X., Ominsky, M.S., Niu, Q.T., Sun, N., Daugherty, B., D'Agostin, D., Kurahara, C., Gao, Y., Cao, J., Gong, J.*, et al.* (2008). Targeted deletion of the sclerostin gene in mice results in increased bone formation and bone strength. J Bone Miner Res *23*, 860-869.

Li, X., Zhang, Y., Kang, H., Liu, W., Liu, P., Zhang, J., Harris, S.E., and Wu, D. (2005). Sclerostin binds to LRP5/6 and antagonizes canonical Wnt signaling. J Biol Chem *280*, 19883-19887.

Li, Y., He, J., He, X., and Lindgren, U. (2013). Nampt expression increases during osteogenic differentiation of multi- and omnipotent progenitors. Biochem Biophys Res Commun *434*, 117-123.

Lindsay, R., Cosman, F., Zhou, H., Bostrom, M.P., Shen, V.W., Cruz, J.D., Nieves, J.W., and Dempster, D.W. (2006). A novel tetracycline labeling schedule for longitudinal evaluation of the short-term effects of anabolic therapy with a single iliac crest bone biopsy: early actions of teriparatide. J Bone Miner Res *21*, 366-373.

Liu, J.P., Baker, J., Perkins, A.S., Robertson, E.J., and Efstratiadis, A. (1993). Mice carrying null mutations of the genes encoding insulin-like growth factor I (Igf-1) and type 1 IGF receptor (Igf1r). Cell *75*, 59-72.

Loder, R.T. (1988). The influence of diabetes mellitus on the healing of closed fractures. Clin Orthop Relat Res, 210-216.

Long, F., Chung, U.I., Ohba, S., McMahon, J., Kronenberg, H.M., and McMahon, A.P. (2004). Ihh signaling is directly required for the osteoblast lineage in the endochondral skeleton. Development *131*, 1309-1318.

Long, F., and Ornitz, D.M. (2013). Development of the endochondral skeleton. Cold Spring Harb Perspect Biol *5*, a008334.

Long, F., Zhang, X.M., Karp, S., Yang, Y., and McMahon, A.P. (2001). Genetic manipulation of hedgehog signaling in the endochondral skeleton reveals a direct role in the regulation of chondrocyte proliferation. Development *128*, 5099-5108.

Lu, H., Kraut, D., Gerstenfeld, L.C., and Graves, D.T. (2003). Diabetes interferes with the bone formation by affecting the expression of transcription factors that regulate osteoblast differentiation. Endocrinology *144*, 346-352.

MacDonald, B.T., Tamai, K., and He, X. (2009). Wnt/beta-catenin signaling: components, mechanisms, and diseases. Dev Cell *17*, 9-26.

Maes, M., Ketelslegers, J.M., and Underwood, L.E. (1986). Low circulating somatomedin-C/insulin-like growth factor I in insulin-dependent diabetes and malnutrition: growth hormone receptor and post-receptor defects. Acta Endocrinol Suppl (Copenh) *279*, 86-92.

Maor, G., and Karnieli, E. (1999). The insulin-sensitive glucose transporter (GLUT4) is involved in early bone growth in control and diabetic mice, but is regulated through the insulin-like growth factor I receptor. Endocrinology *140*, 1841-1851.

Mayahara, H., Ito, T., Nagai, H., Miyajima, H., Tsukuda, R., Taketomi, S., Mizoguchi, J., and Kato, K. (1993). In vivo stimulation of endosteal bone formation by basic fibroblast growth factor in rats. Growth Factors *9*, 73-80.

Mishina, Y., Starbuck, M.W., Gentile, M.A., Fukuda, T., Kasparcova, V., Seedor, J.G., Hanks, M.C., Amling, M., Pinero, G.J., Harada, S.*, et al.* (2004). Bone morphogenetic protein type IA receptor signaling regulates postnatal osteoblast function and bone remodeling. J Biol Chem *279*, 27560-27566.

Mundlos, S., Otto, F., Mundlos, C., Mulliken, J.B., Aylsworth, A.S., Albright, S., Lindhout, D., Cole, W.G., Henn, W., Knoll, J.H.*, et al.* (1997). Mutations involving the transcription factor CBFA1 cause cleidocranial dysplasia. Cell *89*, 773-779.

Nakae, J., Kido, Y., and Accili, D. (2001). Distinct and overlapping functions of insulin and IGF-I receptors. Endocr Rev *22*, 818-835.

Nakashima, K., Zhou, X., Kunkel, G., Zhang, Z., Deng, J.M., Behringer, R.R., and de Crombrugghe, B. (2002). The novel zinc finger-containing transcription factor osterix is required for osteoblast differentiation and bone formation. Cell *108*, 17-29.

Natarajan, K., Meyer, M.R., Jackson, B.M., Slade, D., Roberts, C., Hinnebusch, A.G., and Marton, M.J. (2001). Transcriptional profiling shows that Gcn4p is a master regulator of gene expression during amino acid starvation in yeast. Mol Cell Biol *21*, 4347-4368.

Neuman, W.F., Neuman, M.W., and Brommage, R. (1978). Aerobic glycolysis in bone: lactate production and gradients in calvaria. Am J Physiol *234*, C41-50.

Nicodemus, K.K., and Folsom, A.R. (2001). Type 1 and type 2 diabetes and incident hip fractures in postmenopausal women. Diabetes Care *24*, 1192-1197.

Ohara, H., Tamayama, T., Maemura, K., Kanbara, K., Hayasaki, H., Abe, M., and Watanabe, M. (2001). Immunocytochemical demonstration of glucose transporters in epiphyseal growth plate chondrocytes of young rats in correlation with autoradiographic distribution of 2-deoxyglucose in chondrocytes of mice. Acta Histochem *103*, 365-378.

Ohbayashi, N., Shibayama, M., Kurotaki, Y., Imanishi, M., Fujimori, T., Itoh, N., and Takada, S. (2002). FGF18 is required for normal cell proliferation and differentiation during osteogenesis and chondrogenesis. Genes Dev *16*, 870-879.

Olsen, B.R., Reginato, A.M., and Wang, W. (2000). Bone development. Annu Rev Cell Dev Biol *16*, 191-220.

Owen, M. (1963). Cell Population Kinetics of an Osteogenic Tissue. I. J Cell Biol *19*, 19-32.

Owen, O.E., Kalhan, S.C., and Hanson, R.W. (2002). The key role of anaplerosis and cataplerosis for citric acid cycle function. J Biol Chem *277*, 30409-30412.

Panopoulos, A.D., Yanes, O., Ruiz, S., Kida, Y.S., Diep, D., Tautenhahn, R., Herrerias, A., Batchelder, E.M., Plongthongkum, N., Lutz, M.*, et al.* (2012). The metabolome of induced

pluripotent stem cells reveals metabolic changes occurring in somatic cell reprogramming. Cell Res *22*, 168-177.

Peck, W.A., Birge, S.J., Jr., and Fedak, S.A. (1964). Bone Cells: Biochemical and Biological Studies after Enzymatic Isolation. Science *146*, 1476-1477.

Perl, A., Hanczko, R., Telarico, T., Oaks, Z., and Landas, S. (2011). Oxidative stress, inflammation and carcinogenesis are controlled through the pentose phosphate pathway by transaldolase. Trends Mol Med *17*, 395-403.

Picard, F., Kurtev, M., Chung, N., Topark-Ngarm, A., Senawong, T., Machado De Oliveira, R., Leid, M., McBurney, M.W., and Guarente, L. (2004). Sirt1 promotes fat mobilization in white adipocytes by repressing PPAR-gamma. Nature *429*, 771-776.

Portais, J.C., Voisin, P., Merle, M., and Canioni, P. (1996). Glucose and glutamine metabolism in C6 glioma cells studied by carbon 13 NMR. Biochimie *78*, 155-164.

Pun, K.K., Lau, P., and Ho, P.W. (1989). The characterization, regulation, and function of insulin receptors on osteoblast-like clonal osteosarcoma cell line. J Bone Miner Res *4*, 853-862.

Quattrin, T., Thrailkill, K., Baker, L., Kuntze, J., Compton, P., and Martha, P. (2001). Improvement of HbA1c without increased hypoglycemia in adolescents and young adults with type 1 diabetes mellitus treated with recombinant human insulin-like growth factor-I and insulin. rhIGF-I in IDDM Study Group. J Pediatr Endocrinol Metab *14*, 267-277.

Raisz, L.G. (2005). Pathogenesis of osteoporosis: concepts, conflicts, and prospects. J Clin Invest *115*, 3318-3325.

Riganti, C., Gazzano, E., Polimeni, M., Aldieri, E., and Ghigo, D. (2012). The pentose phosphate pathway: an antioxidant defense and a crossroad in tumor cell fate. Free Radic Biol Med *53*, 421-436.

Roberts, D.J., Tan-Sah, V.P., Smith, J.M., and Miyamoto, S. (2013). Akt phosphorylates HK-II at Thr-473 and increases mitochondrial HK-II association to protect cardiomyocytes. The Journal of biological chemistry *288*, 23798-23806.

Rodan, G.A., Rodan, S.B., and Marks, S.C., Jr. (1978). Parathyroid hormone stimulation of adenylate cyclase activity and lactic acid accumulation in calvaria of osteopetrotic (ia) rats. Endocrinology *102*, 1501-1505.

Rodda, S.J., and McMahon, A.P. (2006). Distinct roles for Hedgehog and canonical Wnt signaling in specification, differentiation and maintenance of osteoblast progenitors. Development *133*, 3231-3244.

Roholl, P.J., Blauw, E., Zurcher, C., Dormans, J.A., and Theuns, H.M. (1994). Evidence for a diminished maturation of preosteoblasts into osteoblasts during aging in rats: an ultrastructural analysis. J Bone Miner Res *9*, 355-366.

Rolland, F., Winderickx, J., and Thevelein, J.M. (2001). Glucose-sensing mechanisms in eukaryotic cells. Trends Biochem Sci *26*, 310-317.

Rosen, D.M., and Luben, R.A. (1983). Multiple hormonal mechanisms for the control of collagen synthesis in an osteoblast-like cell line, MMB-1. Endocrinology *112*, 992-999.

Sabatakos, G., Sims, N.A., Chen, J., Aoki, K., Kelz, M.B., Amling, M., Bouali, Y., Mukhopadhyay, K., Ford, K., Nestler, E.J.*, et al.* (2000). Overexpression of DeltaFosB transcription factor(s) increases bone formation and inhibits adipogenesis. Nat Med *6*, 985-990.

Sambrook, P.N., Roux, C., Devogelaer, J.P., Saag, K., Lau, C.S., Reginster, J.Y., Bucci-Rechtweg, C., Su, G., and Reid, D.M. (2012). Bisphosphonates and glucocorticoid osteoporosis in men: results of a randomized controlled trial comparing zoledronic acid with risedronate. Bone *50*, 289-295.

Sandhu, M.S. (2005). Insulin-like growth factor-I and risk of type 2 diabetes and coronary heart disease: molecular epidemiology. Endocr Dev *9*, 44-54.

Schoolwerth, A.C., and LaNoue, K.F. (1985). Transport of metabolic substrates in renal mitochondria. Annu Rev Physiol *47*, 143-171.

Seck, T., Scheppach, B., Scharla, S., Diel, I., Blum, W.F., Bismar, H., Schmid, G., Krempien, B., Ziegler, R., and Pfeilschifter, J. (1998). Concentration of insulin-like growth factor (IGF)-I and -II in iliac crest bone matrix from pre- and postmenopausal women: relationship to age, menopause, bone turnover, bone volume, and circulating IGFs. J Clin Endocrinol Metab *83*, 2331-2337.

St-Jacques, B., Hammerschmidt, M., and McMahon, A.P. (1999). Indian hedgehog signaling regulates proliferation and differentiation of chondrocytes and is essential for bone formation. Genes Dev *13*, 2072-2086.

Taylor, T.G. (1960). The nature of bone citrate. Biochim Biophys Acta *39*, 148-149.

Teo, C.F., Wollaston-Hayden, E.E., and Wells, L. (2010). Hexosamine flux, the O-GlcNAc modification, and the development of insulin resistance in adipocytes. Mol Cell Endocrinol *318*, 44-53.

Thomas, D.M., Hards, D.K., Rogers, S.D., Ng, K.W., and Best, J.D. (1996a). Insulin receptor expression in bone. J Bone Miner Res *11*, 1312-1320.

Thomas, D.M., Maher, F., Rogers, S.D., and Best, J.D. (1996b). Expression and regulation by insulin of GLUT 3 in UMR 106-01, a clonal rat osteosarcoma cell line. Biochem Biophys Res Commun *218*, 789-793.

Thomas, D.M., Rogers, S.D., Ng, K.W., and Best, J.D. (1996c). Dexamethasone modulates insulin receptor expression and subcellular distribution of the glucose transporter GLUT 1 in UMR 106-01, a clonal osteogenic sarcoma cell line. J Mol Endocrinol *17*, 7-17.

Tsukiyama, K., Yamada, Y., Yamada, C., Harada, N., Kawasaki, Y., Ogura, M., Bessho, K., Li, M., Amizuka, N., Sato, M.*, et al.* (2006). Gastric inhibitory polypeptide as an endogenous factor promoting new bone formation after food ingestion. Mol Endocrinol *20*, 1644-1651.

Tu, X., Joeng, K.S., Nakayama, K.I., Nakayama, K., Rajagopal, J., Carroll, T.J., McMahon, A.P., and Long, F. (2007). Noncanonical Wnt signaling through G protein-linked PKCdelta activation promotes bone formation. Dev Cell *12*, 113-127.

Vaes, G., and Nichols, G., Jr. (1961). Metabolic studies of bone in vitro. III. Citric acid metabolism and bone mineral solubility. Effects of parathyroid hormone and estradiol. J Biol Chem *236*, 3323-3329.

van Daele, P.L., Stolk, R.P., Burger, H., Algra, D., Grobbee, D.E., Hofman, A., Birkenhager, J.C., and Pols, H.A. (1995). Bone density in non-insulin-dependent diabetes mellitus. The Rotterdam Study. Ann Intern Med *122*, 409-414.

Vander Heiden, M.G., Cantley, L.C., and Thompson, C.B. (2009). Understanding the Warburg effect: the metabolic requirements of cell proliferation. Science *324*, 1029-1033.

Verhaeghe, J., van Herck, E., Visser, W.J., Suiker, A.M., Thomasset, M., Einhorn, T.A., Faierman, E., and Bouillon, R. (1990). Bone and mineral metabolism in BB rats with long-term diabetes. Decreased bone turnover and osteoporosis. Diabetes *39*, 477-482.

Wakasugi, M., Wakao, R., Tawata, M., Gan, N., Koizumi, K., and Onaya, T. (1993). Bone mineral density measured by dual energy x-ray absorptiometry in patients with non-insulin-dependent diabetes mellitus. Bone *14*, 29-33.

Wamelink, M.M., Struys, E.A., and Jakobs, C. (2008). The biochemistry, metabolism and inherited defects of the pentose phosphate pathway: a review. J Inherit Metab Dis *31*, 703-717.

Wang, Y., Nishida, S., Boudignon, B.M., Burghardt, A., Elalieh, H.Z., Hamilton, M.M., Majumdar, S., Halloran, B.P., Clemens, T.L., and Bikle, D.D. (2007). IGF-I receptor is required for the anabolic actions of parathyroid hormone on bone. J Bone Miner Res *22*, 1329-1337.

Wise, D.R., DeBerardinis, R.J., Mancuso, A., Sayed, N., Zhang, X.Y., Pfeiffer, H.K., Nissim, I., Daikhin, E., Yudkoff, M., McMahon, S.B.*, et al.* (2008). Myc regulates a transcriptional program that stimulates mitochondrial glutaminolysis and leads to glutamine addiction. Proc Natl Acad Sci U S A *105*, 18782-18787.

Wolinsky, I., and Cohn, D.V. (1969). Oxygen uptake and 14CO2 production from citrate and isocitrate by control and parathyroid hormone-treated bone maintained in tissue culture. Endocrinology *84*, 28-35.

Wu, X., Tu, X., Joeng, K.S., Hilton, M.J., Williams, D.A., and Long, F. (2008). Rac1 activation controls nuclear localization of beta-catenin during canonical Wnt signaling. Cell *133*, 340-353.

Xian, L., Wu, X., Pang, L., Lou, M., Rosen, C.J., Qiu, T., Crane, J., Frassica, F., Zhang, L., Rodriguez, J.P.*, et al.* (2012). Matrix IGF-1 maintains bone mass by activation of mTOR in mesenchymal stem cells. Nat Med *18*, 1095-1101.

Xie, D., Cheng, H., Hamrick, M., Zhong, Q., Ding, K.H., Correa, D., Williams, S., Mulloy, A., Bollag, W., Bollag, R.J.*, et al.* (2005). Glucose-dependent insulinotropic polypeptide receptor knockout mice have altered bone turnover. Bone *37*, 759-769.

Xie, D., Zhong, Q., Ding, K.H., Cheng, H., Williams, S., Correa, D., Bollag, W.B., Bollag, R.J., Insogna, K., Troiano, N.*, et al.* (2007). Glucose-dependent insulinotropic peptide-overexpressing transgenic mice have increased bone mass. Bone *40*, 1352-1360.

Yanes, O., Clark, J., Wong, D.M., Patti, G.J., Sanchez-Ruiz, A., Benton, H.P., Trauger, S.A., Desponts, C., Ding, S., and Siuzdak, G. (2010). Metabolic oxidation regulates embryonic stem cell differentiation. Nat Chem Biol *6*, 411-417.

Yang, X., Matsuda, K., Bialek, P., Jacquot, S., Masuoka, H.C., Schinke, T., Li, L., Brancorsini, S., Sassone-Corsi, P., Townes, T.M.*, et al.* (2004). ATF4 is a substrate of RSK2 and an essential regulator of osteoblast biology; implication for Coffin-Lowry Syndrome. Cell *117*, 387-398.

Yuneva, M., Zamboni, N., Oefner, P., Sachidanandam, R., and Lazebnik, Y. (2007). Deficiency in glutamine but not glucose induces MYC-dependent apoptosis in human cells. J Cell Biol *178*, 93-105.

Zeng, X., Tamai, K., Doble, B., Li, S., Huang, H., Habas, R., Okamura, H., Woodgett, J., and He, X. (2005). A dual-kinase mechanism for Wnt co-receptor phosphorylation and activation. Nature *438*, 873-877.

Zhang, M., Xuan, S., Bouxsein, M.L., von Stechow, D., Akeno, N., Faugere, M.C., Malluche, H., Zhao, G., Rosen, C.J., Efstratiadis, A.*, et al.* (2002). Osteoblast-specific knockout of the insulin-like growth factor (IGF) receptor gene reveals an essential role of IGF signaling in bone matrix mineralization. J Biol Chem *277*, 44005-44012.

Zhang, Y., Marsboom, G., Toth, P.T., and Rehman, J. (2013). Mitochondrial respiration regulates adipogenic differentiation of human mesenchymal stem cells. PLoS One *8*, e77077.

Zhao, G., Monier-Faugere, M.C., Langub, M.C., Geng, Z., Nakayama, T., Pike, J.W., Chernausek, S.D., Rosen, C.J., Donahue, L.R., Malluche, H.H.*, et al.* (2000). Targeted overexpression of insulin-like growth factor I to osteoblasts of transgenic mice: increased

trabecular bone volume without increased osteoblast proliferation. Endocrinology *141*, 2674-2682.

Zhou, S., Greenberger, J.S., Epperly, M.W., Goff, J.P., Adler, C., Leboff, M.S., and Glowacki, J. (2008). Age-related intrinsic changes in human bone-marrow-derived mesenchymal stem cells and their differentiation to osteoblasts. Aging Cell *7*, 335-343.

Zoidis, E., Ghirlanda-Keller, C., and Schmid, C. (2011). Stimulation of glucose transport in osteoblastic cells by parathyroid hormone and insulin-like growth factor I. Mol Cell Biochem *348*, 33-42.

CHAPTER 2

WNT-LRP5 Signaling Induces Warburg Effect through mTORC2 Activation during Osteoblast Differentiation

---

This chapter includes the manuscript:
Esen, E., Chen, J., Karner, C. M., Okunade, A. L., Patterson, B. W., and Long, F. (2013) *Cell Metab* **17**, 745-755

1. Abstract

WNT signaling controls many biological processes including cell differentiation in metazoans. However, how WNT reprograms cell identity is not well understood. We have investigated the potential role of cellular metabolism in WNT-induced osteoblast differentiation. WNT3A induces aerobic glycolysis known as Warburg effect by increasing the level of key glycolytic enzymes. The metabolic regulation requires LRP5 but not β-catenin and is mediated by mTORC2-AKT signaling downstream of RAC1. Suppressing WNT3A-induced metabolic enzymes impairs osteoblast differentiation in vitro. Deletion of Lrp5 in the mouse, which decreases postnatal bone mass, reduces mTORC2 activity and glycolytic enzymes in bone cells and lowers serum lactate levels. Conversely, mice expressing a mutant Lrp5 that causes high bone mass exhibit increased glycolysis in bone. Thus, WNT-LRP5 signaling promotes bone formation in part through direct reprogramming of glucose metabolism. Moreover, regulation of cellular metabolism may represent a general mechanism contributing to the wide-ranging functions of WNT proteins.

2. Introduction

WNT signaling controls cell proliferation, fate decision, polarity, and migration throughout the evolution of metazoans (Croce and McClay, 2008). WNT proteins, by engaging various receptors and coreceptors at the cell membrane, activate an intracellular signaling network highly dependent on the cellular context, to induce diverse biological responses (van Amerongen and Nusse, 2009). WNT signaling through β-catenin has been most extensively studied. In this mechanism, binding of WNT to a Frizzled (Fz) receptor and a LRP5/6 coreceptor leads to stabilization of β-catenin, which subsequently translocates to the nucleus, where it interacts with members of the TCF/LEF transcription factors to activate transcription of downstream target genes (Clevers, 2006). In addition, WNT proteins can activate the Rho family of small GTPases (Habas et al., 2001, 2003; Wu et al., 2008), the Ca^{2+} pathway (Kühl et al., 2000), and PKCδ (Kinoshita et al., 2003; Tu et al., 2007). WNT has also been shown to activate mTORC1 (mammalian target of rapamycin complex 1), one of the two complexes formed by mTOR (Inoki et al., 2006). Whereas mTORC1 uniquely contains raptor and is the main target of rapamycin, mTORC2 contains rictor and is relatively insensitive to the drug (Laplante and Sabatini, 2012; Wullschleger et al., 2006). Among many other functions, mTORC1 is best known to control protein synthesis through phosphorylation of the translational regulators 4E-BP1 and S6K1, the latter of which in turn phosphorylates the ribosomal protein S6 and other substrates (Ma and Blenis, 2009). mTORC2 is known to activate Akt through phosphorylation at Ser473, which is necessary for its activity toward some but not all substrates (Guertin et al., 2006; Hresko and Mueckler, 2005; Jacinto et al., 2006; Sarbassov et al., 2005). Other targets of mTORC2 include PKCα, FOXO3, and SGK1 (García-Martínez and Alessi, 2008; Guertin et al., 2006). Earlier studies with siRNA have implicated mTORC2 signaling in regulating the actin

cytoskeleton (Jacinto et al., 2004; Sarbassov et al., 2004), but this function was not confirmed in embryonic fibroblasts derived from knockout mice (Guertin et al., 2006). On the other hand, mTORC2 has been shown to regulate whole-body glucose and lipid metabolism through its action in the liver and the adipose tissue (Cybulski et al., 2009; Hagiwara et al., 2012; Kumar et al., 2010; Lamming et al., 2012). Recent studies have shown that the small GTPase RAC1 localizes mTOR to specific membranes and mediates the activation of both mTORC1 and mTORC2 in response to growth factors (Saci et al., 2011). In addition, ribosomes activate mTORC2 through physical association (Zinzalla et al., 2011). Whether or not WNT signaling activates mTORC2 has not been explored.

WNT signaling has emerged as an important mechanism regulating bone formation in mammals (Long, 2012). In the mouse embryo, deletion of β-catenin, or both LRP5 and LRP6, in the skeletogenic progenitors abolishes osteoblast differentiation, indicating that WNT signaling through β-catenin is critical for embryonic osteoblastogenesis (Day et al., 2005; Hill et al., 2005; Hu et al., 2005; Joeng et al., 2011; Rodda and McMahon, 2006). Postnatally, loss- and gain-of-function mutations in LRP5 cause low and high bone mass syndromes, respectively, in humans (Boyden et al., 2002; Gong et al., 2001; Little et al., 2002). Moreover, deficiency in SOST, a secreted inhibitor that prevents the binding of WNT to LRP5 or LRP6, results in high bone mass in human patients (Balemans et al., 2001, 2002). In the mouse, deletion of LRP5 causes osteopenia (Cui et al., 2011; Kato et al., 2002), whereas loss of SOST increases bone mass (Li et al., 2008). The mechanism through which WNT signaling stimulates osteoblast differentiation, however, remains to be elucidated.

Emerging evidence has implicated WNT signaling in the regulation of cellular metabolism. A missense mutation in LRP6 has been linked with abnormal whole-body

metabolism in humans (Mani et al., 2007). Genomic polymorphism of TCF7L2, a transcriptional effector of WNT/β-catenin signaling, is associated with type II diabetes (Grant et al., 2006). In cell culture models, prolonged WNT treatment induced mitochondria biogenesis in a β-catenin-dependent manner (Yoon et al., 2010). In the mouse, hepatic manipulation of β-catenin was shown to regulate glucose and glutamine metabolism (Cadoret et al., 2002; Chafey et al., 2009; Liu et al., 2011). However, whether WNT regulates cellular metabolism via β-catenin-independent mechanisms has not been examined. Moreover, it is not known whether metabolic regulation by WNT contributes to cell differentiation.

Here we investigate the potential regulation of glucose metabolism by WNT during osteoblast differentiation. We report that multiple WNT proteins acutely stimulate aerobic glycolysis to control osteoblast differentiation. Distinct from the previous findings, the metabolic regulation described here is independent of β-catenin signaling but requires mTORC2 activation. Importantly, mouse genetic models demonstrate that WNT-LRP5 signaling concurrently increases glycolysis and bone formation in vivo. Thus, WNT signaling reprograms glucose metabolism through a direct mechanism, and WNT-induced metabolic reprogramming contributes to osteoblast differentiation.

3. Results

3.1. WNT Induces Aerobic Glycolysis Independent of β-Catenin

To investigate a potential link between WNT signaling, cellular metabolism, and osteoblast differentiation, we examined the effect of WNT proteins on glucose metabolism in ST2 cells, a mouse bone marrow stromal cell line known to undergo osteoblast differentiation in response to WNT (Tu et al., 2007). Because we were interested in direct regulation by WNT

instead of adaptive effects secondary to the differentiated state, we focused on the response within the first 24 hr of treatment. Purified WNT3A progressively increased glucose consumption over the control, reaching statistical significance at 6 hr and exhibiting a marked increase at 12 and 24 hr (Figure 1A). Importantly, during this time period, WNT3A did not increase the number of cells or alter the cell-cycle distribution (see Figures S1A and S1B). Compared to WNT3A, insulin at high concentrations (1 or 2 μg/ml) was less effective in stimulating glucose consumption in ST2 cells (Figure S1C). Moreover, WNT3A stimulated glucose consumption in the absence of serum even though overall glucose consumption was lower at both basal and stimulated conditions (Figure S1D). Consistent with the increased glucose consumption, glucose uptake, as assayed by fluorescently labeled 2-deoxyglucose, was enhanced following 1, 12, or 24 hr of WNT3A treatment (Figure 1B). Thus, WNT3A acutely induces glucose consumption in ST2 cells.

We then examined whether the regulation was limited to WNT3A and undifferentiated ST2 cells. WNT10B has been shown to induce osteoblast differentiation in ST2 cells (Kang et al., 2007). We found that virally expressed WNT10B increased glucose consumption to an extent comparable to that of purified WNT3A (Figure 1C). In contrast, recombinant WNT5A did not have a similar effect (Figure S1E). BMP2, a known inducer of osteoblast differentiation in ST2 cells, did not stimulate glucose consumption after 24 hr of treatment (Figure S1F). To determine the effect of WNT3A on differentiating ST2 cells, we stimulated them with an established osteogenic media containing dexamethasone, β-glycerophosphate, and ascorbate for up to 15 days and then assessed their response to WNT3A for 24 hr at each differentiation stage. WNT3A stimulated glucose consumption in ST2 cells at all stages (Figures S1G and S1H). We then tested the effect of WNT3A on other cell lines as well as primary cell cultures. We found

that WNT3A stimulated glucose consumption in C2C12 (myoblast), M2-10B4 (bone marrow stromal cell), MC3T3 (preosteoblast), MLO-Y4 cells (osteocyte), and 3T3-L1 cells (preadipocytes), as well as primary cultures of mouse embryonic fibroblasts (MEFs) and osteoblast-lineage cells from the mouse calvaria (Figures 1D–1G). Thus, multiple osteogenic WNT ligands increase glucose consumption, but all osteogenic signals do not exhibit the same regulation. Furthermore, WNT3A stimulates glucose consumption in a variety of cell types.

We next examined potential metabolic changes in ST2 cells. WNT3A markedly increased the concentration of lactate in the culture media at both 6 and 24 hr of treatment (Figure 2A). Similarly, WNT10B increased lactate levels at 24 hr (Figure 2B). WNT5A, on the other hand, did not affect lactate levels (Figure S1I), even though it induced phosphorylation of MARC.KS in ST2 cells (Figure S1J). We next measured extracellular acidification rate (ECAR) as an indicator for lactate production rate, and the oxygen consumption rate (OCR) with the Extracellular Flux Analyzer after 6 hr of WNT stimulation. WNT3A notably increased ECAR both at the basal state and during mitochondria stress tests with oligomycin or FCCP, but had no effect on the OCR under all conditions (Figures 2C and 2D). Similarly, after 24 hr, WNT3A increased ECAR but not OCR (Figure 2E). Moreover, WNT3A did not alter the intracellular ATP levels after 24 hr of treatment (Figure 2F). Thus, WNT signaling stimulated lactate production but not oxidative phosphorylation.

To demonstrate that WNT3A stimulates lactate production directly from glucose, we tracked the fate of glucose through isotopomer distribution analyses of stable isotopically labeled substrates through GC/MS. Briefly, cells were first stimulated with WNT3A for 6, 12, or 24 hr and then incubated with ^{13}C-labeled glucose ([U-$^{13}C_6$]-glucose, m+6 isotopomer tracer) for 1 hr, and its contribution to lactate through glycolysis was determined by measuring the abundance of

the labeled [U-$^{13}C_3$]-lactate (m+3 isotopomer) relative to the unlabeled (m+0) pool. After 6, 12, or 24 hr of stimulation, WNT3A markedly increased the relative abundance of m+3 lactate in the cell lysate, indicating a greater portion of lactate derived through glycolysis (Figures 2G–2I). Moreover, at all time points, the WNT3A-induced enrichment of labeled lactate was greater than that of the intracellular labeled glucose (m+6/m+0), indicating that a greater portion of the intracellular glucose underwent glycolysis in response to WNT3A (Figures 2G–2I). Thus, WNT signaling stimulates glycolysis despite the abundance of oxygen, a phenomenon known as the Warburg effect.

We next examined the molecular basis for the increased glycolysis. GLUT1, a main glucose transporter, and hexokinase II (HK2) that catalyzes the first rate-limiting step of glucose catabolism were both induced by WNT3A at 1 hr and remained high at 6, 12, and 24 hr of treatment (Figure 3A and data not shown). Phosphofructokinase 1 (PFK1), a key regulatory enzyme for the "committed step" of glycolysis, and 6-phosphofructo-2-kinase/fructose-2, 6-bisphosphatase 3 (PFKFB3), which controls the concentration of fructose 2,6-bisphosphate, a potent allosteric activator of PFK1, were both induced by WNT3A, although PFKFB3 returned to control levels by 24 hr of treatment (Figure 3A). Finally, lactate dehydrogenase A (LDHA), which catalyzes the conversion of pyruvate to lactate, and pyruvate dehydrogenase kinase 1 (PDK1) that inactivates the pyruvate dehydrogenase complex to suppress pyruvate from entering the TCA cycle were both induced by 6 hr of WNT3A stimulation and remained high at the later time points (Figure 3A). Quantification of western blots from multiple independent experiments confirmed that the glycolytic regulators were consistently induced by WNT3A after 1, 6, and 24 hr of treatment (Figures S2A–S2C). Interestingly, when ST2 cells were first starved for serum, WNT3A induced not only HK2 but also LDHA and PDK1 after 1 hr of stimulation (Figure 3B).

Further experiments revealed that these enzymes were in fact upregulated by WNT3A within 5 min of stimulation in the serum-starved cells (Figure S2D). The quick induction of the enzymes is not likely to be due to transcriptional regulation, as their mRNA levels stayed relatively unchanged even after 6 hr of WNT3A treatment (Figure S2E). After 24 hr, only Ldha and Pdk1 mRNA but not the others were increased over the control (Figure S2F). Knockdown of either LDHA or PDK1 partially suppressed WNT3A-induced glucose consumption (Figures 3C and 3D). Thus, WNT3A acutely increases the protein levels of a number of key glycolytic regulators to stimulate glycolysis.

We next investigated the signal transduction mechanism through which WNT3A induces glycolysis. Because WNT3A inhibits GSK3β activity, we first investigated the potential importance of GSK3β inhibition. Inhibition of GSK3β activity by either genetic knockdown or LiCl did not increase glucose consumption by itself, nor did it affect WNT3A-induced glucose consumption (Figure 3E and data not shown), even though it increased β-catenin levels as expected (Figure 3F, and data not shown). Similarly, knockdown of β-catenin did not alter WNT3A-induced glucose consumption, although it suppressed the induction of IRS1, known to be induced transcriptionally by β-catenin (Yoon et al., 2010) (Figures 3G and 3H). Knockdown of β-catenin with a second shRNA also did not suppress WNT3A-induced glucose consumption (Figure S3A). Finally, stabilization of AXIN1/2 with the tankyrase inhibitor XAV939 inhibited β-catenin stabilization by WNT3A but did not impair the induction of glucose consumption (Huang et al., 2009) (Figures 3I and 3J). Thus, regulation of AXIN, GSK3, or β-catenin is not the principle mechanism for WNT3A to induce glycolysis.

3.2. WNT-LRP5 Signaling Activates mTORC2 via RAC1 to Induce Glycolysis

We next investigated the potential role of mTOR signaling in WNT-induced glycolysis. WNT3A acutely activated mTORC1, as indicated by increased phosphorylation of the ribosomal protein S6, which was evident at 1 hr of stimulation and maintained after 24 hr (Figure 4A). In addition, WNT3A activated mTORC2, as Ser473-phosphorylation of AKT was elevated at these time points (Figure 4A). Quantification of western blots from multiple independent experiments confirmed these findings (Figures S2A–S2C). We further explored the temporal regulation of mTOR signaling under serum-starved conditions. We found that WNT3A activated both mTOR complexes in serum-starved ST2 cells within 5 min of stimulation and throughout 24 hr of treatment (Figures 4B and 4C). In contrast, WNT5A, which did not induce glycolysis, did not stimulate mTORC2 (Figure S1J). Confirming the activation of mTORC2 signaling by WNT3A, phosphorylation of PKCα at S657, FOXO3A at T32, and NDRG1 at T346, all previously shown to require mTORC2 activity (García-Martínez and Alessi, 2008; Guertin et al., 2006), were also induced (Figures 4B and 4D). Furthermore, as in ST2 cells, WNT3A activated mTORC2 and induced the glycolytic enzymes in MEFs and primary osteoblast-lineage cells from the mouse calvaria (Figure 4E). Knockdown of RICTOR, an mTORC2-specific component, greatly reduced both basal and induced mTORC2 signaling, but not mTORC1 (Figure 5A and Figure S4A). RICTOR knockdown also abolished the upregulation of HK2 and LDHA by WNT3A, as well as WNT3A-induced glucose consumption, lactate production, and media acidification (Figures 5B–5D and Figure S4B). The effects of RICTOR knockdown on WNT3A-induced mTOR signaling, glycolytic enzymes, and glucose consumption were all confirmed with a second shRNA (Figures S4C–S4E). Similarly, PP242 and Torin 1, inhibitors of both mTORC1 and mTORC2, greatly suppressed WNT3A-induced glucose consumption (Figures S4F and S4G). MK-2206, an

allosteric AKT inhibitor preventing S473 phosphorylation, completely abolished WNT3A-induced glucose consumption as well as LDHA and PDK1 upregulation (Figures 5E and 5F). Use of a lower concentration (0.1 μM) of MK2206 suppressed WNT3A-induced glucose consumption to a lesser degree, but an even lower concentration (0.01 μM) did not have an effect (Figure S4H). MK-2206 at the effective dosages did not affect cell numbers (Figure S4I). In contrast to RICTOR, knockdown of RAPTOR, an mTORC1-specific component, suppressed mTORC1, but not mTORC2 activation or the induction of PDK1, LDHA, and HK2 by WNT3A (Figures 5G and 5H and Figure S4J). Interestingly, RAPTOR knockdown activated basal mTORC2 and increased the basal levels of the glycolytic enzymes without WNT stimulation (Figures 5G and 5H), which was likely responsible for the increased basal glucose consumption (Figure 5I). Nonetheless, RAPTOR knockdown did not prevent further stimulation of glucose consumption or lactate production by WNT3A (Figures 5I and 5J). Conversely, activation of mTORC1 by knockdown of TSC2 did not increase glucose consumption by itself, nor did it affect WNT3A-induced glucose consumption (Figure 5K, data not shown). Thus, WNT3A stimulates glycolysis predominantly through mTORC2 activation.

How does WNT signaling activate mTORC2? DKK1, which prevents WNT from binding to LRP5 or LRP6, abolished LRP6 phosphorylation, mTORC2, but not mTORC1 activation by WNT3A at 1 hr (Figure 6A). Moreover, DKK1 abrogated the induction of β-catenin, HK2, LDHA, GLUT1, and PDK1 after 24 hr of WNT3A treatment (Figure 6B). Importantly, DKK1 abolished the increase in glucose consumption in response to WNT3A (Figure 6C). To distinguish the relative contribution of LRP5 versus LRP6 in this regulation, we performed knockdown experiments. Remarkably, knockdown of LRP5 alone essentially recapitulated the effect of either DKK1, or double knockdown of LRP5 and LRP6, in abolishing WNT3A-induced

glucose consumption, whereas knockdown of LRP6 had a relatively minor effect (Figures 6D and 6E). The differential effect of LRP5 versus LRP6 knockdown was confirmed with a second shRNA for each molecule (Figures S3A and S3B). We further examined potential compensation between LRP5 and LRP6 when either molecule was knocked down. Interestingly, LRP6 knockdown doubled Lrp5 mRNA but did not increase its protein level, whereas LRP5 knockdown did not affect either mRNA or protein of LRP6 (data not shown). Confirming the importance of mTORC2, knockdown of LRP5 but not LRP6 suppressed mTORC2 activation, even though either knockdown similarly suppressed the accumulation of the stabilized form of β-catenin in response to WNT3A (Figure 6F). Moreover, knockdown of LRP5 but not LRP6 eliminated the induction of HK2 by WNT3A (Figure 6F). Thus, LRP5 appears to be the principle mediator for WNT3A to stimulate glycolysis.

We next investigated how WNT-LRP5 signaling activates mTORC2. Because we have previously shown that WNT-LRP5/6 signaling activates the Rho family small GTPase RAC1 (Wu et al., 2008), and others have reported that RAC1 mediates both mTORC1 and mTORC2 activation (Saci et al., 2011), we examined the relevance of RAC1 in WNT3A-induced mTORC2 signaling. Knockdown of RAC1 suppressed the induction of P-AKT, P-FOXO3A, and LDHA by WNT3A (Figure 6G and Figure S5A), as well as WNT3A-induced glucose consumption (Figure 6H). A second shRNA against RAC1 confirmed its role in mTORC2 activation and glycolysis stimulation by WNT3A (Figures S5B–S5D). Because the previous study demonstrated that RAC1 membrane translocation, but not its GFP-bound form, mediates mTOR activation (Saci et al., 2011), we examined the effect of WNT on RAC1 subcellular localization by confocal microscopy. Indeed, WNT3A induced accumulation of RAC1 at the plasma membrane (Figure 6I). Specifically, out of 85 cells counted, 23 in the control but 61 in the

WNT3A-treated sample showed membrane localization of RAC1. Similarly, virally expressed WNT10B also induced RAC1 accumulation at the plasma membrane (Figure S5E). Thus, WNT activates mTORC2 through LRP5 and RAC1 to stimulate glycolysis.

3.3. Metabolic Regulation Contributes to WNT-Induced Osteoblast Differentiation

We then tested whether the metabolic regulation plays a role in WNT-induced osteoblast differentiation in ST2 cells. Because WNT induced glucose consumption, we hypothesized that glucose concentrations may impact osteoblast differentiation. Indeed, reducing glucose concentration from the normal 5 mM to 1 mM greatly impaired osteoblast differentiation in response to WNT3A, as indicated by the decreased expression of Alpl and Ibsp (Figure 7A), even though β-catenin was similarly stabilized by WNT3A under both conditions (Figure 7B). The lower glucose concentration did not affect cell numbers but markedly reduced the extent of induction in glucose consumption by WNT3A (Figure 7C and Figure S6A). The cells also produced much less lactate with or without WNT3A (Figure S6B). The inhibitory effect of low glucose was specific to WNT3A, as BMP2 induced osteoblast differentiation similarly with either 5 mM or 1 mM glucose (Figure S6C). Next, we tested the role of mTORC2 in WNT3A-induced osteoblast differentiation. RICTOR knockdown suppressed osteoblast differentiation (Figure 7D). Similarly, Torin 1, which inhibits both mTORC1 and mTORC2, greatly diminished the expression of Alpl and Ibsp in response to WNT3A (Figure S6D). Finally, we examined the roles of glycolytic enzymes. Knockdown of either LDHA or PDK1, both normally induced by WNT3A, greatly reduced the induction of osteoblast marker genes Col1a1 and Ibsp by WNT3A (Figure 7E). In addition, either knockdown suppressed the level of Alpl expression in response to WNT3A, whereas PDK1 knockdown also reduced the basal level (Figure S6E). In contrast,

neither knockdown impaired osteoblast differentiation in response to BMP2 (Figure S6F and data not shown). Thus, reprogramming of glucose metabolism specifically contributes to WNT-induced osteoblast differentiation.

3.4. WNT-LRP5 Signaling Increases Glycolysis *in vivo*

Lastly, we tested whether WNT-LRP5 signaling reprograms glucose metabolism in vivo. We first examined the Lrp5−/− mice that are known to be defective in bone formation (Holmen et al., 2004; Kato et al., 2002). These mutants at 6 weeks of age contained a much lower level of HK2, LDHA, and PDK1 in their bones when compared to the littermate controls (Figure 7F). Moreover, the serum lactate levels in 1-month-old Lrp5−/− mice were significantly lower than those in their littermate controls (Figure 7G). To rule out the possibility that the metabolic changes in bone were secondary to the effects on other tissues, we generated Osx-Cre;Lrp5f/f mice (CKO) containing bone-specific deletion of Lrp5. We found a notable decrease in the levels of HK2, PDK1, and LDHA in the bones of CKO mice at 10 weeks of age, coupled with reduced mTORC2 activity (Figure 7H). Analyses with μCT techniques revealed obvious osteopenia in the CKO mice when compared to the littermate control (Figure 7I and Figures S7A and S7B). Consistent with reduced bone formation, the serum P1NP (procollagen type I N-terminal propeptide) level was lower in the CKO mice than in the control (Figure 7J). To further establish the link between LRP5 and metabolic regulation in bone, we studied the high-bone-mass (HBM) mice harboring the point mutation of A214V in LRP5 (Cui et al., 2011). We confirmed by μCT analyses that mice either heterozygous or homozygous for the mutant allele exhibited markedly higher bone mass at 2 months of age (data not shown). Importantly, bones from the HBM mice expressed higher levels of HK2, PDK1, and LDHA (Figure 7K). The bone marrow stromal cells

isolated from the HBM mice consumed more glucose than their control counterparts when cultured in vitro, and the increase in glucose consumption was suppressed by the mTOR inhibitor Torin 1 (Figures 7L and 7M). Thus, LRP5 signaling modulates glucose metabolism in bone cells in the mouse.

4. Discussion

We have provided evidence that WNT signaling directly regulates glucose metabolism independent of β-catenin signaling. Specifically, WNT3A signals through LRP5 and RAC1 to activate mTORC2 and AKT, resulting in upregulation of key glycolytic enzymes. Functionally, the metabolic regulation contributes to WNT-induced osteoblast differentiation in vitro and correlates with the bone-forming activity of LRP5 signaling in vivo. This study not only uncovers a mechanism through which WNT signaling regulates cellular metabolism but also demonstrates that metabolic regulation contributes to WNT-induced cell differentiation.

The present study further expands the repertoire of signaling cascades activated by WNT3A. In addition to β-catenin stabilization, we have previously shown that WNT3A signals through heterotrimeric G proteins to activate both PLCβ-PKCδ and PI3K-RAC1 signaling in ST2 cells (Tu et al., 2007; Wu et al., 2008). Here we show that WNT3A activates mTORC2 downstream of RAC1. Activation of the different pathways by WNT3A may require distinct cell-surface receptor complexes, as β-catenin stabilization and RAC1 activation are inhibited by DKK1, but PKCδ activation is not. Taken together, these studies support the notion that WNT proteins activate multiple intracellular signaling cascades highly dependent on the cellular context, and do not possess intrinsic “canonical” or “noncanonical” signaling properties (van Amerongen et al., 2008).

The mechanism through which mTORC2 induces glycolytic enzymes remains to be further elucidated. The fact that the induction occurs abruptly following WNT3A treatment with no change in mRNA levels indicates a transcription-independent mechanism at work. We show that AKT, a direct target of mTORC2, is critical for the induction of glycolytic enzymes and glycolysis in response to WNT3A. Future studies are necessary to determine whether and how mTORC2-AKT signaling affects protein stability or translation of the glycolytic enzymes.

Our data identify LRP5 as a major coreceptor for WNT3A to induce glycolysis. Although RNA-seq experiments revealed that ST2 cells expressed three times as much Lrp6 mRNA as Lrp5 (data not shown), knockdown of LRP6 did not have a major effect on WNT3A-induced glucose consumption. In light of the finding that LRP6 has a more potent function in mediating β-catenin signaling (MacDonald et al., 2011), the two homologous coreceptors may have evolved to preferentially execute different WNT signaling cascades. However, because we have analyzed glucose metabolism only within the first 24 hr of WNT3A treatment, LRP6 may regulate cell metabolism at later time points through β-catenin signaling. Indeed, we found that both Ldha and Pdk1 mRNA were induced by WNT3A at 24 hr (Figure S2F), and that knockdown of β-catenin partially suppressed the induction of LDHA and PDK1 proteins at this time point (data not shown). Furthermore, induction of IRS1 by β-catenin signaling may contribute to glucose metabolism in response to insulin (Yoon et al., 2010) (this study). Thus, WNT signaling may control glucose metabolism both through the fast-acting, β-catenin-independent mechanism described here and other slow-acting, β-catenin-dependent mechanisms, which may be preferentially mediated by LRP5 and LRP6, respectively. This conclusion is in agreement with the previous reports that implicated LRP5, LRP6, and β-catenin in the regulation of whole-body metabolism (Fujino et al., 2003; Liu et al., 2011; Mani et al., 2007).

The finding that LRP5 mediates WNT-induced metabolic reprogramming may have important implications for understanding the pathogenesis of bone disorders caused by LRP5 mutations. Although the role of LRP5 in regulating both osteoblast number and function in postnatal mice is well established, the mechanism underlying LRP5 function has been a matter of debate (Cui et al., 2011; Yadav et al., 2008). We have recently reported that β-catenin is necessary for normal osteoblast life span and activity in postnatal mice, lending support to the notion that β-catenin may mediate some aspects of LRP5 signaling in postnatal bones (Chen and Long, 2012). The current study provides an additional mechanism through which LRP5 may regulate osteoblast differentiation and function independent of β-catenin. Future studies are necessary to determine the relative contributions of the different mechanisms to LRP5 function in vivo.

Beyond cells of the osteoblast lineage, WNT signaling may be a general paracrine mechanism that modulates cellular metabolism in the body. Besides cell differentiation, changes in cellular metabolism are likely to influence other aspects of cell physiology, as well as whole-body metabolism. Furthermore, because insulin is an endocrine signal that controls glucose metabolism, we expect that WNT may intersect with insulin signaling to coordinate cellular metabolism. Indeed, a recent report has shown physical interaction between LRP5 and insulin receptor and interdependence between WNT and insulin signaling (Palsgaard et al., 2012). We observed greater potency for WNT3A than insulin in inducing glucose consumption in ST2 cells, and that WNT3A exerted a similar effect in the absence of serum (hence no insulin). Thus, WNT can operate independent of insulin signaling in our setting. Future studies are necessary to elucidate the interaction between WNT and insulin signaling in regulating glucose metabolism.

"Warburg effect" originally describes the phenomenon whereby cancer cells often utilize

glucose through glycolysis over oxidative phosphorylation despite the abundance of oxygen (Warburg, 1956). The phenomenon is now known to be common to proliferating cells in culture. The reason for Warburg effect continues to be an area of active research, but it has been proposed that glycolysis produces the necessary intermediate metabolites for fueling cell proliferation (Vander Heiden et al., 2009). In our experiments, WNT induced cell differentiation without an obvious effect on proliferation. How increased glycolysis promotes differentiation remains to be investigated in the future, but it may alter the levels of key intermediate metabolites that regulate gene expression. Overall, our study has identified metabolic regulation as a new mechanism for WNT proteins to induce cell differentiation.

5. Experimental Procedures

5.1. Mouse Strains

Osx-Cre, Lrp5f/f, Lrp5−/−, Lrp5HBM mice are as previously described (Cui et al., 2011; Holmen et al., 2004; Joeng et al., 2011; Rodda and McMahon, 2006). The Animal Studies Committee at Washington University has reviewed and approved all mouse procedures used in this study.

5.2. Antibodies

Antibodies for p-Lrp6 (cat#2568), p-Akt(S473) (cat#9271), Akt (cat#9272), p-S6 (cat#2215), S6 (cat#2217), Raptor (cat#2280), Rictor (cat#2140), Lrp5 (cat#5731), β-actin (cat#4970), FoxO3a (cat#2497S), p-FoxO3a-T32 (cat#9464S), p-NDRG1-Thr346 (cat#3217S), and P-S6K (cat#9205) are from Cell Signaling Technologies. Hk2 (sc-6521), Ldha (sc-27230), Pfk1 (sc-31712), Lrp6 (sc-25317), α-tubulin (sc-8035), and p-PKCα-Ser 657 (sc-12356) total

PKCα (sc-208) antibodies are from Santa Cruz Biotechnology. Pfkfp3 (ab96699) antibody is from Abcam. Antibody for unphosphorylated β-catenin (05-665) is from Millipore. Pdk1 (KAP-pk112) antibody is from Assay Designs. RAC1 antibody (610650) is from BD Biosciences. Glut1 polyclonal antibody F350 is as previously described and was kindly provided by Dr. Michael Mueckler (Washington University School of Medicine) (Haney et al., 1991). HRP-conjugated anti-rabbit secondary antibody is from GE Healthcare (NA934V), and HRP-conjugated anti-mouse (sc-2005) and anti-goat (sc-2352) secondary antibodies are from Santa Cruz Biotechnology.

5.3. Western Blot

Protein extracts from cells or bone were prepared in RIPA buffer containing phosphatase and proteinase inhibitors. Membranes were imaged with Molecular Imager ChemiDoc XRS+ System (Bio-Rad). Quantification of western blots was performed with ImageLab software or Photoshop CS3. Detailed procedure is provided in the Supplemental Experimental Procedures.

5.4. Quantitative PCR

RNA was isolated from whole cells with QIAGEN RNeasy kit (#74104) and was transcribed into cDNA using iScript cDNA synthesis kit (Bio-Rad). Fast-start SYBR Green (Bio-rad) and 0.05 μM primers were used in each reaction. 18S RNA was used for normalization. The primer sequences and additional information are provided in the Supplemental Experimental Procedures.

5.5. Cell Culture

For routine cultures, ST2 cells were grown in α-MEM (GIBCO, cat#12561), MC3T3 subclone 4 cells were grown in α-MEM (GIBCO catalog number A1049001), HEK293T and 3T3-L1 cells were grown in DMEM (GIBCO catalog number 11965), and M2-10B4 cells (ATCC CRL-1972) were grown in RPMI (GIBCO, catalog number 11875), all supplemented with 10% heat-inactivated FBS (GIBCO) and Pen Strep (GIBCO, catalog number 14140). MLO-Y4 cells were grown on pre-collagen-coated plates in α-MEM containing nucleosides (GIBCO, catalog number 12571-063) supplemented with heat-inactivated FBS (2.5%), calf serum (2.5%), and Pen Strep.

For all experiments, unless indicated otherwise, cells were cultured in glucose- and glutamine-free α-MEM (GIBCO, custom made from catalog number 12561) containing 10% FBS and Pen Strep, and freshly supplemented with 5.5 mM glucose plus 2 mM glutamine. Recombinant mouse Wnt3a (R&D Systems) was used at 50 ng/ml unless indicated otherwise. As a vehicle control for Wnt3a, PBS with 0.5% CHAPS and 0.1 mM EDTA was used. Recombinant human BMP2 (R&D Systems) was used at 300 ng/ml. Recombinant mouse Dkk1 (R&D Systems) was used at 500 ng/ml, and cells were pretreated with Dkk1 for 30 min before the addition of Wnt3a. Torin1 (Tocris Biosciences), PP242 (Sigma), and rapamycin (Sigma), all dissolved in DMSO, were used at 20, 10, and 100 nM, respectively. Insulin (Sigma) was used at 1 or 2 μg/ml.

Bone marrow stromal cells (BMSCs), calvarial cells, and MEFs were isolated from mouse adult long bones, newborn calvaria, and E13.5 embryos, respectively, according to established protocols.

5.6. Glucose Consumption and Uptake Assays, Lactate and ATP Measurements

For glucose consumption measurements, aliquots of the media and glucose standards were assayed with Glucose (HK) Assay Kit (Sigma catalog number GAHK20) and read at 340 OD using a plate reader (BioTek model SAMLFTA, Gen5 software). For glucose uptake assays, cells were incubated with 100 μM 2-NBDG for 30 min and then prepared for fluorescence reading following the manufacturer's instructions (Glucose Uptake Cell-Based Assay Kit, Cayman Chemical). Fluorescence intensity measured at 485/535 nm (excitation/emission) using a plate reader (BioTek model SAMLFTA, Gen5 software) was normalized to the protein content in each well. For lactate measurements, L-lactate assay kit from Eton biosciences (catalog number 1200011002) was used. To measure lactate levels in the serum, mice were fasted for 8 hr before blood was collected from the periorbital venous sinus under anesthesia. Intracellular ATP was measured based on a method previously described (Chi et al., 2002).

5.7. OCR and ECAR Measurements with Seahorse Cellular Flux Assays

ST2 cells were plated in XF96 plates at 20,000 cells per well after coating the plates with cell-tak (BD Biosciences). The next day, the cells were treated with 100 ng/ml Wnt3a for 6 hr, then switched to XF Assay Medium Modified DMEM (Seahorse cat#101022-100) supplemented with 5.5 mM glucose, and further incubated in CO_2-free incubator for 1 hr. Oligomycin and FCCP (Seahorse Stress Kit) were prepared in XF assay medium with final concentration of 5 μM and 1 μM, respectively, and were injected during the measurements. At the end of the assays, protein concentrations were measured for normalization.

5.8. shRNA Knockdown and Retroviral Infection

Lentiviral shRNA targeting vectors were purchased from Genome Center at Washington University. Targeted sequences and virus production procedure are provided in the Supplemental Experimental Procedures. Retroviruses expressing WNT10B or GFP were generated according to a procedure as previously described (Hu et al., 2005).

5.9. Analyses of Postnatal Mouse Bones

Micro-CT analyses were performed with Scanco μCT 40 (Scanco Medical AG) according to ASBMR guidelines (Bouxsein et al., 2010). Quantification of the trabecular bone in the proximal tibia was performed with 100 μCT slices (1.6 mm total) immediately below the growth plate. To measure P1NP in the serum, serum was collected from mice after 6 hr of fasting and analyzed with Rat/Mouse P1NP EIA kit (Immunodiagnostic Systems, Ltd., catalog number DS-AC33F1).

Bone protein extracts were prepared from femurs and tibias of postnatal mice with RIPA buffer. After removal of both epiphyses of each bone, bone marrow cells were removed by brief centrifugation. The remaining bone shafts were rinsed twice in the cold PBS, flash frozen in liquid nitrogen, and then manually ground into a fine power with a mortar/pestle. The bone power was incubated on ice for 30 min, with 200 μl RIPA buffer containing phosphatase inhibitors (Roche, catalog number 04906845001) and proteinase inhibitors (Roche, catalog number 11 836 170 001). The protein extracts were then collected after centrifugation for 10 min.

5.10. GC/MS Analyses

At the end of the Wnt3a treatment, [U-^{13}C6] glucose was added to the medium at a final

concentration of 0.55 mM and incubated for 1 hr. At the end of the [U-13C6] incubation, an aliquot of medium from each sample was collected for analyses. The cells were then washed with cold PBS and extracted three times with −80 C methanol on dry ice. Extracts were dried in a centrifugal concentrator (Savant SpeedVac, Thermo Scientific, Millford, MA) and derivatized at 70°C for 30 min with either 1:1 acetonitrile:N-methyl-N(tert-butyldimethylsilyl)trifluoroacetamide (MTBSTFA, to make tert-butyldimethylsilyl derivatives [tBDMS] of lactate) or 10% heptafluorobutyric anhydride in ethyl acetate (to make heptafluorobutyryl derivative [HFB] of glucose).

GC-MS/EI analyses were performed with Hewlett-Packard 6890 series gas chromatograph interfaced to an Agilent 5973N mass spectrometer. Helium was the carrier gas at constant flow rate of 1.0 mL/min. The injector and the transfer line temperatures were set at 250°C and 280°C, respectively. GC analysis was performed with a DB-5MS column (30 m × 0.25 mm × 0.25 mm; Agilent). The initial temp of the oven was 90°C held for 0 min and then ramped at 20°C per min to 230°C, and next ramped at 70°C per min to 275°C held for 3.5 min for a total run of 11 min. Sample (2.0 μl) in heptane was injected with a 7683 autosampler (split mode; split ratio of 5:1). The electron energy was set at 70 eV and the ion source temperature kept at 230°C.

Isotopomer distributions were measured by electron impact ionization for tBDMS derivative of lactate (m/z 261–264) and for the HFB derivative of glucose (m/z 519–525). All isotopomer distributions were corrected for natural abundance and for spectral overlap (Wolfe and Chinkes, 2004).

5.11. Statistical Analyses

All quantitative data are presented as mean ± STDEV with a minimum of three independent samples. Statistical significance is determined by Student's t test.

6. Figures

Figure 1. WNT Stimulates Glucose Consumption in Cell Culture

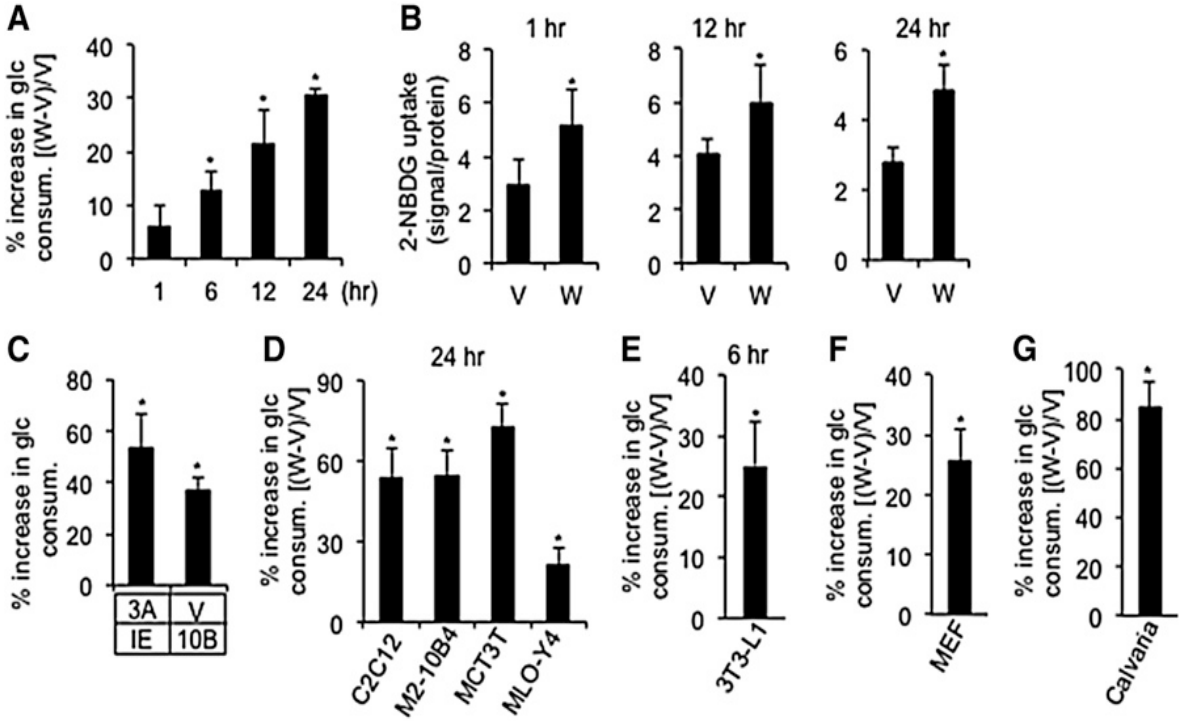

(A) Increase in glucose consumption by ST2 cells treated with WNT3A (W) over vehicle (V) for indicated times.

(B) Glucose uptake assay following WNT3A (W) or vehicle (V) treatment for indicated times.

(C) Induced glucose consumption after 24 hr by purified WNT3A (3A) or virally expressed WNT10B (10B). Increases as percent over control cells incubated with vehicle (V) and a GFP-producing virus (IE).

(D–G) Induced glucose consumption by WNT3A in indicated cell lines, MEFs, and mouse calvarial cells. Increases as percent over vehicle-treated cells. Asterisk denotes significant difference over respective controls, $n = 3$, $p < 0.05$. Error bars, SD.

Figure 2. WNT3A Stimulates Aerobic Glycolysis in ST2 Cells

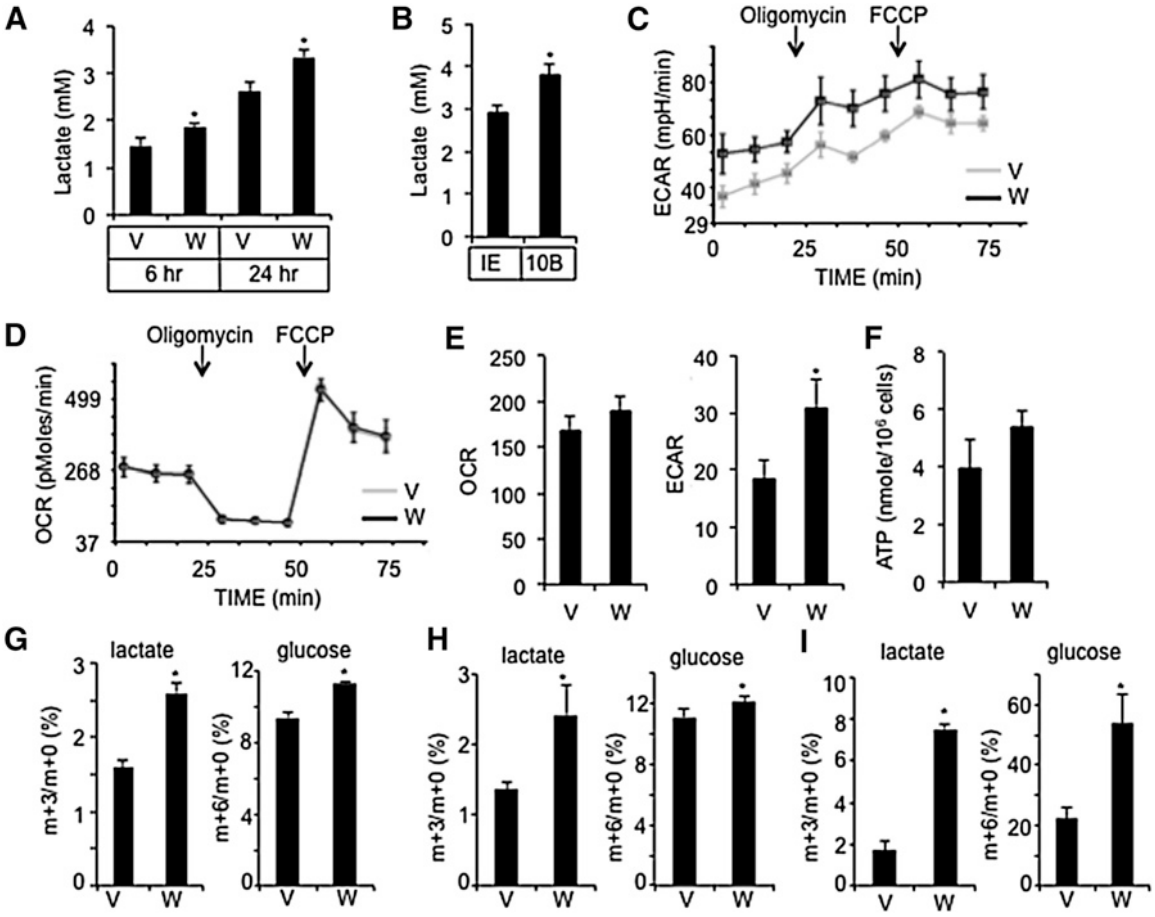

(A) Media lactate levels following vehicle (V) or WNT3A (W) treatments.

(B) Media lactate levels following viral expression of GFP (IE) or WNT10B for 24 hr.

(C and D) Extracellular acidification rate (ECAR) (C) and oxygen consumption rate (OCR) (D) after 6 hr of WNT3A (W) or vehicle (V) treatment.

(E) Measurements of ECAR and OCR after 24 hr of treatment.

(F) Intracellular ATP levels after 24 hr of treatment.

(G–I) Isotopomer enrichment of [U-13C3]-lactate and [U-13C6]-glucose in cell lysates after 6 (G), 12 (H), or 24 (I) hr of WNT3A (W) or vehicle (V) treatment. Asterisk, $n = 3$, $p < 0.05$. Error bars, SD.

Figure 3. WNT3A Induces Glycolysis Independent of GSK3b and β-Catenin

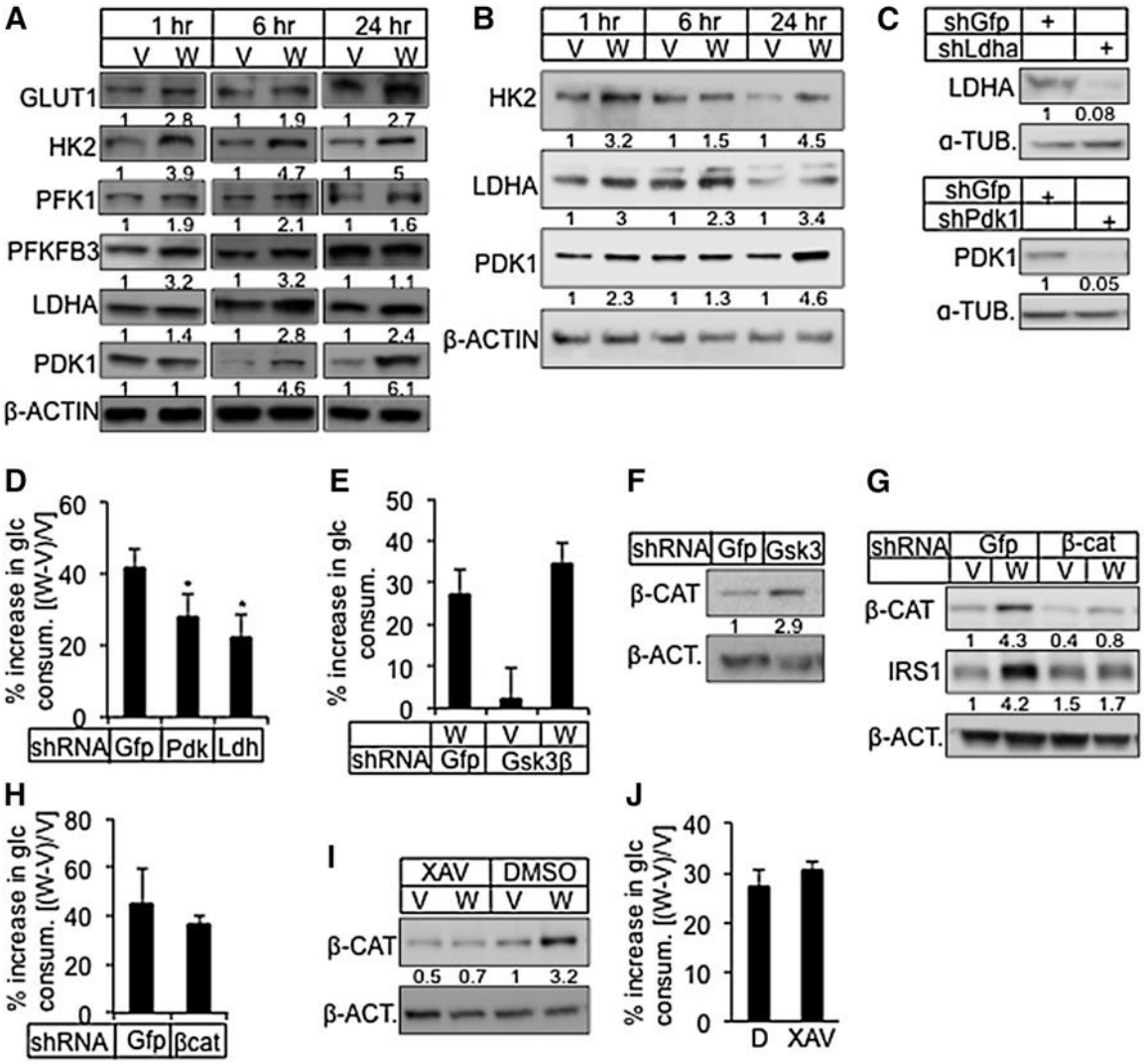

Figure 3. WNT3A Induces Glycolysis Independent of GSK3b and β-Catenin

(A and B) Representative western blots of glycolytic regulators in ST2 cells treated with WNT3A or vehicle in the presence (A) or absence of serum (B) for indicated times. Cells in (B) starved for serum for 12 hr before treatment. Protein abundance normalized to b-actin.

(C) Knockdown of LDHA or PDK1. shGfp as negative control. Protein abundance normalized to a-tubulin.

(D) Effect of LDHA or PDK1 knockdown on WNT3A-induced glucose consumption.

(E) Effect of GSK3b knockdown on WNT3Ainduced glucose consumption. Increase in glucose consumption as percent over cells treated with shGfp and vehicle.

(F) Effect of GSK3b knockdown on b-catenin.

(G) Knockdown of β-catenin and its effect on IRS1.

(H) Effect of β-catenin knockdown on WNT3Ainduced glucose consumption.

(I and J) Effect of XAV-939 on b-catenin (I) and WNT3A-induced glucose consumption (J). All glucose consumption measured after 24 hr of WNT3A or vehicle treatment. D, DMSO; W, WNT3A; V, vehicle. Asterisk, $n = 3$, $p < 0.05$. Error bars, SD.

Figure 4. WNT3A Activates mTORC2

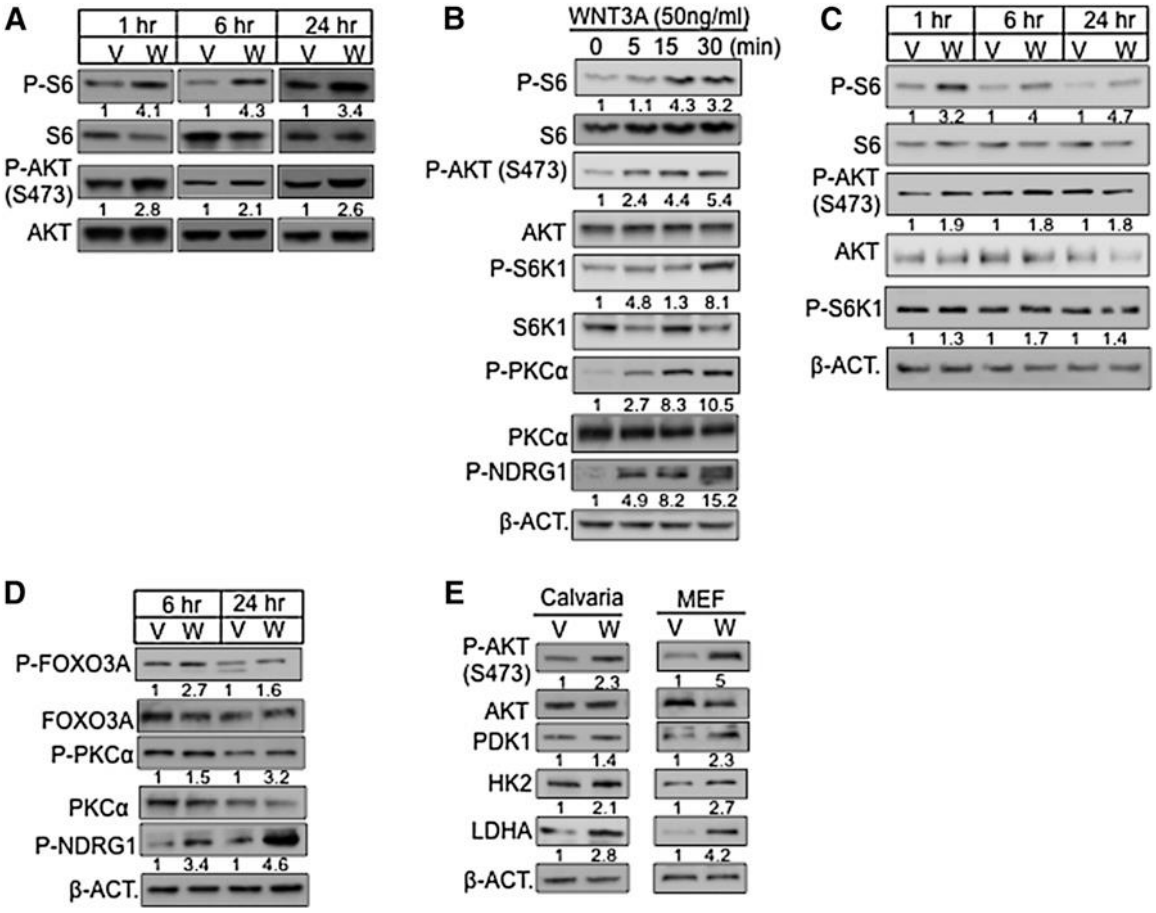

Figure 4. WNT3A Activates mTORC2

(A–D) Representative western blots of mTOR targets in ST2 cells treated with WNT3A (W) or vehicle (V) with (A) or without serum (B–D) for indicated time. Cells in (B)–(D) were serum starved for 24 (B) or 12 (C and D) hr before treatment. ‘‘0 min’’ samples in (B) were treated with vehicle for 30 min.

Phosphoprotein was normalized to respective total protein, except for P-NDRG1 and P-S6K1 in (C), which were normalized to b-actin. (E) Effect of WNT3A on mouse calvarial cells or MEFs. Calvarial cells treated with WNT3A or vehicle for 1 hr after 12 hr serum starvation. MEFs treated with WNT3A or vehicle for 6 hr in the presence of serum.

Figure 5. WNT3A Induces Glucose Consumption via mTORC2 Activation

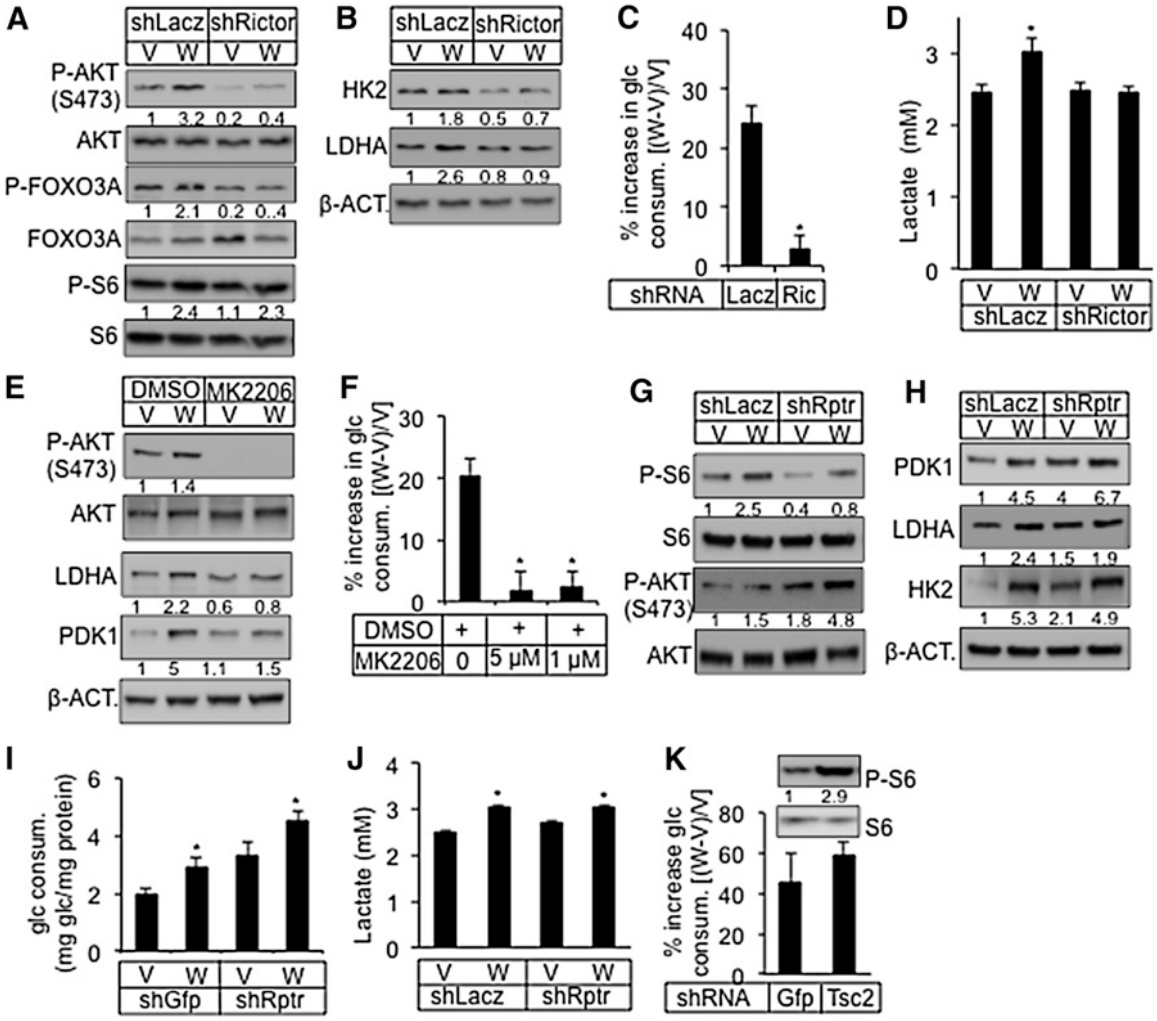

Figure 5. WNT3A Induces Glucose Consumption via mTORC2 Activation

(A–D) Effect of RICTOR knockdown (shRictor) on mTORC1 versus mTORC2 (A), glycolytic enzymes (B), glucose consumption (C), and lactate production

(D) after 24 hr of WNT3A (W) or vehicle (V) treatment.

(E and F) Effect of AKT inhibitor MK2206 on glycolytic enzymes (E) and glucose consumption (F) after 24 hr of WNT3A (W) or vehicle (V) treatment.

(G–J) Effect of RAPTOR knockdown (ShRptr) on mTORC1 versus mTORC2 (G), glycolytic enzymes (H), glucose consumption (I), and lactate production (J) after 24 hr of WNT3A (W) or vehicle (V) treatment.

(K) Effect of TSC2 knockdown (shTSC2) on mTORC1 and glucose consumption after 24 hr of treatment. shGFP or shLacz as negative control.

Asterisk, $n = 3$, $p < 0.05$. Error bars, SD

Figure 6. WNT3A Stimulates Glucose Consumption via LRP5 and RAC1

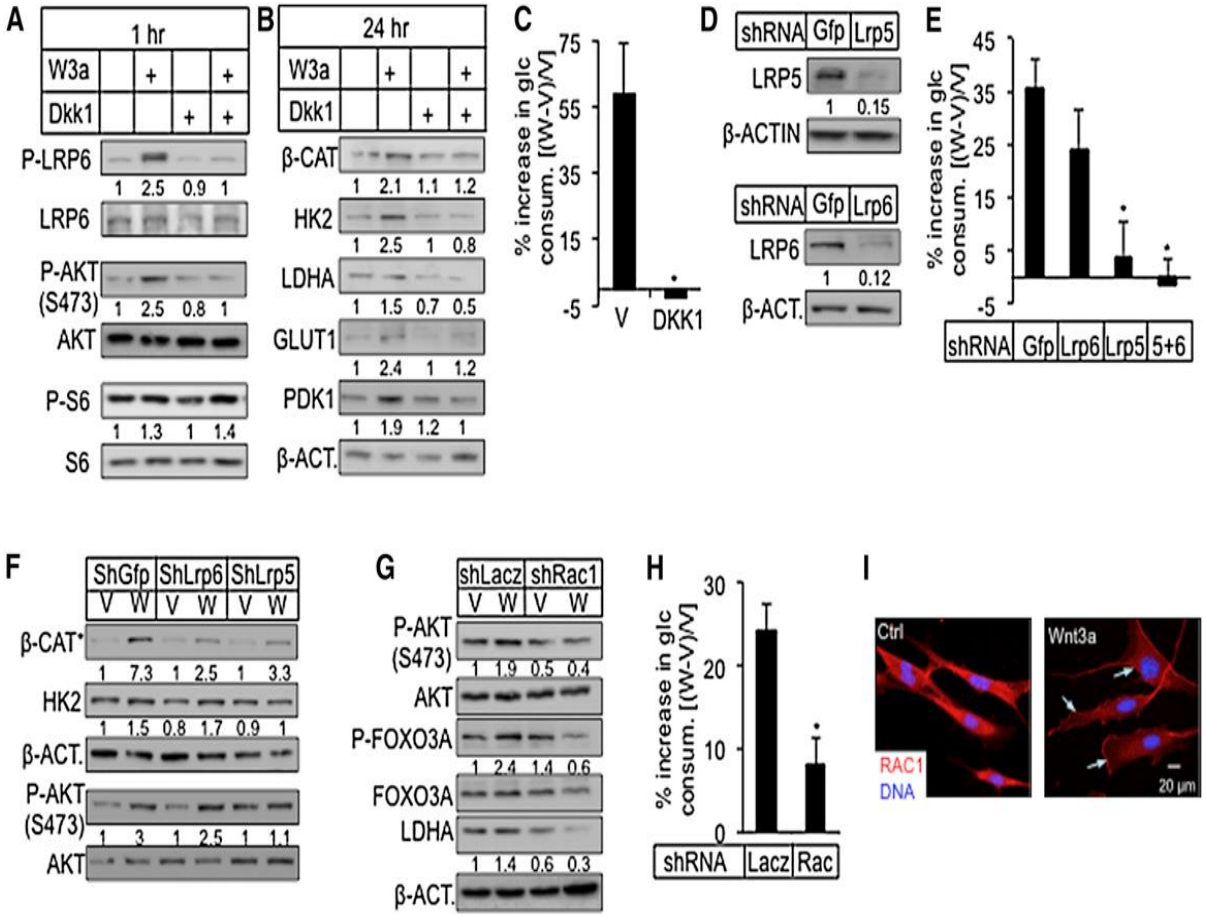

Figure 6. WNT3A Stimulates Glucose Consumption via LRP5 and RAC1

(A and B) Effects of DKK1 on WNT3A-induced phosphorylation and glycolytic enzymes. P-LRP6, P-AKT, and P-S6 normalized to respective total protein. Other

proteins normalized to b-actin.

(C) Effect of DKK1 on WNT3A-induced glucose consumption.

(D–F) Effect of LRP5 or LRP6 knockdown (D) on WNT3A-induced glucose consumption (E), and on signaling events after 1 hr of treatment (F). b-CAT* denotes b-catenin unphosphorylated at N terminus.

(G) Effect of RAC1 knockdown on mTORC2 and LDHA induction by 24 hr WNT3A treatment.

(H) Effect of RAC1 knockdown on WNT3A-induced glucose consumption.

(I) Representative confocal images of RAC1 immunofluorescence. ST2 cells were serum starved overnight before being treated for 2 hr with vehicle (Ctrl) or

Wnt3a. Arrows denote RAC1 membrane localization. All glucose consumption was measured after 24 hr of WNT3A or vehicle treatment. V, vehicle; W, WNT3A.

Asterisk, $n = 3$, $p < 0.05$. Error bars, SD.

Figure 7. Metabolic Reprogramming by WNT-LRP5 Signaling in Osteoblast Lineage

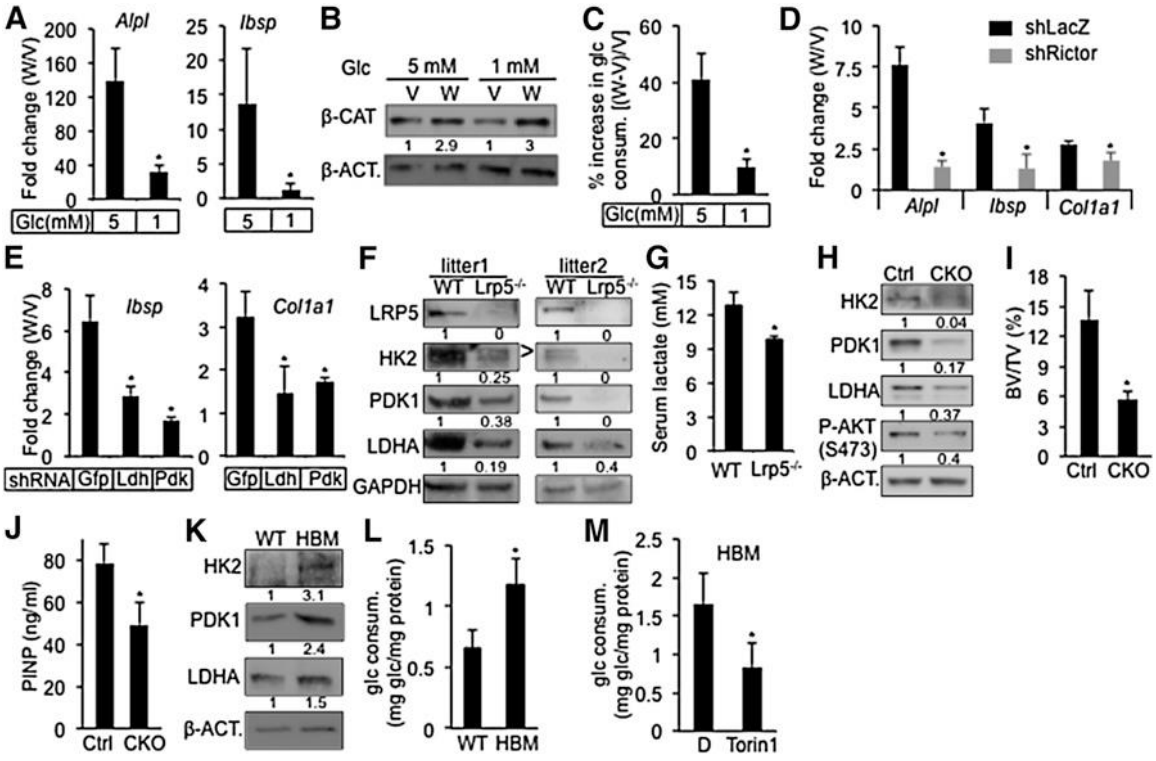

(A) Effect of glucose concentration on WNT3Ainduced osteoblast differentiation in ST2 cells after 4 days of stimulation. Expression of osteoblast markers was determined by qPCR. Fold changes between WNT3A- and vehicle-treated cells were calculated after normalization to 18S RNA.

(B and C) Effect of glucose concentration on b-catenin stabilization (B) and WNT3A-induced glucose consumption (C) after 24 hr of treatment.

(D and E) Effect of RICTOR (D), LDHA, or PDK1 (E) knockdown on WNT3A-induced osteoblast differentiation in ST2 cells after 4 days of treatment. Expression of osteoblast markers was determined by qPCR. Fold changes between WNT3A- and vehicle-treated cells were calculated after normalization to 18S RNA.

Figure 7. Metabolic Reprogramming by WNT-LRP5 Signaling in Osteoblast Lineage

(F) Western blots of glycolytic enzymes in bone protein extracts from Lrp5-/- versus wild-type littermates. > denotes correct band for HK2.

(G) Serum lactate levels from Lrp5-/-versus wild type littermates.

(H) Western blots with bone protein extracts from Lrp5CKO versus Osx-Cre littermates (Ctrl).

(I and J) Bone phenotype analyses of Lrp5CKO versus Osx-Cre littermates (Ctrl) by mCT (I) and serum P1NP assays (J).

(K) Western blots of glycolytic enzymes in bone protein extracts from homozygous LRP5 HBM mice versus wild-type littermates.

(L) Glucose consumption after 48 hr of culture by BMSC from LRP5 HBM (heterozygous or homozygous) mice versus wild-type littermates.

(M) Effect of Torin1 on 48 hr glucose consumption by BMSC from homozygous LRP5 HBM mice. D, DMSO. Asterisk, n R 3, $p < 0.05$. Error bars, SD.

7. Supplemental Figures

Figure S1. Effects of WNT3A, insulin, BMP2 and WNT5A on ST2 cells.

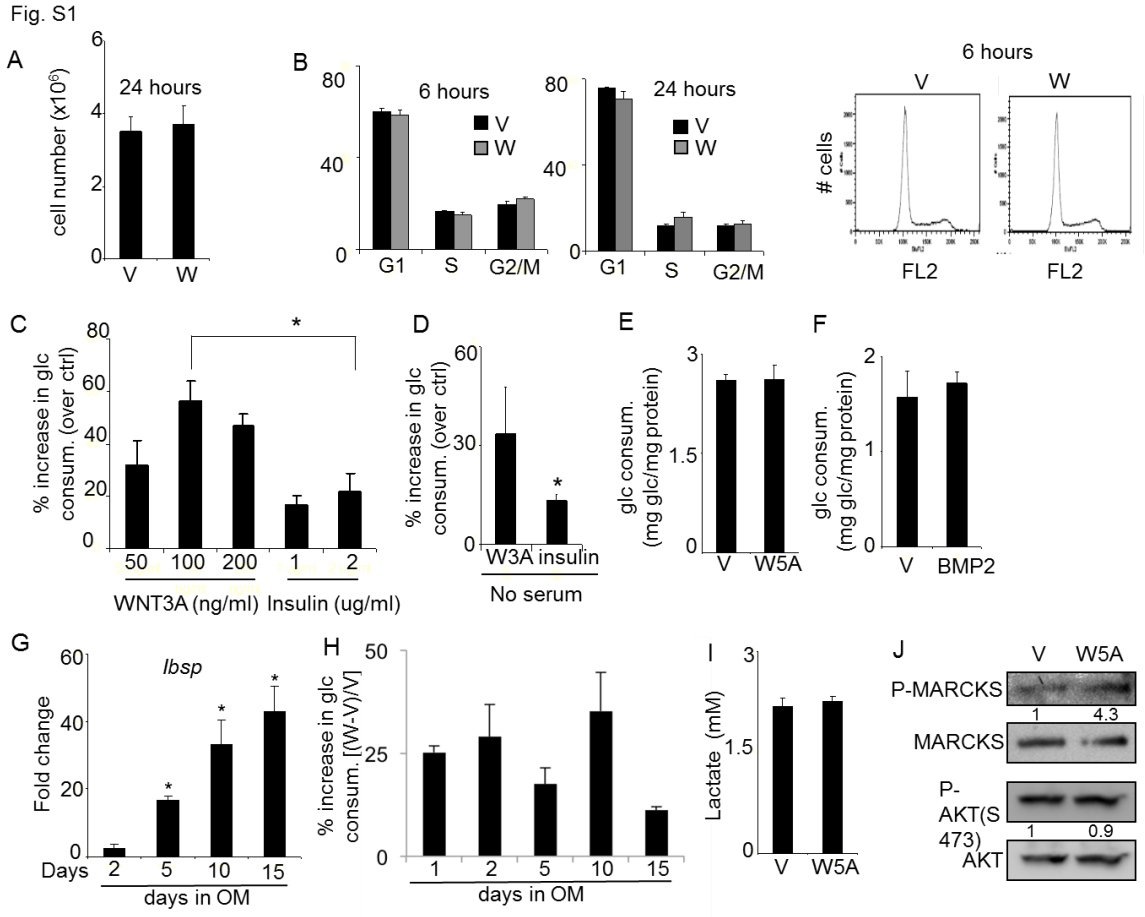

Figure S1. Effects of WNT3A, insulin, BMP2 and WNT5A on ST2 cells.

(A) Cell numbers after WNT3A (W) or vehicle (V) treatment for 24 hours.

(B) Cell cycle profiling after 6 or 24 hours of treatment. A representative profile after 6 hours of treatment is shown to the right.

(C) Glucose consumption induced by insulin versus WNT3A after 24 hours of treatment.

(D) Induction of glucose consumption by WNT3A or insulin after 24 hours in the absence of serum.

(E-F) Effect of WNT5A (100 ng/ml) or BMP2 (300 ng/ml) on glucose consumption after 24 hours.

(G) Expression of Ibsp in ST2 cells assayed by qPCR following incubation in osteogenic medium (OM) for indicated times. Fold change over cells in OM for 1 day after normalized to 18S RNA.

(H) Effect of WNT3A on 24-hour glucose consumption by ST2 cells after incubation in OM for indicated days.

(I) Effect of WNT5A on lactate production after 24 hours of treatment. (J) Effect of WNT5A on P-MARCKS and PAKT (S473) after 1-hour treatment in the absence of serum following 12-hour serum starvation. Phospho-protein levels normalized to respective total protein. *: n=3, $p<0.05$. Error bars: STDEV.

Figure S2. Effects of WNT3A on metabolic regulators in ST2 cells.

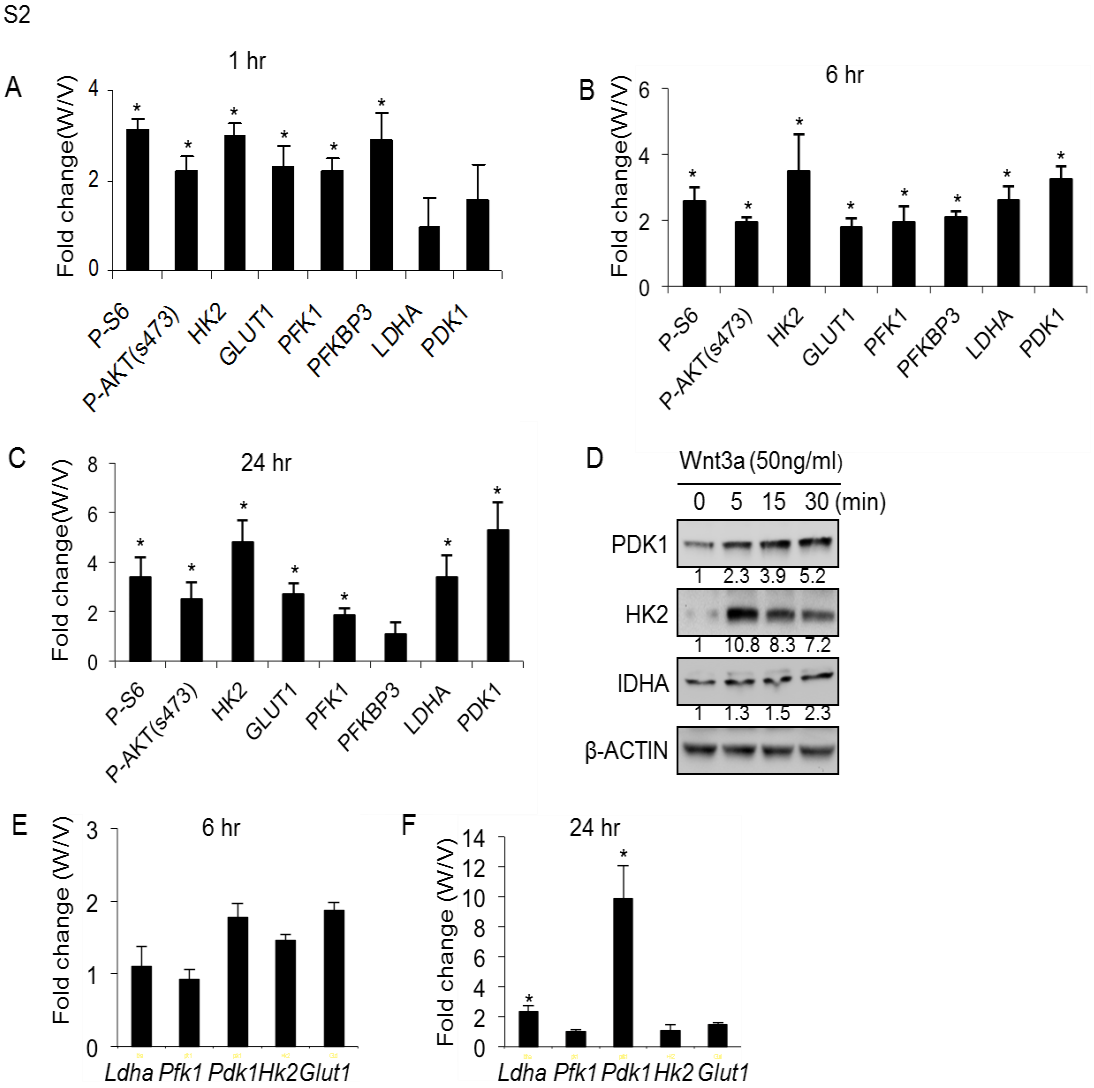

Figure S2. Effects of WNT3A on metabolic regulators in ST2 cells.

(A-C) Quantification of Western blots from independent experiments following WNT3A (W) or vehicle (V) treatment for indicated duration. P-S6 and P-AKT (S473) normalized to respective total protein levels; all other proteins normalized to β-actin.

(D) Western blot of glycolytic

enzymes after WNT3A treatment for indicated time after 24-hr serum starvation. Protein levels normalized to β-ACTIN. "0" treatment cells exposed to vehicle for 30 mins.

(E, F) qPCR analyses of mRNA following 6 (E) or 24 (F) hours of treatment. Fold change calculated between WNT3A (W) and vehicle (V) treatments after expression level first normalized to respective 18S rRNA. Bar graphs: n=3, *: $p<0.05$, error bar = STDEV.

Figure S3. Confirmation of the role of LRP5, LRP6 and β-catenin by a second shRNA construct.

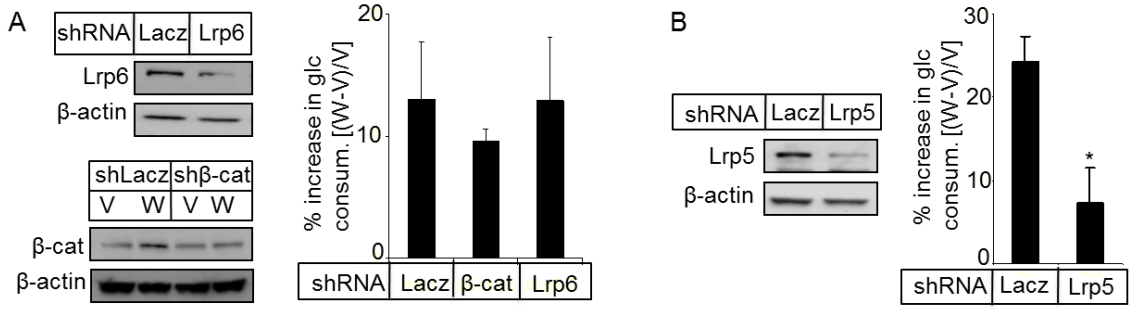

(A) Effect of LRP6 or β-catenin knockdown on WNT3A-induced glucose consumption. (B) Effect of LRP5 knockdown on WNT3A-induced glucose consumption.

Figure S4. Role of mTOR and AKT signaling in WNT3A-induced glucose consumption.

Fig. S4

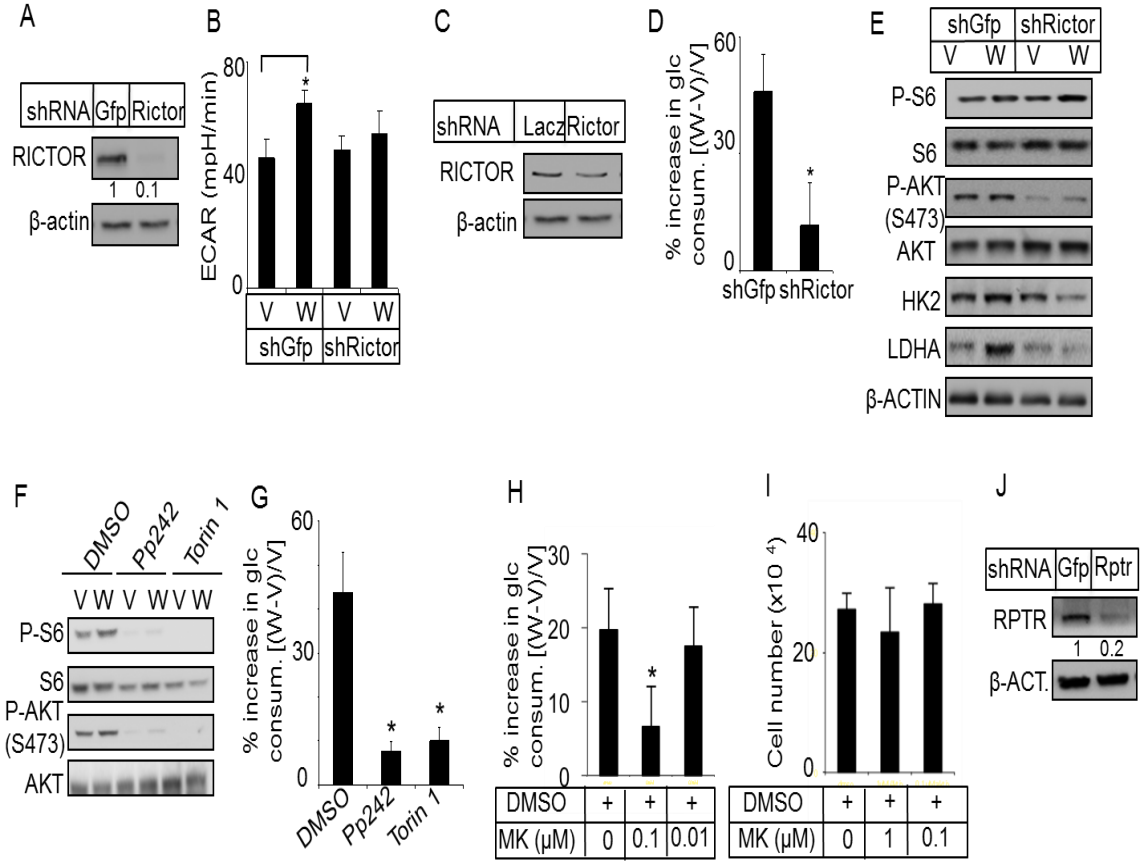

Figure S4. Role of mTOR and AKT signaling in WNT3A-induced glucose consumption.

(A) shRNA knockdown of RICTOR assayed by Western blot.

(B) Effect of Rictor knockdown on ECAR after 6 hours of WNT3A or vehicle treatment.

(C-E) Effect of a second Rictor shRNA on RICTOR levels (C), WNT3A-induced glucose consumption (D), mTOR signaling and glycolytic enzymes (E). (F, G) Effect of mTOR inhibitors on WNT3A-induced mTOR signaling (F) and glucose consumption (G) after 24 hours of treatment.

(H) Effect of different concentrations of MK2206 on WNT3A-induced glucose consumption.

(I) Effect of MK2206 on cell numbers. (J) Knockdown of RAPTOR assayed by Western blot. Bar graphs: n=3, *: $p<0.05$, error bar = STDEV.

Figure S5. Role of RAC1 in WNT-induced mTOR signaling and glycolysis.

Fig. S5

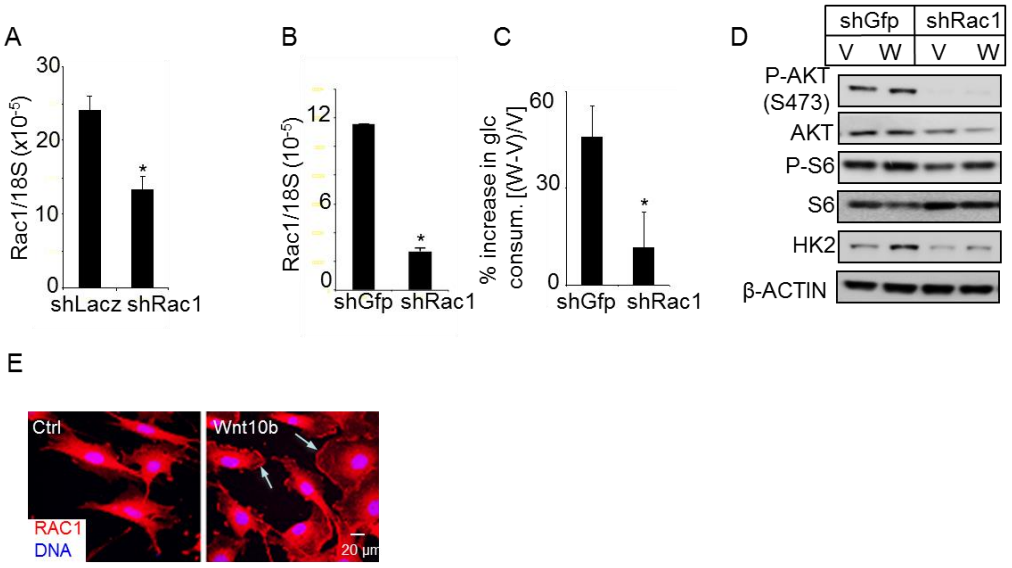

(A) Knockdown of Rac1 assayed by qPCR with 18S RNA as normalizer. (B-D) Effect of a second Rac1 shRNA on Rac1 mRNA (B), WNT3A-induced glucose consumption (C), mTOR signaling and glycolytic enzymes (D). (E) Confocal microscopy of RAC1 immunofluorescence. ST2 cells were infected overnight with retrovirus expressing either GFP (Ctrl) or WNT10B. Bar graphs: n=3, *: $p<0.05$, error bar = STDEV.

Figure S6. Metabolic regulation of osteoblast differentiation in ST2 cells.

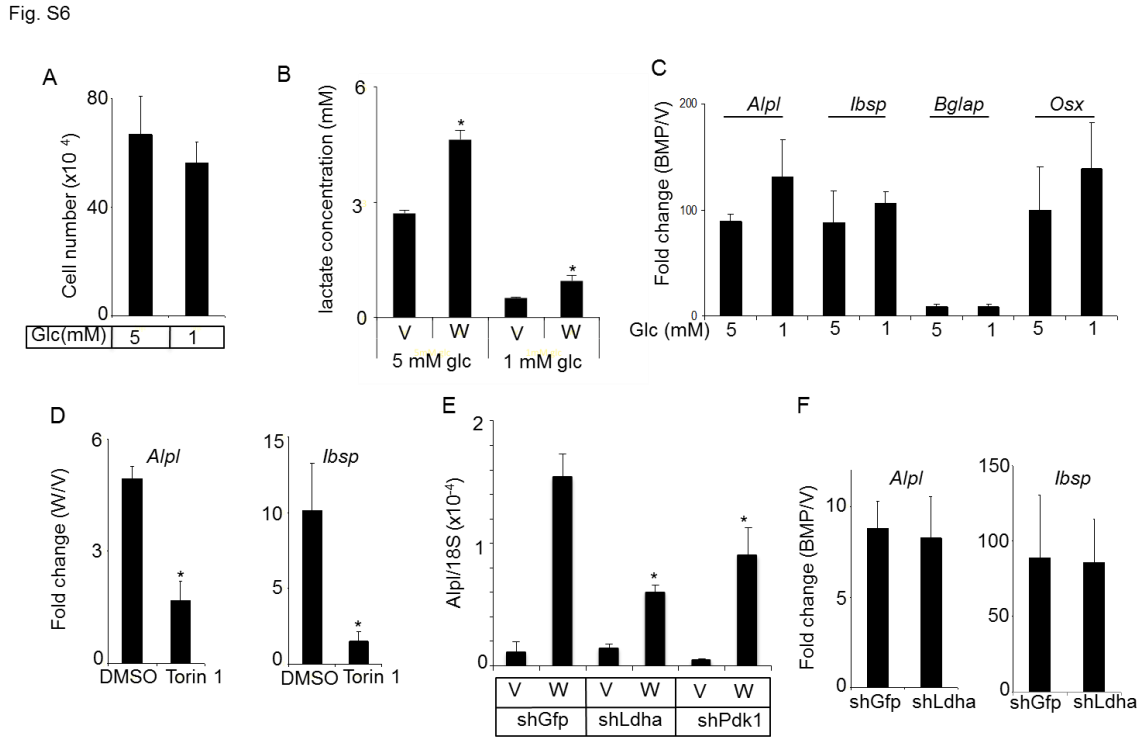

(A) Cell numbers after 4 days of WNT3A treatment in media containing 5 mM or 1 mM glucose.

(B) Lactate levels after 24 hours of WNT3A or vehicle treatment.

(C) Effect of glucose concentration on BMP2-induced expression of osteoblast differentiation markers assayed by qPCR.

(D) Effect of Torin1 on osteoblast differentiation markers after 4 days of WNT3A treatment, assayed by qPCR.

(E) Effect of LDHA or PDK1 knockdown on WNT3A-induced Alpl expression as determined by qPCR.

(F) Effect of LDHA knockdown on BMP2-induced osteoblast differentiation as determined by qPCR. All qPCR data normalized to 18S RNA before calculation of fold changes. Bar graphs: n=3, *: $p<0.05$, error bar = STDEV

Figure S7. Analyses of bone phenotype of Osx-Cre;Lrp5f/f mice at ten weeks of age.

Fig. S7

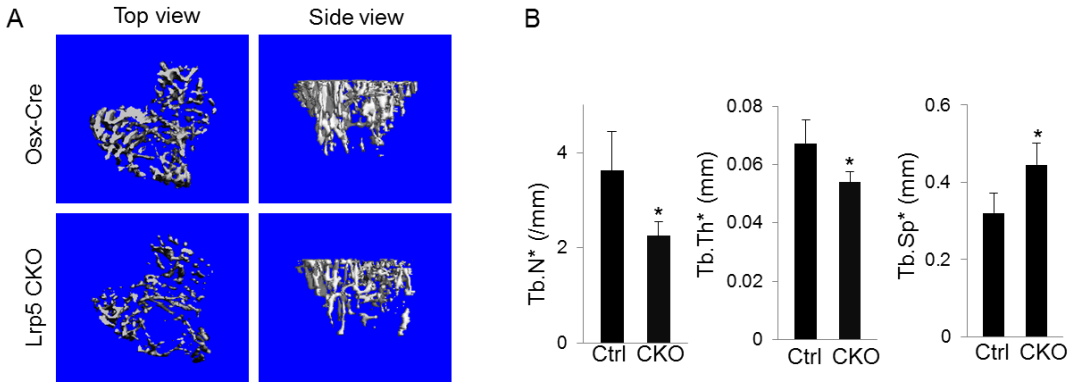

(A) Representative 3-D reconstruction of trabecular bone in proximal tibia by μCT.

(B) Quantification of trabecular bone parameters in proximal tibia by μCT. Data from male littermates. Ctrl: Osx-Cre; CKO: Osx-Cre;Lrp5f/f . Bar graphs: n=3, *: $p<0.05$, error bar = STDEV.

References

Balemans, W., Ebeling, M., Patel, N., Van Hul, E., Olson, P., Dioszegi, M., Lacza, C., Wuyts, W., Van Den Ende, J., Willems, P., et al. (2001). Increased bone density in sclerosteosis is due to the deficiency of a novel secreted protein (SOST). Hum. Mol. Genet. 10, 537–543.

Balemans, W., Patel, N., Ebeling, M., Van Hul, E., Wuyts, W., Lacza, C., Dioszegi, M., Dikkers, F.G., Hildering, P., Willems, P.J., et al. (2002). Identification of a 52 kb deletion downstream of the SOST gene in patients with van Buchem disease. J. Med. Genet. 39, 91–97.

Bouxsein, M.L., Boyd, S.K., Christiansen, B.A., Guldberg, R.E., Jepsen, K.J., and Muller, R. (2010). Guidelines for assessment of bone microstructure in rodents using micro-computed tomography. J. Bone Miner. Res. 25, 1468–1486.

Boyden, L.M., Mao, J., Belsky, J., Mitzner, L., Farhi, A., Mitnick, M.A., Wu, D., Insogna, K., and Lifton, R.P. (2002). High bone density due to a mutation in LDL-receptor-related protein 5. N. Engl. J. Med. 346, 1513–1521.

Cadoret, A., Ovejero, C., Terris, B., Souil, E., Le´ vy, L., Lamers, W.H., Kitajewski, J., Kahn, A., and Perret, C. (2002). New targets of beta-catenin signaling in the liver are involved in the glutamine metabolism. Oncogene 21, 8293–8301.

Chafey, P., Finzi, L., Boisgard, R., Cau¨ zac, M., Clary, G., Broussard, C., Pe´ gorier, J.P., Guillonneau, F., Mayeux, P., Camoin, L., et al. (2009). Proteomic analysis of beta-catenin activation in mouse liver by DIGE analysis identifies glucose metabolism as a new target of the Wnt pathway. Proteomics 9, 3889–3900.

Chen, J., and Long, F. (2012). b-catenin promotes bone formation and suppresses bone resorption in postnatal growing mice. J. Bone Miner. Res. Published online November 27, 2012.

Chi, M.M., Hoehn, A., and Moley, K.H. (2002). Metabolic changes in the glucose-induced apoptotic blastocyst suggest alterations in mitochondrial physiology. Am. J. Physiol. Endocrinol. Metab. 283, E226–E232.

Clevers, H. (2006). Wnt/beta-catenin signaling in development and disease. Cell 127, 469–480.

Croce, J.C., and McClay, D.R. (2008). Evolution of the Wnt pathways. Methods Mol. Biol. 469, 3–18.

Cui, Y., Niziolek, P.J., MacDonald, B.T., Zylstra, C.R., Alenina, N., Robinson, D.R., Zhong, Z., Matthes, S., Jacobsen, C.M., Conlon, R.A., et al. (2011). Lrp5 functions in bone to regulate bone mass. Nat. Med. 17, 684–691.

Cybulski, N., Polak, P., Auwerx, J., Ru¨ egg, M.A., and Hall, M.N. (2009). mTOR complex 2 in adipose tissue negatively controls whole-body growth. Proc. Natl. Acad. Sci. USA 106, 9902–9907.

Day, T.F., Guo, X., Garrett-Beal, L., and Yang, Y. (2005). Wnt/beta-catenin signaling in mesenchymal progenitors controls osteoblast and chondrocyte differentiation during vertebrate skeletogenesis. Dev. Cell 8, 739–750.

Fujino, T., Asaba, H., Kang, M.J., Ikeda, Y., Sone, H., Takada, S., Kim, D.H., Ioka, R.X., Ono, M., Tomoyori, H., et al. (2003). Low-density lipoprotein receptor-related protein 5 (LRP5) is essential for normal cholesterol metabolism and glucose-induced insulin secretion. Proc. Natl. Acad. Sci. USA 100, 229–234.

Garcı´a-Martı´nez, J.M., and Alessi, D.R. (2008). mTOR complex 2 (mTORC2) controls hydrophobic motif phosphorylation and activation of serum- and glucocorticoid-induced protein kinase 1 (SGK1). Biochem. J. 416, 375–385.

Gong, Y., Slee, R.B., Fukai, N., Rawadi, G., Roman-Roman, S., Reginato, A.M., Wang, H., Cundy, T., Glorieux, F.H., Lev, D., et al.; Osteoporosis-Pseudoglioma Syndrome Collaborative Group. (2001). LDL receptor-related protein 5 (LRP5) affects bone accrual and eye development. Cell 107, 513–523.

Grant, S.F., Thorleifsson, G., Reynisdottir, I., Benediktsson, R., Manolescu, A., Sainz, J., Helgason, A., Stefansson, H., Emilsson, V., Helgadottir, A., et al. (2006). Variant of transcription factor 7-like 2 (TCF7L2) gene confers risk of type 2 diabetes. Nat. Genet. 38, 320–323.

Guertin, D.A., Stevens, D.M., Thoreen, C.C., Burds, A.A., Kalaany, N.Y., Moffat, J., Brown, M., Fitzgerald, K.J., and Sabatini, D.M. (2006). Ablation in mice of the mTORC components raptor, rictor, or mLST8 reveals that mTORC2 is required for signaling to Akt-FOXO and PKCalpha, but not S6K1. Dev. Cell 11, 859–871.

Habas, R., Kato, Y., and He, X. (2001). Wnt/Frizzled activation of Rho regulates vertebrate gastrulation and requires a novel Formin homology protein Daam1. Cell 107, 843–854.

Habas, R., Dawid, I.B., and He, X. (2003). Coactivation of Rac and Rho by Wnt/Frizzled signaling is required for vertebrate gastrulation. Genes Dev. 17, 295–309.

Hagiwara, A., Cornu, M., Cybulski, N., Polak, P., Betz, C., Trapani, F., Terracciano, L., Heim, M.H., Ru¨ egg, M.A., and Hall, M.N. (2012). Hepatic mTORC2 activates glycolysis and lipogenesis through Akt, glucokinase, and SREBP1c. Cell Metab. 15, 725–738.

Haney, P.M., Slot, J.W., Piper, R.C., James, D.E., and Mueckler, M. (1991). Intracellular targeting of the insulin-regulatable glucose transporter (GLUT4) is isoform specific and independent of cell type. J. Cell Biol. 114, 689–699.

Hill, T.P., Spa¨ ter, D., Taketo, M.M., Birchmeier, W., and Hartmann, C. (2005). Canonical Wnt/beta-catenin signaling prevents osteoblasts from differentiating into chondrocytes. Dev. Cell 8, 727–738.

Holmen, S.L., Giambernardi, T.A., Zylstra, C.R., Buckner-Berghuis, B.D., Resau, J.H., Hess, J.F., Glatt, V., Bouxsein, M.L., Ai, M., Warman, M.L., et al. (2004). Decreased BMD and limb deformities in mice carrying mutations in both Lrp5 and Lrp6. J. Bone Miner. Res. 19, 2033–2040.

Hresko, R.C., and Mueckler, M. (2005). mTOR.RICTOR is the Ser473 kinase for Akt/protein kinase B in 3T3-L1 adipocytes. J. Biol. Chem. 280, 40406–40416.

Hu, H., Hilton, M.J., Tu, X., Yu, K., Ornitz, D.M., and Long, F. (2005). Sequential roles of Hedgehog and Wnt signaling in osteoblast development. Development 132, 49–60.

Huang, S.M., Mishina, Y.M., Liu, S., Cheung, A., Stegmeier, F., Michaud, G.A., Charlat, O., Wiellette, E., Zhang, Y., Wiessner, S., et al. (2009). Tankyrase inhibition stabilizes axin and antagonizes Wnt signalling. Nature 461, 614–620.

Inoki, K., Ouyang, H., Zhu, T., Lindvall, C., Wang, Y., Zhang, X., Yang, Q., Bennett, C., Harada, Y., Stankunas, K., et al. (2006). TSC2 integrates Wnt and energy signals via a coordinated phosphorylation by AMPK and GSK3 to regulate cell growth. Cell 126, 955–968.

Jacinto, E., Loewith, R., Schmidt, A., Lin, S., Ru¨ egg, M.A., Hall, A., and Hall, M.N. (2004). Mammalian TOR complex 2 controls the actin cytoskeleton and is rapamycin insensitive. Nat. Cell Biol. 6, 1122–1128.

Jacinto, E., Facchinetti, V., Liu, D., Soto, N., Wei, S., Jung, S.Y., Huang, Q., Qin, J., and Su, B. (2006). SIN1/MIP1 maintains rictor-mTOR complex integrityand regulates Akt phosphorylation and substrate specificity. Cell 127, 125–137.

Joeng, K.S., Schumacher, C.A., Zylstra-Diegel, C.R., Long, F., and Williams, B.O. (2011). Lrp5 and Lrp6 redundantly control skeletal development in the mouse embryo. Dev. Biol. 359, 222–229.

Kang, S., Bennett, C.N., Gerin, I., Rapp, L.A., Hankenson, K.D., and Macdougald, O.A. (2007). Wnt signaling stimulates osteoblastogenesis of mesenchymal precursors by suppressing CCAAT/enhancer-binding protein alpha and peroxisome proliferator-activated receptor gamma. J. Biol. Chem. 282, 14515–14524.

Kato, M., Patel, M.S., Levasseur, R., Lobov, I., Chang, B.H., Glass, D.A., 2nd, Hartmann, C., Li, L., Hwang, T.H., Brayton, C.F., et al. (2002). Cbfa1-independent decrease in osteoblast proliferation, osteopenia, and persistent embryonic eye vascularization in mice deficient in Lrp5, a Wnt coreceptor. J. Cell Biol. 157, 303–314.

Kinoshita, N., Iioka, H., Miyakoshi, A., and Ueno, N. (2003). PKC delta is essential for Dishevelled function in a noncanonical Wnt pathway that regulates Xenopus convergent extension movements. Genes Dev. 17, 1663–1676.

Kùhl, M., Sheldahl, L.C., Park, M., Miller, J.R., and Moon, R.T. (2000). The Wnt/Ca2+ pathway: a new vertebrate Wnt signaling pathway takes shape. Trends Genet. 16, 279–283.

Kumar, A., Lawrence, J.C., Jr., Jung, D.Y., Ko, H.J., Keller, S.R., Kim, J.K., Magnuson, M.A., and Harris, T.E. (2010). Fat cell-specific ablation of rictor in mice impairs insulin-regulated fat cell and whole-body glucose and lipid metabolism. Diabetes 59, 1397–1406.

Lamming, D.W., Ye, L., Katajisto, P., Goncalves, M.D., Saitoh, M., Stevens, D.M., Davis, J.G., Salmon, A.B., Richardson, A., Ahima, R.S., et al. (2012). Rapamycin-induced insulin resistance is mediated by mTORC2 loss and uncoupled from longevity. Science 335, 1638–1643.

Laplante, M., and Sabatini, D.M. (2012). mTOR signaling in growth control and disease. Cell 149, 274–293.

Li, X., Ominsky, M.S., Niu, Q.T., Sun, N., Daugherty, B., D'Agostin, D., Kurahara, C., Gao, Y., Cao, J., Gong, J., et al. (2008). Targeted deletion of the sclerostin gene in mice results in increased bone formation and bone strength. J. Bone Miner. Res. 23, 860–869.

Little, R.D., Carulli, J.P., Del Mastro, R.G., Dupuis, J., Osborne, M., Folz, C., Manning, S.P., Swain, P.M., Zhao, S.C., Eustace, B., et al. (2002). A mutation in the LDL receptor-related protein 5 gene results in the autosomal dominant high-bone-mass trait. Am. J. Hum. Genet. 70, 11–19.

Liu, H., Fergusson, M.M., Wu, J.J., Rovira, I.I., Liu, J., Gavrilova, O., Lu, T., Bao, J., Han, D., Sack, M.N., and Finkel, T. (2011). Wnt signaling regulates hepatic metabolism. Sci. Signal. 4, ra6.

Long, F. (2012). Building strong bones: molecular regulation of the osteoblast lineage. Nat. Rev. Mol. Cell Biol. 13, 27–38.

Ma, X.M., and Blenis, J. (2009). Molecular mechanisms of mTOR-mediated translational control. Nat. Rev. Mol. Cell Biol. 10, 307–318.

MacDonald, B.T., Semenov, M.V., Huang, H., and He, X. (2011). Dissecting molecular differences between Wnt coreceptors LRP5 and LRP6. PLoS ONE 6, e23537.

Mani, A., Radhakrishnan, J., Wang, H., Mani, A., Mani, M.A., Nelson-Williams, C., Carew, K.S., Mane, S., Najmabadi, H., Wu, D., and Lifton, R.P. (2007). LRP6 mutation in a family with early coronary disease and metabolic risk factors. Science 315, 1278–1282.

Palsgaard, J., Emanuelli, B., Winnay, J.N., Sumara, G., Karsenty, G., and Kahn, C.R. (2012). Cross-talk between insulin and Wnt signaling in preadipocytes: role of Wnt co-receptor low density lipoprotein receptor-related protein-5 (LRP5). J. Biol. Chem. 287, 12016–12026.

Rodda, S.J., and McMahon, A.P. (2006). Distinct roles for Hedgehog and canonical Wnt signaling in specification, differentiation and maintenance of osteoblast progenitors. Development 133, 3231–3244.

Saci, A., Cantley, L.C., and Carpenter, C.L. (2011). Rac1 regulates the activity of mTORC1 and mTORC2 and controls cellular size. Mol. Cell 42, 50–61.

Sarbassov, D.D., Ali, S.M., Kim, D.H., Guertin, D.A., Latek, R.R., Erdjument- Bromage, H., Tempst, P., and Sabatini, D.M. (2004). Rictor, a novel binding partner of mTOR, defines a rapamycin-insensitive and raptor-independent pathway that regulates the cytoskeleton. Curr. Biol. 14, 1296–1302.

Sarbassov, D.D., Guertin, D.A., Ali, S.M., and Sabatini, D.M. (2005). Phosphorylation and regulation of Akt/PKB by the rictor-mTOR complex. Science 307, 1098–1101.

Tu, X., Joeng, K.S., Nakayama, K.I., Nakayama, K., Rajagopal, J., Carroll, T.J., McMahon, A.P., and Long, F. (2007). Noncanonical Wnt signaling through G protein-linked PKCdelta activation promotes bone formation. Dev. Cell 12, 113–127.

van Amerongen, R., and Nusse, R. (2009). Towards an integrated view of Wnt signaling in development. Development 136, 3205–3214.

van Amerongen, R., Mikels, A., and Nusse, R. (2008). Alternative wnt signaling is initiated by distinct receptors. Sci. Signal. 1, re9.

Vander Heiden, M.G., Cantley, L.C., and Thompson, C.B. (2009). Understanding the Warburg effect: the metabolic requirements of cell proliferation. Science 324, 1029–1033.

Warburg, O. (1956). On the origin of cancer cells. Science 123, 309–314.

Wolfe, R.R., and Chinkes, D.L. (2004). Determination of isotope enrichment. In Isotope Tracers in Metabolic Research: Principles and Practice of Kinetics AnalysisIsotope Tracers in Metabolic Research: Principles and Practice of Kinetics Analysis (New York: John Wiley & Sons).

Wu, X., Tu, X., Joeng, K.S., Hilton, M.J., Williams, D.A., and Long, F. (2008). Rac1 activation controls nuclear localization of beta-catenin during canonical Wnt signaling. Cell 133, 340–353.

Wullschleger, S., Loewith, R., and Hall, M.N. (2006). TOR signaling in growth and metabolism. Cell 124, 471–484.

Yadav, V.K., Ryu, J.H., Suda, N., Tanaka, K.F., Gingrich, J.A., Schu¨ tz, G., Glorieux, F.H., Chiang, C.Y., Zajac, J.D., Insogna, K.L., et al. (2008). Lrp5 controls bone formation by inhibiting serotonin synthesis in the duodenum. Cell 135, 825–837.

Yoon, J.C., Ng, A., Kim, B.H., Bianco, A., Xavier, R.J., and Elledge, S.J. (2010). Wnt signaling regulates mitochondrial physiology and insulin sensitivity. Genes Dev. 24, 1507–1518.

Zinzalla, V., Stracka, D., Oppliger, W., and Hall, M.N. (2011). Activation of mTORC2 by association with the ribosome. Cell 144, 757–768.

CHAPTER 3

Aerobic glycolysis is required for bone anabolism in the mouse

1. Abstract

WNT signaling has emerged as a major mechanism stimulating bone formation, but the downstream signaling mechanism is not fully understood. We have previously shown that WNT signaling stimulates lactate-producing glycolysis in the presence of oxygen (aerobic glycolysis), but the effect of WNT on other metabolic fates of glucose is unknown. Moreover, the role of aerobic glycolysis in bone formation has not been examined *in vivo*. Here, by tracking the production of CO_2 from glucose position-specifically labeled with radioactive ^{14}C, we found that WNT3A suppressed the contribution of glucose to both TCA cycle and pentose phosphate pathway *in vitro*. Pharmacological enhancement of pyruvate entering the TCA cycle attenuated the high-bone mass phenotype caused by hyperactive WNT signaling in the mouse. In addition, genetic deletion of LDHA from osteoblast-lineage cells suppressed normal postnatal bone accrual due to reduced osteoblast number and function. These results supports the model that aerobic glycolysis induced by WNT or other physiologic signals enhances bone anabolism.

2. Introduction

WNTs are a large family of glycoproteins that activate both β-catenin-dependent and -independent intracellular pathways and are involved in bone formation. The first evidence for the role of WNT signaling in bone formation came from human diseases associated with mutations in the co-receptor Lrp5. Loss- and gain-of-function mutations in Lrp5 are linked to low and high bone mass diseases, respectively (Babij et al., 2003; Gong et al., 2001). These phenotypes were confirmed by mouse genetic studies and further supported by evidence revealing the significance of WNT signaling at different stages of osteoblast differentiation. However, the discrepancy between the osteoblast phenotypes obtained by alterations of Lrp5 and β-catenin postnatally (Lrp5 mutations are associated with osteoblast defects, while β-catenin mutations mostly effect osteoclasts) suggests that there might be β-catenin-independent WNT pathways also important for osteoblast differentiation and function (Cui et al., 2011; Gilbert, 2000).

We have shown that WNT signaling increases glucose utilization and directs the usage of glucose towards aerobic glycolysis; this process was regulated by a signaling cascade dependent on Lrp5-Rac1-mTORC2 and independent of β-catenin (Esen et al., 2013). The increase in aerobic glycolysis was accompanied by the enhanced expression of glycolytic enzymes, including lactate dehydrogenase A (LDHA), which converts pyruvate to lactate, and pyruvate dehydrogenase 1 (PDK1) that suppresses pyruvate from entering the TCA cycle by inactivating the pyruvate dehydrogenase complex. These enzymes were also increased in mice with Lrp5 gain-of-function mutation (thereafter Lrp5 HBM), but suppressed in animals lacking Lrp5 (Esen et al., 2013). However, the contribution of aerobic glycolysis to bone formation has not been explored *in vivo*.

Although the previous study detailed that WNT3A increased glucose utilization and lactate production, it did not examine the other metabolic fates of glucose. These other fates include oxidation in TCA cycle, oxidation via Pentose Phosphate Pathway (PPP) and fueling into hexosamine biosynthetic pathway (HBP) (Bouche et al., 2004; Teo et al., 2010). Early studies have established that carbons at specific positions of the glucose molecule are released as CO_2 through the oxidative branch of PPP, the decarboxylation of pyruvate to acetyl-coA at the entry of TCA cycle, or the subsequent rounds of TCA cycle. This knowledge has allowed one to track the various metabolic fates of glucose through positive-specific labeling with radioactive ^{14}C (Reitzer et al., 1979).

Lactate dehydrogenase (LDH) is a tetrameric enzyme consisting of subunits A, B or C expressed from different genes. LDH catalyzes the conversion of pyruvate to lactate in the cytoplasm and replenishes NAD^+, which is an important oxidizing molecule necessary for the continuation of glycolysis. Different homo and hetero combinations of A and B subunits constitute 5 different enzyme forms LDH1-5, which are expressed ubiquitously. On the other hand, the C subunit is specific to the testis and sperms (Kopperschlager and Kirchberger, 1996). The A-subunit of the LDH enzyme, LDHA, is increased in many cancer cells (Goldman et al., 1964). Knocking down LDHA in cancer cells was shown to switch the glucose flux towards TCA cycle and reduced tumor formation, indicating that LDHA is not only a hallmark of altered metabolism but also a key checkpoint to control glycolytic flux (Fantin et al., 2006; Le et al., 2010). We previously showed that LDHA was enhanced by WNT3A and this enhancement was important for WNT3A-induced osteoblast differentiation *in vitro*. However, the role of LDHA in bone formation has never been explored *in vivo*.

In this study, we have investigated the effect of WNT3A on other cellular glucose fates. We have also manipulated the metabolic glucose flux *in vivo* either by genetically removing LDHA or inhibiting PDKs with dichloroacetate (DCA). The results have revealed an important role for glycolysis in bone formation *in vivo*.

3. Results

3.1. WNT3A suppresses glucose oxidation in PPP and TCA cycle

To have a better understanding of the effect of WNT signaling on glucose metabolism, we examined changes in metabolites in response to WNT3A. We performed an unbiased metabolomics study in ST2 cells, a mouse bone marrow stromal cell line that undergo osteoblast differentiation (Tu et al., 2007) and metabolic reprogramming (Esen et al., 2013) in response to WNT signaling. We discovered that 24 hours of WNT3a treatment significantly suppressed the intracellular levels of ribose-5 phosphate as well as ribulose / xylulose-5-phosphate, all of which are intermediates in PPP (Figure 1). Since this result only showed the steady state for the intermediates, we decided to examine the flux of glucose towards PPP. For this, we used glucose specifically labeled at C1 ([$^{14}C_1$]-Glucose) or C6 ([$^{14}C_6$]-Glucose). C_1 in glucose is expected to release as CO_2 through either PPP or after the 2nd cycle following entry of pyruvate to the TCA cycle, whereas C_6 is only released as CO_2 from the latter (Gilbert, 2000) (Figure 2). We treated ST2 cells with WNT3A or vehicle together with one of the labeled glucose in a sealed flask designed to trap CO_2 produced by the cells (Figure 3). We then assessed the radioactivity via a scintillation counter. The labeling index was calculated by normalizing the radioactive CO_2 detected as disintegration per minute (DPM) with the total (labeled and unlabeled) glucose uptake in the same experiment and the total cell number in a parallel

experiment. Relative flux through PPP was calculated as the difference of $^{14}C_1$-C_6 CO_2, normalized to the total glucose uptake and cell number. We found that $^{14}C_1$ labeling index was reduced with WNT3A treatment, while $^{14}C_6$ labeling index was not significantly different. Importantly, the relative PPP flux in the WNT3A-treated samples was suppressed (Figure 4A). Thus, WNT3A suppresses glucose contribution to PPP.

Since the glucose flux to PPP was suppressed by WNT3A, we wanted to determine if glucose metabolism via the TCA cycle was affected. We used the same experimental set-up with radioactively labeled glucose ^{14}C [3, 4] to determine the relative amount of glucose entering the TCA cycle via decarboxylation of pyruvate to acetyl-CoA, as carbons at 3 and 4 positions are only released as CO_2 during this conversion (Figure 2). We calculated the relative TCA contribution index by normalizing the CO_2 radioactivity level to the total glucose uptake and the total cell number in each culture at the end of 24 hours treatment. We detected a suppression of glucose contribution to TCA cycle (Figure 4B). We previously showed that WNT3A did not change mitochondrial oxygen consumption at 24 hours (Esen et al., 2013). The reduced contribution of glucose to TCA cycle suggests that cellular respiration may be fueled by other nutrient sources. Indeed, we observed that WNT3A increased glutamine uptake and its conversion to citrate at 24 hours; the later change was determined by mass isotopomer distribution analyses with stable-isotopically labeled glutamine (data not shown). The reason why WNT3A treatment changes the carbon source for the TCA cycle from glucose to glutamine remains to be investigated. Overall, WNT3A diverts glucose away from the TCA cycle by repressing oxidation of pyruvate to acetyl-coA.

3.2. LDHA is required for bone formation

Our results so far, together with our previous studies, have established that WNT3A enhances glucose contribution to lactate production via enhanced glycolysis while suppressing the contribution to PPP and TCA cycle. We then examined the effect of enhanced glycolysis *in vivo*. We have shown that WNT3A acutely increased LDHA in ST2 cells. To suppress glycolysis, we decided to remove Ldha in osteoblast progenitor cells. We used an allele from Eucomm referred to as "promoterless knockout first cassette". This allele contains a lacz-neo cassette flanked by FRT sites within the 2nd intron of the Ldha gene, which results a null allele. Following the 2nd FRT site, there is a loxP insertion before and after exon 3. We first crossed this mice with Rosa26; Flippase mice to create the floxed allele (Figure 5). Later, by using Cre-LoxP system, we removed Ldha from osteoblast progenitors by using *Osx-Cre*. We used heterozygous animals with the genotype Osx-Cre; Ldha $^{flox/+}$ and Osx-Cre;Ldha $^{-/+}$ as a control and have not observed a difference between the two genotypes (thereafter control animals). We used Osx-Cre;Ldha $^{flox/flox}$ and Osx-Cre;ldha $^{flox/-}$ as mutants and both had comparable bone phenotypes (thereafter Osx-Ldha). More importantly, vivaCT analysis at the proximal tibia indicated that Osx-Ldha animals had reduced bone mass at trabecular region at both 1 month of age (Figure 6); this phenotype persisted at 2 months as analyzed by conventional μCT (Figure 7). Osx-Ldha animals were smaller at 1 month of age, but the size difference was mostly diminished by 2 months (Figure 8A-B). In this study we have not pursued the size difference, but focused on the bone phenotype. Overall, our data demonstrate that LDHA is required for proper trabecular bone formation *in vivo*.

We next explored the Osx-Ldha phenotype to determine whether the reduced bone mass was a result of attenuated bone formation or increased bone resorption. Histologic sections

confirmed the reduced bone mass. Static histomorphometry analyses confirmed the reduced bone mass and indicated a lower osteoblast number per bone surface (Figure 9A-B). On the other hand, serum CTX level (an indicator of osteoclast activity) did not change (Figure 10). Thus, LDHA is a critical regulator of osteoblast number without affecting osteoclast function.

We then examined the osteoblast activity by performing dynamic histomorphometry on the periosteal surface of tibias. We found that mineral apposition rate (MAR), mineralized surface per bone surface (MS/BS) and bone formation rate (BFR/BS) were all reduced in the mutant over the control (Figure 11). Thus, LDHA regulates not only the total number of osteoblasts but also the osteoblast activity.

To characterize the effect of Ldha removal specifically on postnatal bone accrual and to avoid body size-related complications, we took advantage of the fact that Osx-Cre can be suppressed by doxycycline (dox). We raised the Osx-Ldha mice on dox from conception until one month of age, then withdrew dox and analyzed the bones at 2 months. Removal of Ldha via dox withdrawal from 1 through 2 month of age did not affect body weight (Figure 12), but caused a slight by statistically significant reduction in trabecular bone mass in both males and females (Figure13). This result suggests that LDHA plays a role in postnatal bone accrual.

Having determined that perturbation of glycolysis via removal of LDHA suppresses normal bone formation; we next seek to understand the role of increased glycolysis in pathological bone formation caused by hyperactive WNT signaling. Specifically, we treated Lrp5 HBM mice with dichloroacetate (DCA) that inhibits PDK activity to stimulate entry of pyruvate into TCA cycle. We have previously detected an increase in PDK1 protein levels in the bones of Lrp5 HBM animals (Esen et al., 2013). We treated 3-weeks-old Lrp5 HBM mice with DCA for 5 weeks. MicroCT analysis showed that at the beginning of the treatment Lrp5 HBM

mice already manifested a higher trabecular bone mass compared to the littermate wild-type controls (Figure 14). Importantly, DCA significantly reduced bone mass (BV/TV) in the Lrp5 HBM mice (Figure 15A-B). The decrease in bone mass was further confirmed by histology (Figure 15C). On the other hand, DCA had no discernible effect on bone mass in the wild-type mice (data not shown). Thus, the increased aerobic glycolysis contributes to the exuberant bone formation caused by hyperactive WNT signaling.

4. Discussion

In this study, we show that WNT signaling suppresses glucose oxidation through either PPP or TCA cycle. This finding further supports the model that WNT signaling reprograms glucose metabolism towards lactate-producing glycolysis. Functionally, we show that LDHA is required for optimal bone formation in postnatal mice. Moreover, we have demonstrated that the high-bone mass phenotype in Lrp5 HBM mice is partially reversed by enhancing glucose entry to TCA cycle. Overall, increased aerobic glycolysis seems to be necessary for osteoblast differentiation and function.

We show that WNT3A suppresses the contribution of glucose to PPP. This result is unexpected since PPP provides the ribose necessary for nucleotide production and is expected to be active in anabolic reactions. It remains to be investigated why WNT signaling reduces PPP and whether this suppression is a driver for differentiation.

In addition to PPP, WNT3A suppresses glucose oxidation in the TCA cycle. Our finding is consistent with the previous reports that lactate is the major end product of glucose during osteoblast differentiation (Cohn and Forscher, 1962). Despite the reduced glucose contribution to the TCA cycle, mitochondrial oxygen consumption or the cellular ATP level was not changed after 24 hours of WNT3a treatment (Esen et al., 2013). These results suggest that WNT-

stimulated cells utilize alternative fuels for TCA metabolism. Our other parallel studies support that glutamine may be the primary fuel source when the cells are stimulated with WNT3A. Glutamine is the most prominent anaplerotic carbon source for most of cancer cells (DeBerardinis et al., 2007; Portais et al., 1996). It remains to be investigated why WNT3A treated cells switch the TCA fuel source from glucose to glutamine, and how this switch regulates osteoblast differentiation.

In the metabolomics studies, we also detected a lower level of N-acetyl-glucosamine 6-phoshate in WNT3A treated samples (Figure 16). This metabolite is an intermediate of the HBP that produces the end product UDP-N-acetyl glucosamine, a necessary substrate for glycosylation. Glycosylation can regulate protein function (Teo et al., 2010). However, the steady state of the intermediates cannot distinguish whether increased utilization or reduced production was responsible for the lower level in response to WNT3A. We were not able to perform similar flux analysis due to technical limitations since there is not a decarboxylation step in this biosynthesis pathway. Considering the smaller contribution of cellular glucose to HPP, we have not further characterized HBP in this study. Further research is required to characterize the effect of WNT signaling on glucose metabolism through the Hexosamine pathway.

Removal of LDHA in osteoblast progenitor cells showed an osteopenic phenotype. At the cellular level, LDHA is required for proper osteoblast function and number. A decrease in osteoblast number can be due to reduced differentiation from progenitor cells, increased apoptosis or accelerated transition of osteoblasts to osteocytes. These potential mechanisms have not been explored in this study.

We showed that WNT increased LDHA levels both *in vitro* and *in vivo*. Due to the technical limitations we were unable to examine the energetics in LDHA knockout cells *in vivo*.

We expect that LDHA deletion reduced glycolysis and possibly enhanced TCA metabolism of glucose. Future development of techniques that allows for studies of energy metabolism *in vivo* is critical to understand the metabolic requirements of osteoblasts.

LDHA is a part of LDH enzymes that can consist of A and B subunits. There might be functional redundancy between LDHA and LDHB that would result in a lack of complete suppression on LDH activity even when Ldha is completely removed. Assessing LDH enzymatic activity in LDHA knockout osteoblasts will provide insights to this possibility. Moreover, given the fact that we used Ldha heterozygous animals as controls, we might be underestimating the mutant phenotype. Thus, potential redundancy with Ldhb or Ldha haploinsufficiency could have masked the full extent of the effect of blocking pyruvate-to-lactate conversion in this study.

5. Experimental Procedures

5.1. Mouse Strains

$LRP5^{A214V/+}$, referred as Lrp5 HBM, (Cui et al., 2011; Holmen et al., 2004) and Osx-Cre was previously described (Rodda and McMahon, 2006). Ldha mouse strain was from Eucomm; knockout first cassette was crossed with R26;Flippase mice from Jackson Laboratories.

5.2. Analyses of skeleton

μCT analyses were performed with Scanco μCT 40 (Scanco Medical AG) according. Quantification of the trabecular bone in the tibia was performed with 100 μCT slices, total of 1.6 mm right below the growth plate. For paraffin sections, bones were fixed in 10% buffered formalin overnight at room temperature on a rocking platform. After fixation, tissue was washed with PBS and decalcified in 14% EDTA with daily change of solution for 2 weeks. At the end of

decalcification, bones were processed for paraffin embedding and then sectioned at 6 μm thickness. Sections were used for H&E and TRAP staining following the standard protocols. For dynamic histomorphometry, mice were injected intraperitoneally with calcein (20 mg/kg, Sigma, St. Louis, MO) at 6 and 2 days before sacrifice, and bones were fixed in 70% ethanol and embedded in methyl-methacrylate for plastic sections. Both static and dynamic histomorphometry were performed with the commercial software Bioquant II.

Viva-CT analysis was performed with anesthetized mice using xyline/ketamine mixture. Analyses of the scanned bones were done similar to microCT scans.

For serum-based biochemical assays, mice were first fasted for 6 hours and then get anesthetized by using xyline/ketamine mix before blood collection. Blood was incubated at room temperature for 30 mins, spinned down for 5 minutes and then serum was collected. Serum CTX-I assay was performed using the RatLaps ELISA kit (Immunodiagnostic Systems, Ltd.).

5.3. Doxycycline treatment

1 month mice were exposed to doxycycline (Sigma, St. Louis) for one month. Doxycycline was administered through drinking water containing 2% sucrose. 50 mg/L dox was used.

5.4. CO_2 trap experiments

ST2 cells were plated in flasks at a concentration of 40x104/flasks and treated with WNT3A (100ng/ml) along with either 1μ1 Ci/ml glucose [1-C14], glucose [3, 4-C14] or glucose [6-C14] and tube was inserted into the flask and the system is sealed for 24 hours. At the end of 24 hours, 2.5 ml 2.5N H_2SO_4 was injected into the flask to gas the CO_2, and 1 ml NaOH is

injected into the tube. After overnight incubation, liquid in the tube is mixed with scintillation mixture and read in the scintillation counter. A parallel experiment was conducted with the same treatment for cell counting. Labeling index is calculated by normalizing the dpm (disintegration per minute) value by total glucose consumed and by cell number. For glucose consumption, either an aliquot of the medium is used before injecting H_2SO_4, or parallel plates are used. Flux through PPP was calculated by subtracting glucose [6-C14] from glucose [1-C14] and same normalization was performed.

5.5. Metabolomics Studies

ST2 cells were plated on 15-cm plates. Next day, the medium was changed to custom made α-MEM media supplemented with 5 mM glucose, 2 mM glutamine and 50 ng/ml of recombinant WNT3a or vehicle for 24 hours. Cells were washed with cold PBS at the end of incubation and were harvested by scraping and centrifugation. The cell pellets were frozen on dry ice and shipped to Metabolon, Inc for analyses (Durham, NC) on dry ice. Four or five biological replicates (each approximately $8x10^6$ cells) were prepared for each condition. Samples were run on GC/MS and LC/MS/MS by Metabolon pipeline. A total of 208 metabolites were detected. The relative abundance of each metabolite was normalized to protein content. Student t-test was applied to identify biochemical that differed significantly between the groups.

5.5. DCA Treatment

DCA was dissolved in autoclaved water at 2 gr/L concentration and the pH was adjusted to ~ 7.2.

6. Figures

Figure 1. WNT3A Decreases Metabolites in Pentose Phosphate Pathway

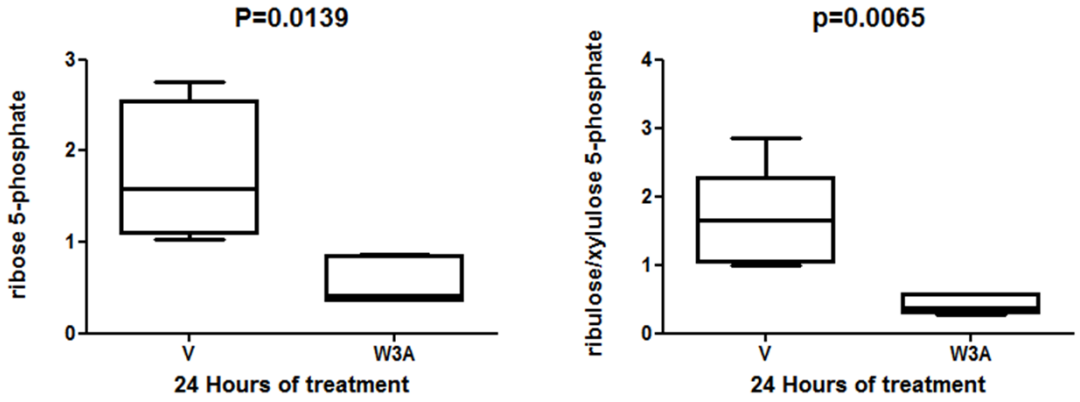

Relative abundance of intracellular ribose 5-phosphate (A) and ribulose 5 phosphate/xylulose 5-phosphate (B) after 24 hours of 50 ng/ml WNT3A treatment. N: 5, V: vehicle, W3A: WNT3A.

Figure 2. Schematic Representation of the Fates of Carbons 1, 3/4 and 6 on Glucose

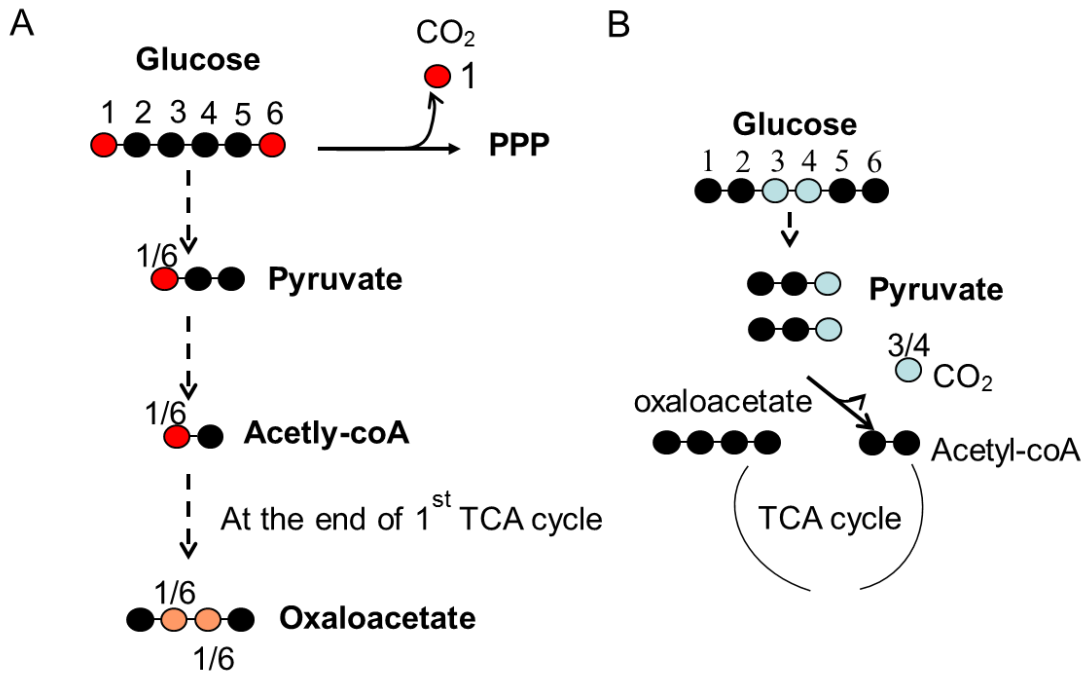

(A) Carbon 1 (red circle) of glucose is released as CO_2 at the step where glucose-6-phosphate is diverted to PPP. Carbon 1 also gets integrated in one of the central carbons in oxaloacetate. It later gets released after 3rd round of TCA cycle. Carbon 6 (red) is only released after the 3rd round of TCA cycle.

(B) Carbons 3 and 4 (blue) are only released when pyruvate is oxidized to acetyl-coA. PPP: pentose phosphate pathway

Figure 3. Schematic Representation of the CO_2-trap Design

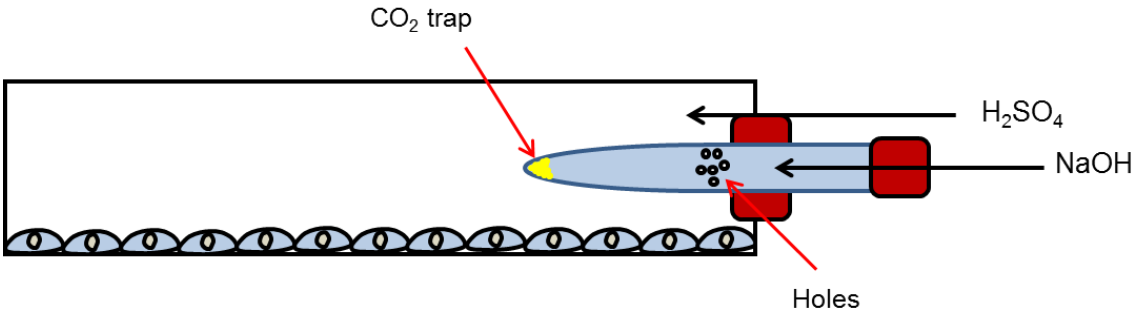

Cells are cultured in flasks sealed with stoppers with a tube containing holes inserted into the flasks during 24 hours of treatment. Treatment includes vehicle (V), WNT3A (W3A) together with radioactively labeled glucose. H_2SO_4 is injected to the cells at the end of treatment to gas the CO_2 that is trapped in the tube with NaOH.

Figure 4. WNT3A Represses Glucose Contribution to TCA Cycle and PPP

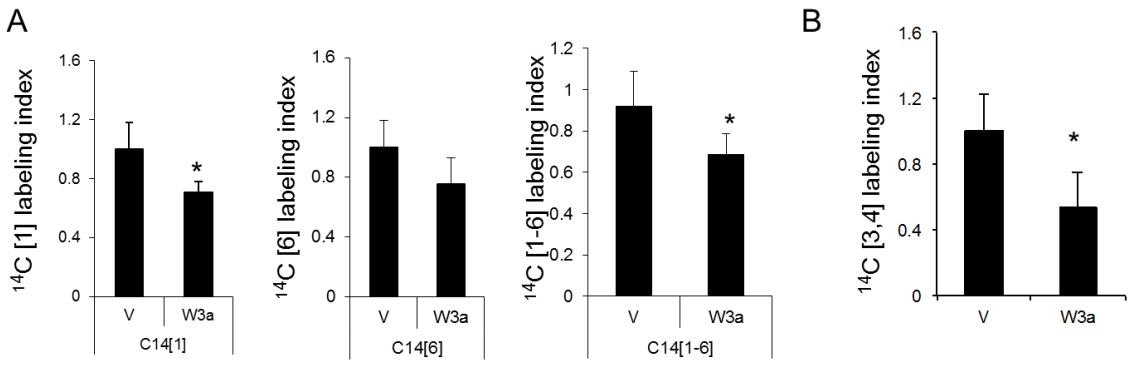

(A) CO_2 trapped during 24 hours of 50ng/ml WNT3A treatment with either $^{14}C_6$-glucose or $^{14}C_1$-glucose. CO_2 trapped from [$^{14}C_6$], [$^{14}C_1$], and [$^{14}C_6$ -$^{14}C_1$] was normalized to total glucose uptake and cell number.

(B) CO_2 trapped during 24 hours of 50ng/ml WNT3A treatment with glucose-^{14}C [3,4]. DPM (disintegration per minute) counts were normalized to total glucose uptake and cell number.

Figure 5. Schematic Representation of Genetic Crosses to Get Osteoblast Specific Ldha Deletion

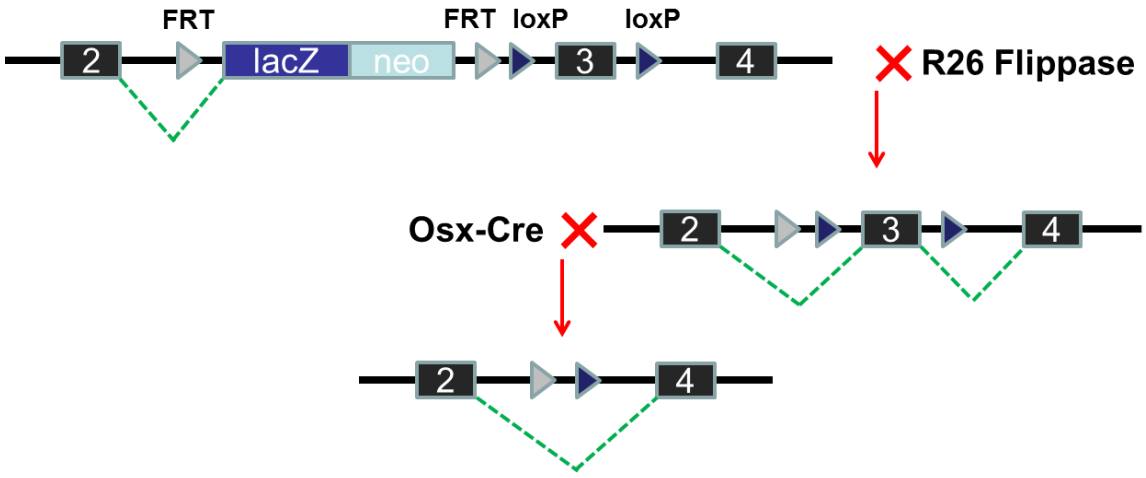

Knockout first allele crossed with Rosa26; Flippase mice to get floxed allele that is later crossed with Osx-Cre mice.

Figure 6. Osx-Ldha Mice have Lower Trabecular Bone at 1 Month of Age

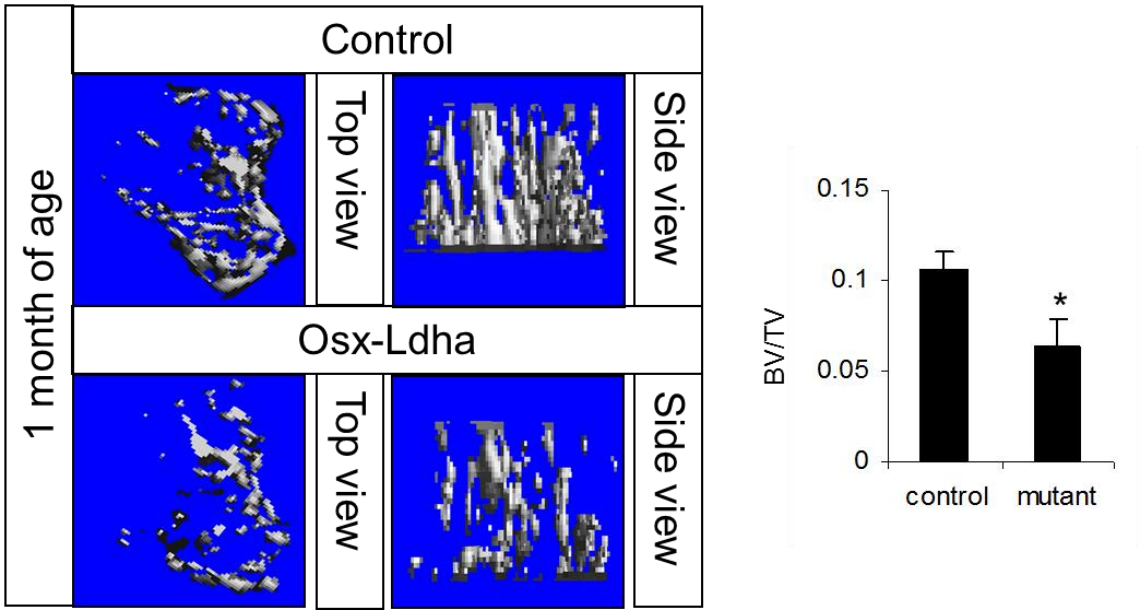

Proximal tibia from control and mutant (Osx-Ldha) mice was scanned with vivaCT at 1 month of age. 50 slides right under the growth plate (total of 0.8 mM) were analyzed and 3D images from the top and side views were prepared with Scanco Medical software. BV: bone volume; TV: tissue volume.

Figure 7. Osx-Ldha Mice have Reduced Trabecular Bone at 2 Months of Age

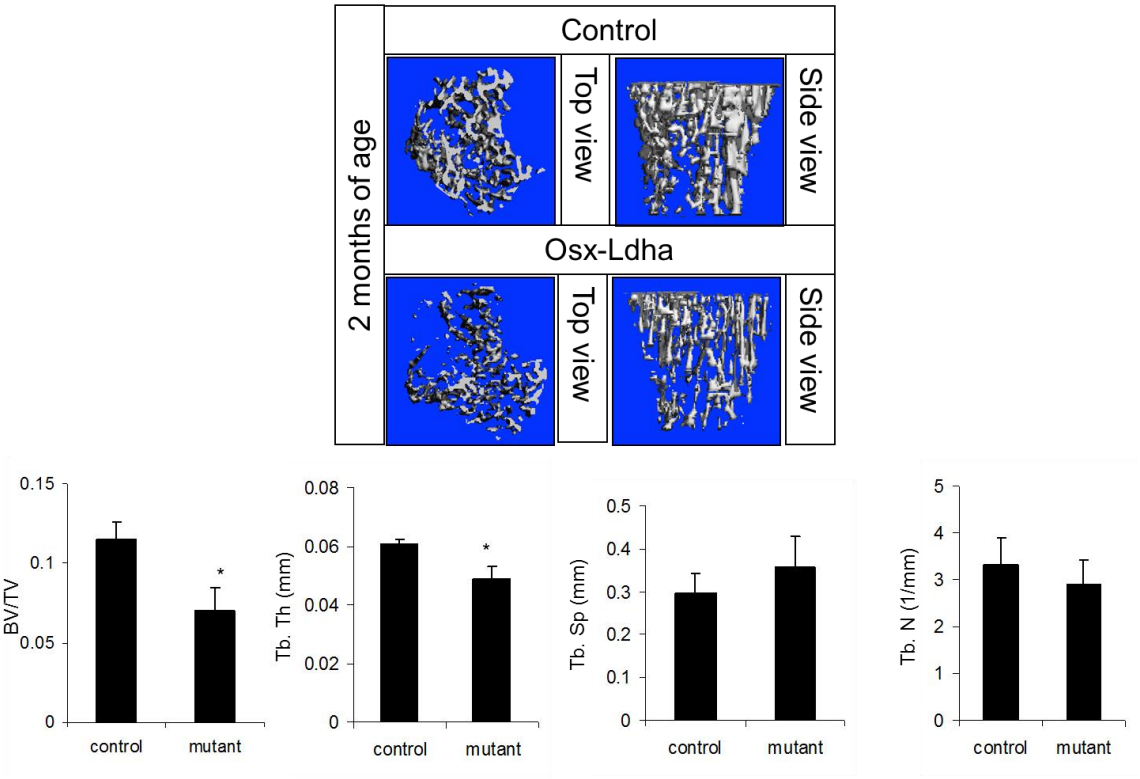

Proximal tibias harvested from control and Osx-Ldha mice were scanned with Scanco μCT 40. 100 slides under the growth plate, with a total of 1.6 mM, were analyzed and 3D structures were prepared with Scanco Medical software. BV: bone volume; TV: tissue volume. Tb. N: trabecular number; Tb. Th: trabecular thickness; Tb. Sp: trabecular spacing.

Figure 8. Body Weight of Control and Osx-Ldha Mice at 1 Month and 2 Months of Age

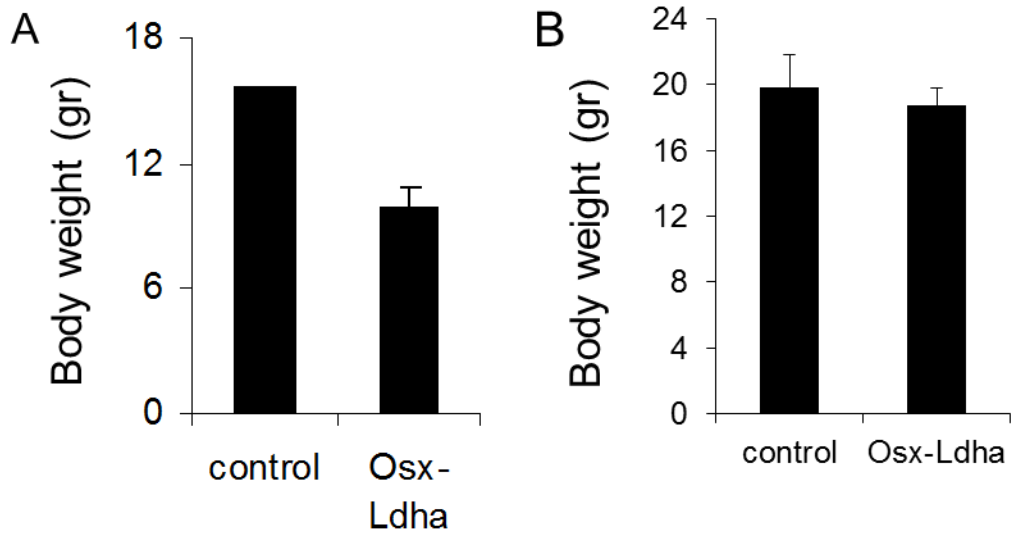

(A-B) Body weight (gr) of control and mutant (Osx-Ldha) animals at 1 month (A) and 2 months (B) of age.

Figure 9. Histology of Control and Osx-Ldha Animals

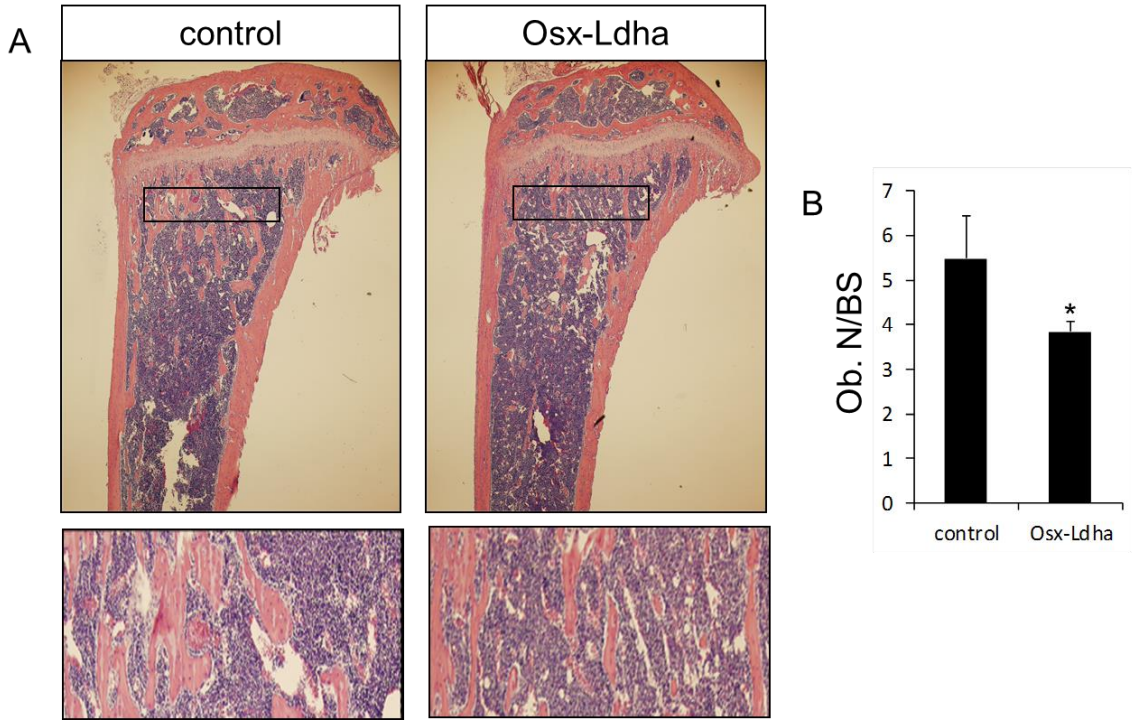

(A) 4x and 20x images of histological sections from control and Osx-Ldha animals at 2 months of age.

(B) Osteoblast number (Ob. N) per bone surface (BS) from experimental animals. Bioquant II is used for counting the cells.

Figure 10. Osteoclast Activity does not Change in Osx-Ldha Mice

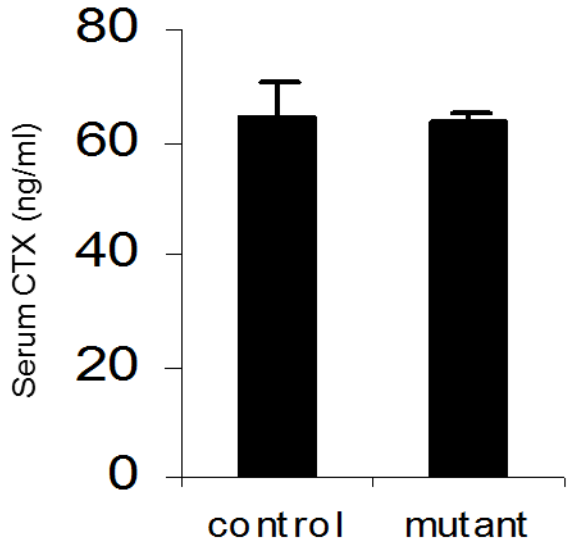

Serum was prepared from control and mutant (Osx-Cre) animals at 2 month of age after 6 hours of fasting. Serum CTX-I (ng/ml) is an indicator of osteoclast activity.

Figure 11. There is Reduced Osteoblast Activity in Osx-Ldha Animals

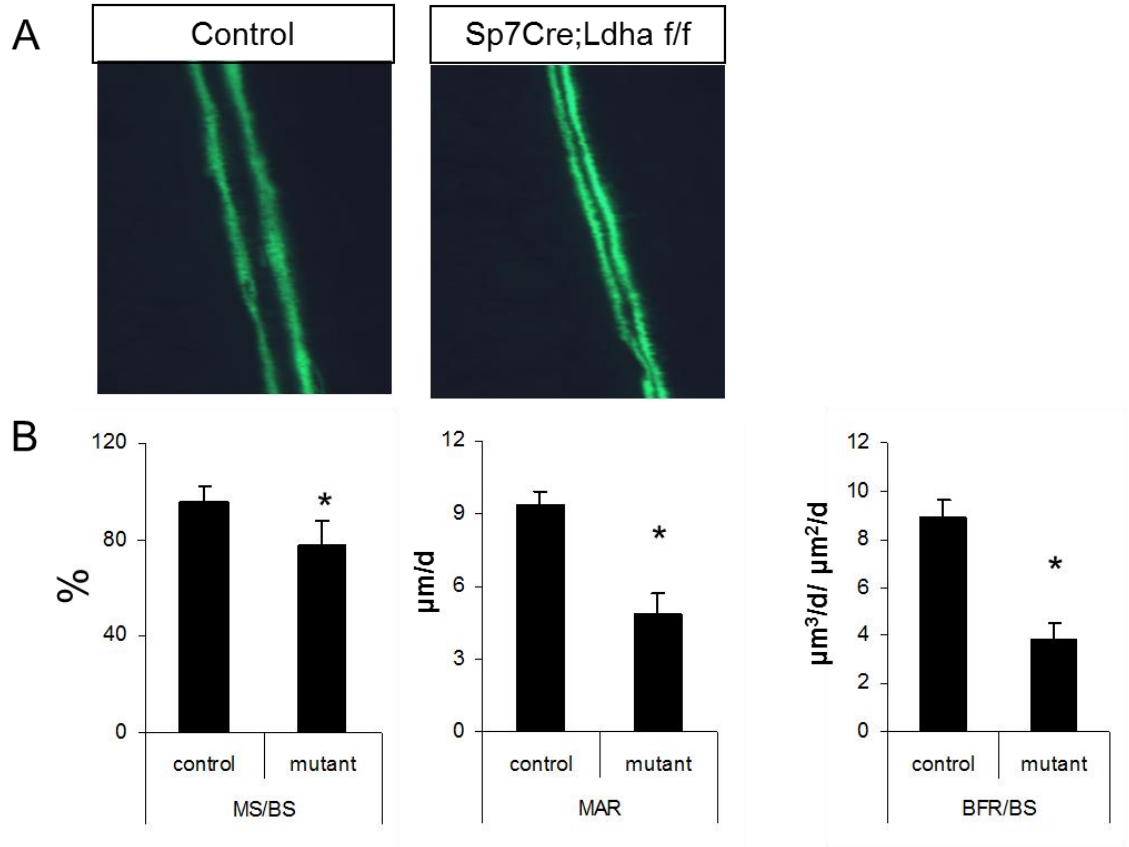

(A) Representative images of calcein double labeling in tibias of control and Osx-Ldha animals at endosteal region at 2 months of age.

(B) Bone formation parameters from endosteum at midshaft of tibias. MS/BS: mineralized surface/ bone surface; MAR: mineral apposition rate; BFR/BS: bone formation rate/bone surface.

Figure 12. Postnatal Ldha Removal does not Cause Size Defect

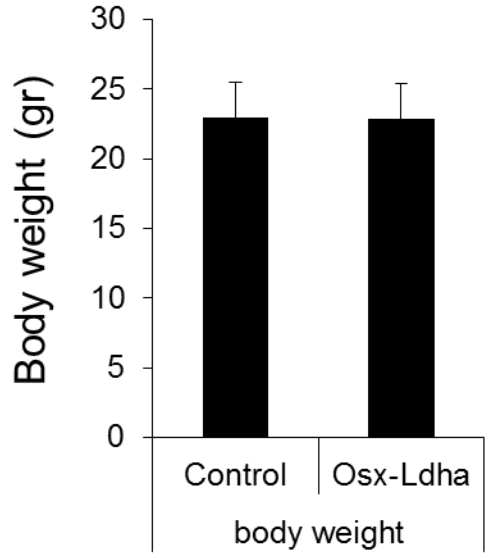

Osx-Ldha male mice were either kept on dox (doxycycline) all the time or were kept on dox from conception until 1 month of age. In the second group, dox was removed from 1 month to 2 months of age and animals in both groups were weighted at 2 months.

Figure 13. Postnatal Removal of Ldha Causes Trabecular Bone Loss

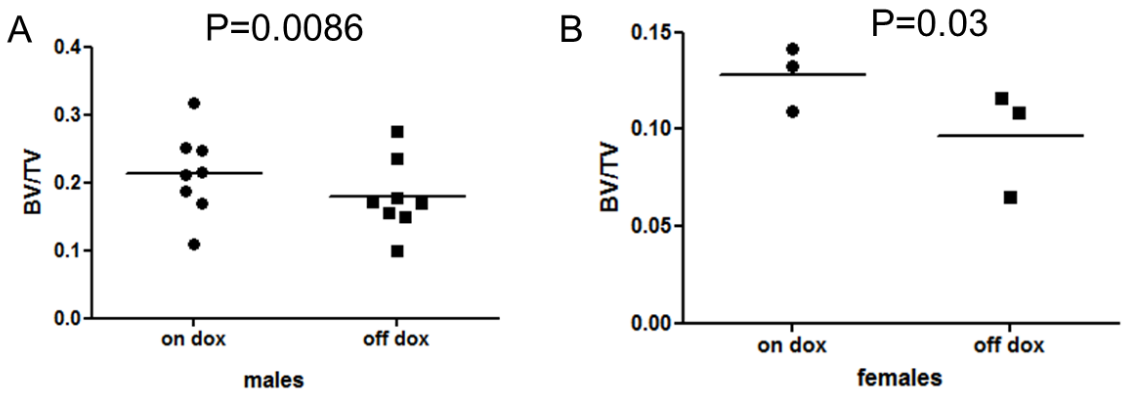

(A-B) Osx-Ldha mice were raised on doxycycline (dox) until one month of age, later half of the animals are removed from dox. Bone volume/tissue volume (BV/TV) from males (A) and females (B).

Figure 14. Increased BV/TV in Lrp5 HBM Animals at 3 Weeks

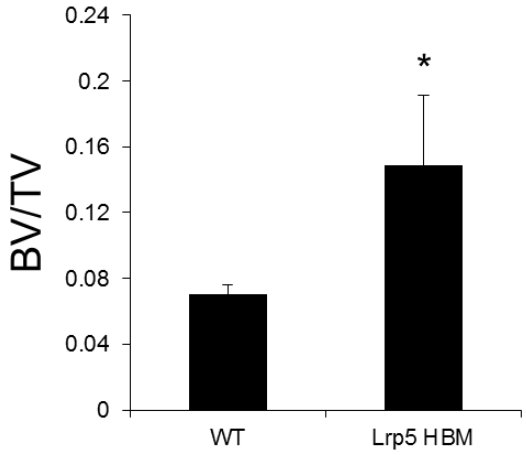

MicroCT analysis of tibias harvested from 3 weeks of wild type (WT) or Lrp5 HBM animals. 100 slices right under the growth plate is analyzed. Bone volume /tissue volume (BV/TV).

Figure 15. DCA Attenuates the High Bone Mass Phenotype in Lrp5 HBM Mice

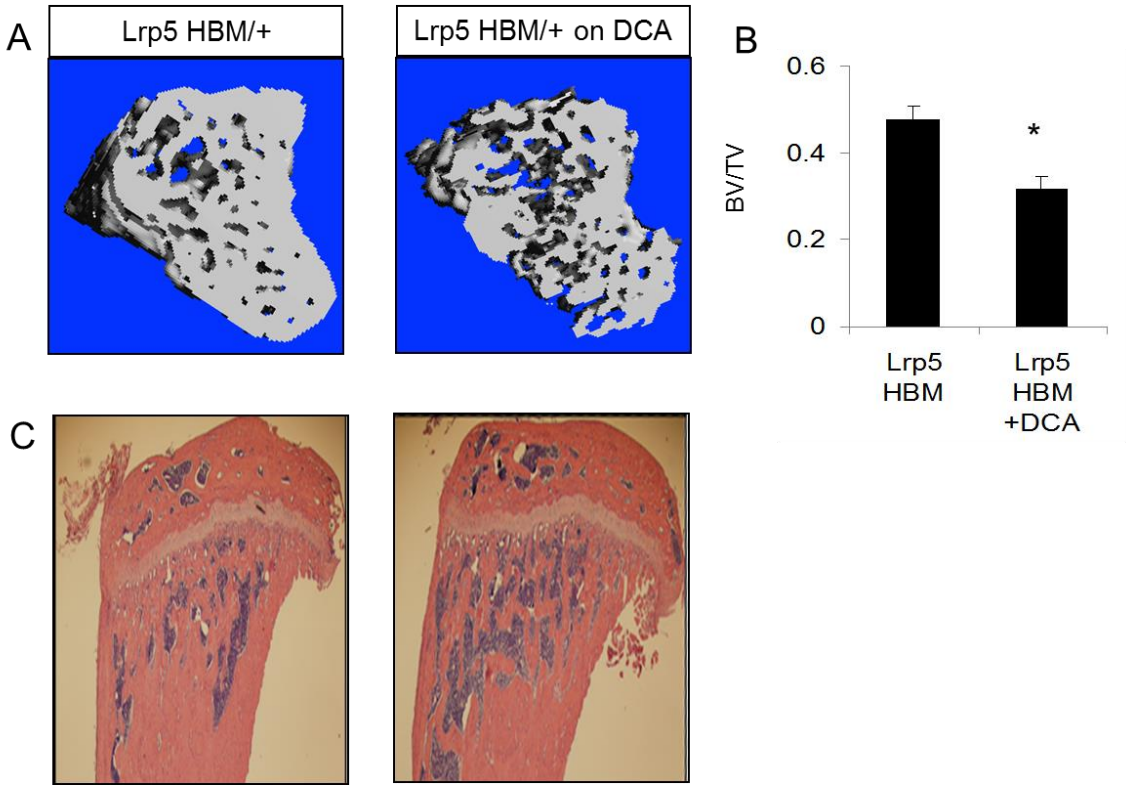

(A) Representative 3D images from Lrp5 HBM control and Dichloroacetate (DCA) treated animals. 100 slides under the growth plate from tibias were analyzed.

(B) Bone volume/Tissue volume (BV/TV) from both groups.

(C) Representative histological sections from control and DCA treated Lrp5 HBM/+ mice.

Figure 16. Hexosamine Biosynthesis Intermediate is reduced in WNT3A (50ng/ml) Treated Samples

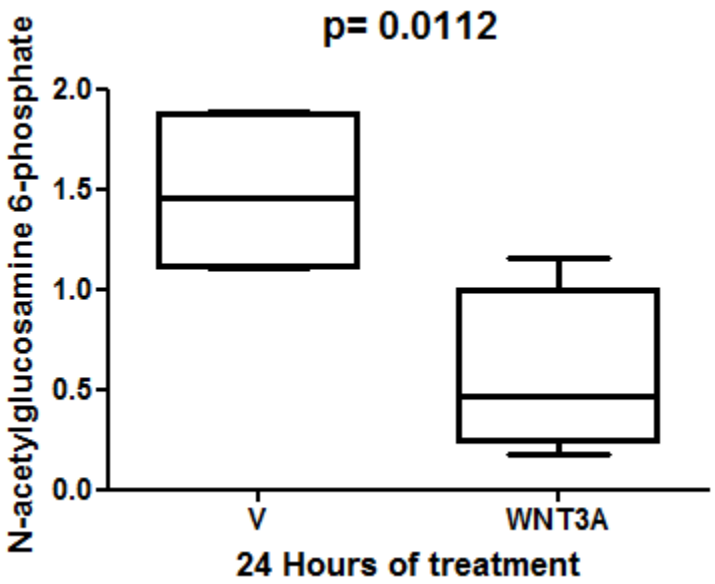

Relative abundance of intracellular N-acetyl glucosamine-6-phosphate in 24 hours treated control (V) and WNT3A (50ng/ml) samples. N=5 for control and N=4 for WNT3A.

References

Babij, P., Zhao, W., Small, C., Kharode, Y., Yaworsky, P.J., Bouxsein, M.L., Reddy, P.S., Bodine, P.V., Robinson, J.A., Bhat, B.*, et al.* (2003). High bone mass in mice expressing a mutant LRP5 gene. J Bone Miner Res *18*, 960-974.

Bouche, C., Serdy, S., Kahn, C.R., and Goldfine, A.B. (2004). The cellular fate of glucose and its relevance in type 2 diabetes. Endocr Rev *25*, 807-830.

Cohn, D.V., and Forscher, B.K. (1962). Aerobic metabolism of glucose by bone. J Biol Chem *237*, 615-618.

Cui, Y., Niziolek, P.J., MacDonald, B.T., Zylstra, C.R., Alenina, N., Robinson, D.R., Zhong, Z., Matthes, S., Jacobsen, C.M., Conlon, R.A.*, et al.* (2011). Lrp5 functions in bone to regulate bone mass. Nat Med *17*, 684-691.

DeBerardinis, R.J., Mancuso, A., Daikhin, E., Nissim, I., Yudkoff, M., Wehrli, S., and Thompson, C.B. (2007). Beyond aerobic glycolysis: transformed cells can engage in glutamine metabolism that exceeds the requirement for protein and nucleotide synthesis. Proc Natl Acad Sci U S A *104*, 19345-19350.

Esen, E., Chen, J., Karner, C.M., Okunade, A.L., Patterson, B.W., and Long, F. (2013). WNT-LRP5 signaling induces Warburg effect through mTORC2 activation during osteoblast differentiation. Cell Metab *17*, 745-755.

Fantin, V.R., St-Pierre, J., and Leder, P. (2006). Attenuation of LDH-A expression uncovers a link between glycolysis, mitochondrial physiology, and tumor maintenance. Cancer Cell *9*, 425-434.

Gilbert, H.F. (2000). Basic Concepts in Biochemistry: A Student's Survival Guide, second edition edn.

Goldman, R.D., Kaplan, N.O., and Hall, T.C. (1964). Lactic Dehydrogenase in Human Neoplastic Tissues. Cancer Res *24*, 389-399.

Gong, Y., Slee, R.B., Fukai, N., Rawadi, G., Roman-Roman, S., Reginato, A.M., Wang, H., Cundy, T., Glorieux, F.H., Lev, D.*, et al.* (2001). LDL receptor-related protein 5 (LRP5) affects bone accrual and eye development. Cell *107*, 513-523.

Holmen, S.L., Giambernardi, T.A., Zylstra, C.R., Buckner-Berghuis, B.D., Resau, J.H., Hess, J.F., Glatt, V., Bouxsein, M.L., Ai, M., Warman, M.L.*, et al.* (2004). Decreased BMD and limb deformities in mice carrying mutations in both Lrp5 and Lrp6. Journal of bone and mineral research : the official journal of the American Society for Bone and Mineral Research *19*, 2033-2040.

Kopperschlager, G., and Kirchberger, J. (1996). Methods for the separation of lactate dehydrogenases and clinical significance of the enzyme. J Chromatogr B Biomed Appl *684*, 25-49.

Le, A., Cooper, C.R., Gouw, A.M., Dinavahi, R., Maitra, A., Deck, L.M., Royer, R.E., Vander Jagt, D.L., Semenza, G.L., and Dang, C.V. (2010). Inhibition of lactate dehydrogenase A induces oxidative stress and inhibits tumor progression. Proc Natl Acad Sci U S A *107*, 2037-2042.

Portais, J.C., Voisin, P., Merle, M., and Canioni, P. (1996). Glucose and glutamine metabolism in C6 glioma cells studied by carbon 13 NMR. Biochimie *78*, 155-164.

Reitzer, L.J., Wice, B.M., and Kennell, D. (1979). Evidence that glutamine, not sugar, is the major energy source for cultured HeLa cells. J Biol Chem *254*, 2669-2676.

Rodda, S.J., and McMahon, A.P. (2006). Distinct roles for Hedgehog and canonical Wnt signaling in specification, differentiation and maintenance of osteoblast progenitors. Development *133*, 3231-3244.

Teo, C.F., Wollaston-Hayden, E.E., and Wells, L. (2010). Hexosamine flux, the O-GlcNAc modification, and the development of insulin resistance in adipocytes. Mol Cell Endocrinol *318*, 44-53.

Tu, X., Joeng, K.S., Nakayama, K.I., Nakayama, K., Rajagopal, J., Carroll, T.J., McMahon, A.P., and Long, F. (2007). Noncanonical Wnt signaling through G protein-linked PKCdelta activation promotes bone formation. Dev Cell *12*, 113-127.

CHAPTER 4

Intermittent PTH promotes bone anabolism by stimulating glycolysis via IGF-SGK1 signaling

1. Abstract

Teriparatide, a recombinant peptide corresponding to amino acids 1-34 of human parathyroid hormone (PTH), has been an effective bone anabolic drug in the clinic. However, it is not well understood how PTH signaling stimulates bone formation. Although multiple downstream effectors and crosstalk with different pathways have been uncovered, there remains uncertainty regarding the importance of these effectors in mediating the anabolic effects of PTH on bone. Here we have investigated a potential role of cellular glucose metabolism in PTH function. Using both MC3T3-E1 cells and primary calvarial cells, we showed that PTH enhanced glucose uptake and induced aerobic glycolysis while reducing the contribution of glucose to TCA cycle. These changes in glucose metabolism were mediated through a cAMP-IGF-PI3K-SGK1 signaling cascade. Moreover, in the mouse, pharmacological enhancement of pyruvate entering the TCA cycle suppressed the bone anabolic effect by PTH. Thus, stimulation of glycolysis via IGF signaling may be an important mechanism mediating the anabolic effect of intermittent PTH.

2. Introduction

PTH, a hormone secreted by parathyroid glands, plays a central role in calcium and phosphate metabolism. Calcium homeostasis is crucial for mineralization of newly formed bone among other processes. To maintain calcium homeostasis, PTH increases osteoclast activity to mobilize calcium from bone; it also promotes intestinal absorption and renal reabsorption of calcium. Patients with primary hyperparathyroidism experience bone loss due to enhanced bone resorption. Although continuously elevated PTH levels as in the case of hyperparathyroidism drive bone remodeling toward bone resorption, intermittent PTH (iPTH) treatment drive bone remodeling toward bone formation. Thus, depending on the duration and pattern of the elevation, increased PTH levels can lead to either bone anabolism or catabolism (Frolik et al., 2003; Kousteni and Bilezikian, 2008; Kraenzlin and Meier, 2011).

Daily injections of both the full length PTH (1-84) and the fragment of PTH (1-34), which is known as teriparatide, increase bone mass and reduce fractures in osteoporotic patients (Hodsman et al., 2005). The anabolic effect of PTH administration has been studied in mice and rats extensively. Although less studied, intermittent administration of parathyroid hormone related protein (PTHrP) peptide 1–36, a fragment of the other principal ligand of the PTH receptor, is also an anabolic agent (Horwitz et al., 2003).

The primary target of PTH is osteoblasts. PTH stimulates bone formation on the surface of cancellous and cortical bone, and increases the trabecular connectivity and improves the microarchitecture of the skeleton. Based on the histological studies, the increase in bone formation in response to PTH is mostly due to increased osteoblast numbers (Arlot et al., 2005; Dobnig and Turner, 1997). Different mechanisms have been proposed for the increase in osteoblast number, these including increased osteoblast differentiation via suppression of cell

replication (Pettway et al., 2005), attenuation of osteoblast apoptosis (Bellido et al., 2003; Jilka et al., 2009), and activation of quiescent lining cells (Dobnig and Turner, 1995; Kim et al., 2012). The relative contribution of each proposed mechanism has been controversial, depending on the site studied, duration of iPTH administration and the model used (Jilka, 2007; Kousteni and Bilezikian, 2008). iPTH also indirectly stimulates the development and activation of osteoclasts through regulation of the pro-osteoclastogenic receptor activator of nuclear factor kappa-B ligand (RANKL) and the anti-osteoclastogenic osteoprotegerin, both expressed by osteoblasts (Huang et al., 2004). There is evidence that osteoclasts might contribute to the anabolic action of PTH either by releasing stored growth factors from the bone matrix (IGFs, BMPs, TGF-β) or via factors secreted by osteoclasts (Martin and Sims, 2005). The anabolic function of iPTH treatment is suggested to be bi-phasic. In the early phase, PTH stimulates bone modeling (bone formation in new space) whereas extended PTH administration stimulates bone remodeling by enhancing both osteoblasts and osteoclasts with a positive balance towards bone formation (Dobnig et al., 2005; Hodsman and Steer, 1993; Lindsay et al., 2006).

The actions of PTH and PTHrP are mediated by a G protein coupled receptor, referred to as PTH receptor 1 (PTHR1) (Potts, 2005). Activation of PTH1R initiates several parallel signaling pathways. One of them is Gαs-mediated activation of adenylyl cyclase, which stimulates cAMP production, and subsequently activates protein kinase A (PKA). PKA then phosphorylates and activates CREB that translocates to the nucleus and binds the cAMP responsive elements (CRE). PTHR1 also stimulates Gαq-mediated activation of protein kinase C (PKC). In addition, PTH activates extracellular regulated kinase (ERK) signaling through both conventional G-protein dependent pathway and G-protein independent pathway via β-arrestins (Gesty-Palmer et al., 2006). By the use of different PTH fragments differentially activating the

various pathways, cAMP/PKA is proposed to be the main signaling cascade important for bone anabolism. For example, daily injections of PTH (1–31), which only activates cAMP production, produced an equivalent anabolic effect in rats compared to PTH (1-34), the teriparatide (Whitfield et al., 1996). On the other hand, PTH (3–38), which activates PKC but not cAMP production, did not cause an anabolic effect (Armamento-Villareal et al., 1997). Another PTH analog, D-Trp^{12}, Tyr^{34}-PTH (7–34) referred as PTH-βarr that selectively activates β-arrestin pathway, enhances trabecular but not cortical bone formation (Gesty-Palmer et al., 2009). Mice lacking β -arrestin2 have an altered anabolic response to PTH, but do not completely lose the response (Ferrari et al., 2005; Yang et al., 2007). Overall, PTH increases several signaling cascades, cAMP/PKA being the most characterized and prominent pathway for the bone anabolic function of PTH.

IGF signaling is required for the anabolic effect of iPTH. PTH stimulates the synthesis of IGF-I in rat and mouse osteoblasts *in vitro* (Linkhart and Mohan, 1989; McCarthy et al., 1989; Verheijen and Defize, 1995). IGF1 inhibition with a neutralizing antibody prevented the PTH-induced collagen synthesis (Canalis et al., 1989), alkaline phosphatase (ALP) activity and the expression of osteocalcin mRNA (Ishizuya et al., 1997). In rats, iPTH increased IGF-I mRNA levels more than 2-fold (Watson et al., 1995). IGF1 knockout mice failed to increase bone anabolism in response to iPTH (Bikle et al., 2002; Miyakoshi et al., 2001). More importantly, osteoblast-specific deletion of IGF1 receptor (IGF1R) ablated PTH-induced bone formation in the mouse (Wang et al., 2007). In patients, 12 to 24 months of teriparatide treatment increase IGF-II expression on periosteal surfaces (Ma et al., 2006). Thus, IGF level is increased by PTH and IGF signaling is tightly linked with the anabolic function of PTH.

PTH has also been shown to cross talk with WNT signaling, an established pathway that regulates osteoblast differentiation and function. Based on mRNA micro-array data, PTH regulates the expression of WNT signaling components both *in vitro* and *in vivo*, mostly through cAMP/PKA (Kulkarni et al., 2005; Li et al., 2007; Qin et al., 2003). More strikingly, PTH increases protein levels of β-catenin, a key transducer of WNT signaling, in a manner dependent on both PKA and PKC (Tobimatsu et al., 2006). Knocking down β-catenin attenuates PTH-induced osteoblast differentiation *in vitro* (Tian et al., 2011). PTH was shown to stabilize β-catenin through inactivation of GSK-3β in a PKA/cAMP dependent manner (Suzuki et al., 2008). PTH can also regulate WNT signaling through regulation of WNT antagonists, as PTH inhibits DKK1 (Kulkarni et al., 2005) and SOST (Keller and Kneissel, 2005), both of which interfere with WNT interaction with the co-receptors LRP5/6. Moreover, PTH1R has been shown to dimerize with LRP6 to activate WNT/β-catenin signaling (Wan et al., 2008). More recently, PTH1R was demonstrated to directly interact with disheveled proteins, the intracellular adaptor proteins important for WNT-β-catenin signaling (Romero et al., 2010). However, PTH is still able to enhance bone formation either in the presence of Dkk1 overexpression (Yao et al., 2011), or in the absence of SOST (Kramer et al., 2010), suggesting that PTH can induce bone anabolism independent of WNT signaling.

PTH can alter cellular glucose metabolism. PTH induces glucose uptake in rat osteoblastic cells (PyMS) (Zoidis et al., 2011). In early studies, PTH was shown to alter cellular metabolism towards generating more lactate. Metaphyseal bone prepared from PTH injected mice (Borle et al., 1960), or PTH treated calvarial cells (Neuman et al., 1978; Rodan et al., 1978) exhibited more active lactate production than the controls even in aerobic condition. However,

the relevance of these metabolic alterations in the context of bone anabolism has remained unknown.

We recently showed that enhanced aerobic glycolysis is critical for WNT3A induced osteoblast differentiation (Esen et al., 2013). In light of this work, here we investigate the potential role of metabolic alterations for the anabolic effect of PTH. In MC3T3-E1 cells and neonatal calvarial cells, we showed that PTH enhances glucose uptake, induces aerobic glycolysis, activates pentose phosphate pathway but reduces contribution of glucose to TCA cycle. PTH-induced glucose utilization required IGF-PI3K-SGK1 signaling. In the mouse, co-administration of PTH and a chemical that promotes pyruvate entering the TCA cycle impaired the bone anabolic effect by PTH alone. Thus, changes in cellular glucose metabolism may be an important mechanism mediating the anabolic effect of intermittent PTH.

3. Results

3.1 PTH Enhances Aerobic Glycolysis

To uncover a potential link between the PTH and cellular metabolism, we investigated the effect of PTH on glucose consumption in preosteoblastic MC3T3-E1 cells. Direct measurements of glucose in the culture media indicated that PTH significantly increased glucose consumption after 48 hours of treatment in a dose-dependent manner (Figure 1A, B). A similar effect was observed with PTHrP (Figure S1). Importantly, primary cultures of calvarial osteoblastic cells from neonatal mice also increased glucose consumption in response to PTH (Figure 1C). Moreover, cells treated with PTH for 24 or 48 hours exhibited a progressive increase in the rate of glucose uptake (Figure 1D). In contrast, PTH treatment did not alter total cellular protein content in MC3T3-E1 cells after 48 hours (Fig S2). Stimulation of glucose

consumption by PTH did not require serum (Fig S3). Thus, PTH increases glucose utilization in both primary and cell culture systems.

We then examined the metabolic changes in response to PTH. We first monitored metabolic activities with the Seahorse extracellular flux analyzer. PTH treatment noticeably enhanced both oxygen consumption rate (OCR) and extracellular acidification rate (ECAR) after 24 hours of treatment (Figure 2A). Quantification of oxygen consumption in response to the various mitochondria stressors revealed an increase in all parameters of mitochondrial activity in the PTH-treated cells (Figure 2B). Similarly, the extracellular acidification rate (ECAR), likely driven by lactate production, was higher in the PTH-treated cells both under the basal condition and in response to the mitochondria stress tests (Figure 2C, D). Consistent with the ECAR data, lactate concentration in the medium increased significantly by PTH treatment in both MC3T3 and calvarial cells after 48 hours (Figure 2E, F). Thus, PTH enhances both mitochondrial respiration and lactate production.

We then looked into molecular changes that could lead to metabolic changes in response to PTH. One-hour treatment of MC3T3 cells with PTH or PTHrP increased Hexokinase II (HK2, phosphorylating glucose at the very first and rate-limiting step of glucose catabolism), lactate dehydrogenase A (LDHA, catalyzing the conversion of pyruvate to lactate), and pyruvate dehydrogenase kinase 1 (PDK1, inactivating the pyruvate dehydrogenase complex to suppress pyruvate from entering the TCA cycle) (Figure 3A, left). These enzymes remained elevated after 48 hours of PTH treatment in MC3T3 cells (Figure, 3A, right). Similarly, PTH increased the levels of these enzymes in calvarial cells after 24 hours of treatment (Figure 3B). Importantly, intraperitoneal injection of PTH increased the enzymes in bone protein extracts within 6 hours in a dose-dependent manner (Figure 3C and S4A); the enzymes remained upregulated for at least

12 hours *in vivo* (Figure S4B). Therefore, PTH stimulates critical glucose metabolism enzymes both in *in vivo* and *in vitro* models.

To begin to address the role of the metabolic enzymes in regulating glucose metabolism, we performed functional studies with LDHA. We knocked down LDHA in MC3T3 cells by using shRNA that was followed by 48 hours PTH treatment. LDHA knockdown cells did not increase glucose consumption in response to PTH, while controls infected by lentivirus with GFP targeting shRNA responded as expected (Figure 3D). We also prepared calvarial cells from Ldha $^{f/f}$ animals. Similarly, removing LDHA from calvarial cells by infecting with adenovirus expressing Cre recombinase blunts the effect of PTH on glucose consumption (Figure 3E). Thus, upregulation of LDHA is an important step for PTH-induced glucose consumption.

3.2 PTH Suppresses Glucose Oxidation in TCA cycle but Stimulates PPP

PTH has been shown to have a more robust effect on differentiated MC3T3 cells (McCauley et al., 1996; Schiller et al., 1999). To take advantage of this feature, we performed subsequent PTH experiments with MC3T3 cells that underwent differentiation in an osteogenic medium containing ascorbic acid and β-glycerol phosphate for three days. We confirmed that the cells exhibited an increase in the osteoblast marker Alkaline Phosphates (AP) together with a slight change in the levels of PTH1R (Figure S5). Differentiated MC3T3 cells significantly increased glucose utilization and lactate production as early as 6 hours of treatment, which was consistent with increased phosphorylation of IGF1R at 1 hr and 6 hrs of PTH treatment (Figure 4A-C). To gain further insights about the fate of glucose, we examined the contribution of glucose towards TCA cycle. To this end, we used a glucose tracer radioactively labeled at carbon positions 3 and 4 (^{14}C [3, 4]-glucose) to determine the relative amount of glucose entering the

TCA cycle, by tracking the amount of radioactive CO_2 produced during the conversion of pyruvate to acetyl-CoA (Figure S6, S7). We calculated the relative TCA contribution index by normalizing the CO_2 radioactivity level to the total glucose uptake and the total cell number in each culture. We found that 24 hours of PTH treatment reduced the glucose contribution to TCA by ~70% (Figure 4E), even though it increased glucose consumption and lactate production by ~40% and ~60 % respectively (Figure S8). We next examined the flux of glucose towards pentose phosphate pathway (PPP) using glucose specifically labeled at C_1 ([$^{14}C_1$]-Glc) or C_6 ([$^{14}C_6$]-Glc). C_1 in glucose is expected to release as CO_2 through either PPP or after the 3rd cycle after pyruvate enters the TCA cycle, whereas C_6 is only released as CO_2 from the latter (Figure S7). We found that CO_2 released from C_6, after normalization to total glucose consumption and cell number, was reduced in the PTH-treated group (Figure 4F). This could be due to simply reduced contribution of glucose towards TCA cycle, which is consistent with the previous data (Figure 4E); or due to exit of TCA cycle intermediates in the first two cycles before the release of C_6- CO_2. Since the reduction of C [3, 4] and C_6 release is comparable, the former possibility is more likely to happen. The flux through PPP, calculated as the difference of C_1-C_6 CO_2, was elevated in the PTH-treated cells. Thus, PTH enhances PPP and lactate-producing glycolysis while suppressing contribution of glucose to TCA cycle.

3.3 PTH Regulates Glycolysis through IGF Signaling

We next investigated the potential involvement of WNT and IGF signaling in PTH induced metabolic alterations. Neither DKK1 nor Frizzled-8 Fc Chimera blocked augmented glucose utilization (Figure 5A), and the effect of PTH and WNT3A was additive (Figure 5B), indicating that PTH regulates glucose metabolism independent of WNT signaling. We then

tested the involvement of IGF in the PTH-driven metabolic changes. In keeping with previous findings, PTH increased mRNA levels of Igf1, Igf2 and Igfbp5 by 6 hours of treatment (Figure 5C). Furthermore, intraperitoneal injection of PTH enhanced the phosphorylation of IGF1R, readout of IGF signaling, in mice that was detected in bone extracts after 6 hours (Figure 5D). Importantly, inhibition of IGF signaling with two different inhibitors blocked PTH-induced glucose consumption, phosphorylation of IGF1 receptor (IGF1R), as well as LDHA and HK2 induction (Figure 5E and S9). We also confirmed that inhibition of IGF1R suppressed PTH-induced glucose utilization by the differentiated MC3T3 cells (Figure 4D). To further test the function of IGF1R, we genetically deleted Igf1R in primary calvarial cells *in vitro* by infecting Igf1R $^{f/f}$ cells with an adenovirus expressing Cre. Removal of IGF1R completely abolished the PTH-induced increase in glucose consumption (Figure 5F). Finally, IGF1 can replace PTH to increase glucose consumption and lactate production in both MC3T3 and calvarial cells (Figure 4G, H). In summary, IGF signaling is required for the PTH-induced glucose consumption and enzyme up-regulation.

3.4 PTH-IGF Signaling Activates SGK1 through PI3K to Regulate Metabolism

We then investigated the signal transduction mechanism downstream of IGF signaling. IGF1 signaling is known to activate PI3K (phosphatidylinositol 3-kinase). Inhibition of PI3K with LY294002 partially suppressed PTH-induced glucose consumption at 5-10 μM, and completely abolished it at 25-100 μM (Figure 6A). It is noteworthy that PI3K inhibition blocked basal glucose metabolism at all concentrations (Figure 6A). The drug also suppressed PDK1 and HK2 levels (Figure 6C). On the other hand, specific inhibition of p110β-specific PI3K activation with TGX-221 did not significantly affect PTH-induced glucose consumption even though it

suppressed basal-level P-AKT S473 (Figure 6B). Because PTH induced P-AKT both *in vivo* and *in vitro* (Figure 5D) (Figure 6E), we tested the role of AKT by inhibiting its activity with MK2206 in MC3T3 cells. MK2206 greatly suppressed AKT phosphorylation but did not impair PTH-induced glucose consumption (Figure 6G). Thus, PTH regulates glucose metabolism independent of AKT activation.

We next explored the potential role of SGK1 in PTH-stimulated glucose metabolism. PTH treatment increased phosphorylation of NDRG1, a target of Serum- and glucocorticoid-inducible kinase 1 (SGK1) (Garcia-Martinez and Alessi, 2008) both *in vivo*, in calvarial cells and in MC3T3 cells (Figure 5D, 6E and 6F). Previous studies have established that the activation of SGK1 is dependent on the activation of PI3K (Park et al., 1999). This was confirmed by our finding that LY 294002 but not TGX-221 abolished P-NDRG1 (Figure 6D). Inhibition of SGK1 with two different inhibitors each abolished glucose consumption, LDHA upregulation and lactate production (Figure 6H). Furthermore, SGK1 inhibition suppressed PTH-induced ECAR or OCAR both at the basal condition and in the presence of various mitochondria stressors, whereas AKT inhibition had little or no effect (Figure 6I). Thus, PTH alters cellular metabolism through a PI3K-IGF-SGK1 dependent signaling cascade.

3.5 PTH Regulates Glucose Metabolism through a cAMP-dependent Mechanism

Our results so far have established that PTH reprograms glucose metabolism through Igf-Sgk1 signaling. We next investigated the upstream signaling mechanism leading to IGF-SGK1 activation. PTH activates three main signaling cascades that are cAMP/PKA, PLC/PKC, and ERK. To distinguish which signaling pathway is more important for PTH to activate SGK1 and glucose metabolism, we assessed the effect of different PTH fragments known to activate

differentially the various intracellular signaling cascades (Armamento-Villareal et al., 1997; Whitfield et al., 1996). PTH (1-31), mostly activating cAMP/PKA, enhanced glucose consumption and activated SGK1, with potency similar to that of teriparatide (Figure 7A, B). In contrast, PTH (3-34), activating mostly PKC, only modestly stimulated glucose consumption at the higher concentration (Figure 7A), and did not enhance SGK1 activity even at the higher concentration (Figure 7B). To test whether cAMP was sufficient to cause the metabolic changes, we used Forskolin to activate adenylyl cyclase. Forskolin stimulated glucose consumption potently (Figure 7C); this result is consistent with the literature demonstrating that Forskolin can increase IGF1 production (McCarthy et al., 1990). More importantly, we were able to block the Forskolin effect with an IGF1R inhibitor (Figure 7D). Interestingly however, the PKA inhibitor H-89 had no effect on PTH-induced glucose consumption or SGK1 activation, even though it blocked β-catenin accumulation (Figure 7E). H89 also had minimal effects on PTH-induced expression of Igf1 and igfbp5 mRNA (Figure 7F). Unexpectedly, H-89 at higher concentrations increased basal glucose consumption (Figure S10). Inhibition of the PKC pathway with either the PLC inhibitor U73112 or PKC inhibitor ro-318220 had no effect on glucose metabolism (Figure S11). Finally, inhibition of ERK pathway with two different inhibitions, PD98059 and U0126, did not impair PTH-induced glucose consumption (Figure S12 A, B). Overall, PTH enhances glucose metabolism through a cAMP-dependent but PKA-independent mechanism.

3.6 Metabolic Regulation Contributes to the Anabolic Effect of iPTH *in vivo*

We finally examined the role of metabolic alterations in PTH-induced bone formation *in vivo*. We showed *in vitro* that PTH enhanced glucose utilization while suppressing glucose entry to TCA cycle. To investigate the importance of this metabolic switch, we decided to use

dichloroacetate (DCA) that represses the activity of PDKs, thus enhancing glucose metabolism via the TCA cycle. As expected, DCA prevented PTH-induced glucose utilization in both undifferentiated and differentiated MC3T3 cells (Figure 8A). We administered PTH intermittently to 3-month-old BL6 male mice for one month with or without DCA co-treatment. PTH did not alter body weight whereas DCA caused a slight but statistical significant decrease in body weight (Figure 8B). PTH increased serum lactate levels, but the effect was abolished by co-administration of DCA, even though DCA alone did not affect serum lactate levels (Figure 8C). As expected, PTH alone increased proximal tibial trabecular BV/TV as determined by microCT analyses; this was coupled with a statistically significant increase in trabecular thickness (table 1) (Figure 8D). Importantly, co-administration of DCA attenuated the PTH-induced increase in BV/TV (Figure 8D) (table 1). The effect of PTH on cortical bone, although relatively mild in comparison, was also suppressed by DCA (table 2). Histology confirmed that PTH alone increased trabecular bone mass but the effect was suppressed by DCA (Figure 8E). Thus, suppressing the glucose oxidation in TCA cycle is critical for the anabolic role of PTH.

We next investigated the underlying cellular basis for the DCA-mediated suppression of PTH effect. Histomorphometry showed a higher osteoblast number per bone surface in PTH-treated over control mice, and that the increase was reduced by DCA co-administration (Figure 8F-left). Dynamic histomorphometry revealed that mineral apposition rate (MAR) and bone formation rate (BFR/BS) were increased by PTH, but were suppressed by DCA co-administration (Figure 8H, I). PTH alone or together with DCA did not cause a significant change in osteoclast number per bone surface (Figure 8F-right). However, PTH alone increased the serum level of CTX-I (a degradation product of type I collagen used as an indicator of total osteoclast activity), and DCA co-treatment did not significantly affect the PTH effect (Figure

8G). Overall, PTH-induced glucose metabolism is required for enhances osteoblast number and function.

4. Discussion

Here we have provided evidence that PTH stimulates bone anabolism in part through reprogramming of cellular glucose metabolism. Specifically, PTH treatment increases overall glucose consumption and lactate-producing glycolysis. PTH also enhances glucose metabolism through PPP, but suppresses mitochondrial metabolism of glucose despite increased mitochondrial respiration. The metabolic regulation by PTH appears to be indirect as it is mediated through upregulation of Igfs that in turn activates SGK1 to stimulate glycolysis and mitochondrial respiration (Figure S13 for proposed model). Functionally, reversing the PTH-induced metabolic reprogramming with DCA suppressed the bone anabolic effect of PTH.

The present study improves our understanding of signaling cascades downstream of PTH. Here we showed that PTH regulates SGK1 through a cAMP-IGF1-PI3K dependent pathway. SGK1 can be phosphorylated by the phosphoinositide-dependent protein kinase (PDK1) at Thr^{256} in the activation loop following the priming phosphorylation at Ser^{422} by mTORC2 (Tessier and Woodgett, 2006). In our experiments, PI3K inhibitor completely blocked glucose uptake and SGK1 activation in response to PTH. However, phosphorylation of AKT at Ser^{473}, another target for mTORC2, did not correlate with SGK1 activation (Figure 4C, S14 A). Thus, PTH seems to activate SGK1 without stimulating the overall activity of mTORC2. The role of SGK1 in bone and its contribution for the bone anabolic effect of PTH *in vivo* remains to be investigated.

DCA alone did not have any effect on the bone parameters we looked at as well as osteoblast, osteoclast numbers or activities. This might be explained by couple theories; under basal conditions PDK activities might be so low that inhibiting further would not have a phenotype. On the other hand, PTH treatment increases PDK levels so that suppressing PDK activities by DCA has a robust effect. Pyruvate dehydrogenase complex (PDC), which controls pyruvate oxidation, is regulated not only by PDKs but also by pyruvate dehydrogenase phosphatases that catalyze the dephosphorylation and activation of the complex. It is also possible that PTH might reduce phosphatases making PDC activity more prone to changes in PDK1 activity. Further studies are required to answer these questions.

The importance of increased mitochondrial respiration and capacity in response to PTH remains to be investigated further. The suppression of glucose flux towards TCA cycle suggests an increase in mitochondrial metabolism from other nutrient sources. The fact that SGK1 inhibition blocks mitochondrial parameters suggests a central role for SGK1 in metabolic regulation in general besides PTH-induced glycolysis.

Establishing an *in vitro* culture system mimicking the bone anabolic effect of PTH *in vivo* has been a roadblock to studying the mechanism of PTH action. It is difficult to discriminate between anabolic and catabolic actions of PTH *in vitro.* We mostly focused on 24 to 48 hours of treatments in undifferentiated MC3T3 cells, or 6 to 24 hours treatment in differentiated MC3T3 cells, because at those time points we observed the most striking effects on glucose uptake, glycolysis and mitochondrial respiration. One concern is that PTH has a short life in the circulation *in vivo* while it stays stable up to 72 hours *in vitro*. However, the activation of downstream signaling cascades in the samples prepared from 48 hours of *in vitro* PTH treatment were comparable with samples prepared 6 hours after one time PTH injection *in vivo*. During

PTH treatment, downstream signaling pathways have been regulated temporally (Fig S14B). Moreover, differentiated MC3T3 cells reprogrammed their glucose metabolism more acutely and robustly. Further research is needed to define the changes in the signaling pathways in response to PTH at different stages and its relationship with the metabolic regulation to better understand this process.

The current finding that PTH regulates cellular metabolism may have implications to understanding the association of metabolic disorders with PTH elevation. Hyperparathyroidism has long been linked with a high frequency of glucose intolerance and type 2 diabetes mellitus (DM) (Taylor, 1991; Werner et al., 1974) as well as cardiovascular abnormalities (Valdemarsson et al., 1998).

On the other hand, intermittent PTH treatment only showed an adverse effect on glucose tolerance acutely and this effect was diminished after chronic administration (Anastasilakis et al., 2007). It is critical to assess the effect of PTH on different tissues to understand the systemic responses. Overall, our study describes PTH induced metabolic alterations in which glucose utilization is increased and used through glycolysis and PPP over oxidative phosphorylation despite the abundance of oxygen. More importantly, these alterations are critical for the anabolic effect of PTH.

5. Experimental Procedures

5.1 Mouse Strains

C57BL/6J mice from Jackson Laboratory were used for PTH injections. LDHA strain was from Eucomm and IGF1R floxed mice (B6;129-*Igf1r*^{tm2Arge}/J**)** was from Jackson Laboratories.

5.2 Analyses of Postnatal Skeleton

μCT analyses were performed with Scanco μCT 40 (Scanco Medical AG) according. Quantification of the trabecular bone in the tibia was performed with 35 μCT slices, total of 0.56 mm right below the growth plate. For cortical bone, 50 slices from midshalf were analyzed.

For paraffin sections, bones were fixed in 10% buffered formalin overnight at room temperature on a rocking platform. After fixation, tissue was washed with PBS and decalcified in 14% EDTA with daily change of solution for 2 weeks. At the end of decalcification, bones were processed for paraffin embedding and then sectioned at 6 μm thickness. Sections were used for H&E and TRAP staining following the standard protocols. For dynamic histomorphometry, mice were injected intraperitoneally with calcein (20 mg/kg, Sigma, St. Louis, MO) at 10 and 2 days before sacrifice, and bones were fixed in 70% ethanol and embedded in methyl-methacrylate for plastic sections. Both static and dynamic histomorphometry were performed with the commercial software Bioquant II.

For serum-based biochemical assays, mice were first fasted for 6 hours and then get anesthetized by using xyline/ketamine mix before blood collection. Blood was incubated at room temperature for 30 mins, spinned down for 5 minutes and then serum was collected. Serum CTX-I assay was performed using the RatLaps ELISA kit (Immunodiagnostic Systems, Ltd.). Serum lactate was measured using Lactate assay kit from Eton Biosciences.

5.3 Calvarial Osteoblast Culture

Calvarial cells were prepared as explained in chapter 2. Briefly, frontal and parietal bones (FPN) are dissected out from newly born mice (0-5 days) and incubated with collagenase for

digestion. Cells were strained through 70μM filters and plated in culture medium (alpha MEM with 20% FBS and 1% Pen Strep)

5.4 Western blot

Western blots were done as explained in chapter 2

5.5 Quantitative PCR

RNeasy kit (Qiagen) was used for RNA extraction. RNase-free DNase kit (Qiagen) was used following manufacturer's instructions. RNA, cDNA preparation Real Time PCR was done as discussed in chapter 2. The primer sequences are as follows:

18S F CGGCTACCACATCCAAGGAA

18S R GCTGGAATTACCGCGGCT

Ldha F: TGGAAGACAAACTCAAGGGCGAGA

Ldha R: TGACCAGCTTGGAGTTCGCAGTTA

Igf1 F CTGGACCAGAGACCCTTTGC

Igf1 R GGACGGGGACTTCTGAGTCTT

Igf2 F CCGTGGGCAAGTTCTTCCAATATG

Igf2 R ACGATGACGTTTGGCCTCTCTGAA

Igfbp5 F TGGTGTGTGGACAAGTACGGAATG

Igfbp5 R ACTCAACGTTACTGCTGTCGAAGG

5.6 Cell Culture, Glucose and Lactate Measurements

For routine cultures, MC3T3 E1 subclone 4 cells were grown in ascorbic acid free α-MEM medium (Gibco a10490-01) and switched to complete α-MEM (Gibco, cat#12561) during treatments, both of which supplemented with 10% heat inactivated FBS (Gibco) and Pen Strep (Gibco, cat#14140).

PTH (1-34), PTH (3-34) and PTH (1-31) are obtained from Bachem Biosciences. All PTH fragments were dissolved in a solution containing 0.9% NaCI, 0.1% BSA, 0.001 N HCI mixed in sterile water. This solution is used as vehicle control in all the PTH administrations. Recombinant mouse Dkk1 (R&D systems) and Recombinant Mouse Frizzled-8 Fc Chimera (R&D systems) was used at 500ng/ml and cells were pretreated with Dkk1 for 30 minutes before the addition of PTH.

Glucose and lactate measurements were done as discussed in chapter 2.

Osteogenic media (Mineralization media): alpha MEM with 10% FBS , 1% Pen Strep, 100 nM Dexamethasone, 50 μg/ml Ascorbic Acid and 10 mM β-glycerol phosphate.

5.7 2-NBDG Uptake Experiments

MC3T3 cells were plated in 96-well clear bottom culture plates the day before each experiment. The cells were stimulated with PTH for the indicated time. After treatments cells were switched to fresh medium containing 100 μM 2-NBDG for 30 minutes, and then prepared for fluorescence reading following the manufacturer's instructions (Glucose Uptake Cell-based Assay Kit, Cayman Chemical). 2-NBDG uptake was measured at 485/535nm (excitation/emission) using a plate reader (BioTek model SAMLFTA, Gen5 software). Fluorescence intensity was normalized to the protein content in each well.

5.8 OCR and ECAR measurements with Seahorse Cellular Flux assays

The day before the experiment cells were plated at 5,000 cells/well density in XF96 plates after coating the plates with cell-tak (BD Biosciences). The next day, the cells were treated with 500 ng/ml PTH for 24 hours with or without inhibitors (2 uM for Sgk I inhibitor and 0.5 uM for Akt inhibitor, then switched to XF Assay Medium Modified DMEM and further incubated in CO2-free incubator for 1 hour. Oligomycin (ATP synthase inhibitor), FCCP (carbonyl cyanide p-trifluoromethoxyphenylhydrazone, proton ionophore), antimycin A (complex III inhibitor) and rotenone (complex I inhibitor) (Seahorse Stress Kit) were prepared in XF assay medium with final concentration of 5 uM for oligomycin and 1 uM for the rest and were injected during the measurements. At the end of the assays, protein concentrations were measured for normalization. OCR and ECAR were measured simultaneously. Mitochondrial parameters are calculated as follows: basal respiration is the difference in OCR before treatment of mitochondrial inhibitors and after antimycin A/rotenone treatment; spare respiratory capacity is difference in OCR following treatment of FCCP and basal respiration; oxidative ATP turnover is the difference in OCR following oligomycin treatment and before FCCP treatment; maximal respiratory capacity is the difference in OCR after FCCP and before antimycin A/rotenone).

5.9 shRNA knockdown and adenovirus infection

Lentiviral shRNA targeting vectors were purchased from Genome Center at Washington University. Targeting sequences are as follows:

Gfp TGACCCTGAAGTTCATCTGCA,

Ldha CGTGAACATCTTCAAGTTCAT

Lentivirus was prepared as discussed in chapter 2.

Adenovirus targeting Gfp (adGfp) and Cre (adCre) were bought from University of Iowa. Sub confluent calvarial cells were infected with adGfp or adCre at 50 MOI (multiplicity of infection) in 2% serum containing medium overnight. The medium was changed to 10% serum containing medium next day and PTH treatment started after 72 hours.

5.10 In vivo PTH Injections

3 months old male C57BL/6J mice were injected intraperitoneally with either 80 μg/kg PTH (1-34) or the vehicle control 5 days a week for 1 month. Half of the vehicle and PTH treated animals were fed with 2 g/L DCA containing water. DCA was dissolved in sterile water pH was adjusted around 7.2.

For *in vivo* signaling studies, PTH (1-34) or vehicle was injected intraperitoneally at the indicated concentration and the bones were harvested 6 or 12 hours after injection. Bone protein extracts were prepared from femurs and tibias of postnatal mice. The muscle was cleaned out carefully, the ends of the bones were surgically removed, and the bone marrow was discarded by centrifugation. The bones were chapped and rinsed twice with cold PBS. Flash-frozen bones were powerized by using. The bone power was incubated with 150 μl RIPA buffer containing proteinase and phophatase inhibitors on ice for 45 minutes, centrifuged down and the supernatant was collected for Western analysis.

5.11 Antibodies

Antibodies for p-Akt(S473)(9271), Akt (9272), β-actin (4970)) p-NDRG1-Thr346 (3217S), LDHA (2012), p-IGFIR (3024) are from cell signaling technologies. Hk2 (sc-6521), α-tubulin (sc-8035) antibodies are from Santa Cruz Biotechnology. Pdk1 (KAP-pk112) antibody is

from Assay Designs. HRP-conjugated anti-rabbit secondary antibody is from GE healthcare (NA934V), HRP-conjugated anti-mouse (sc-2005) and anti-goat (sc-2352) secondary antibodies are from Santa Cruz Biotechnology.

5.12 CO_2 trap experiments

MC3T3 cells were plated in flasks at a concentration of 40x104/flasks and treated with mineralization medium for 3 days. At the end of 3 days the cells are treated with PTH along with either 1µ1 Ci/ml glucose [1-C14], glucose [3, 4-C14] or glucose [6-C14] and tube was inserted into the flask and the system is sealed for 24 hours. At the end of 24 hours, 2.5 ml 2.5 H_2SO_4 was injected into the flask to gas the CO_2, and 1 ml NaOH is injected into the tube. After overnight incubation, liquid in the tube is mixed with scintillation mixture and read in the scintillation counter. A parallel experiment was conducted with the same treatment for cell counting. Labeling index is calculated by normalizing the dpm (disintegration per minute) value by glucose consumed and by cell number. For glucose consumption, either an aliquot of the medium is used before injecting H_2SO_4, or parallel plates are used. Flux through PPP was calculated by subtracting glucose [6-C14] from glucose [1-C14].

6. Figures

Figure 1. PTH Increases Glucose Utilization in Cell Culture

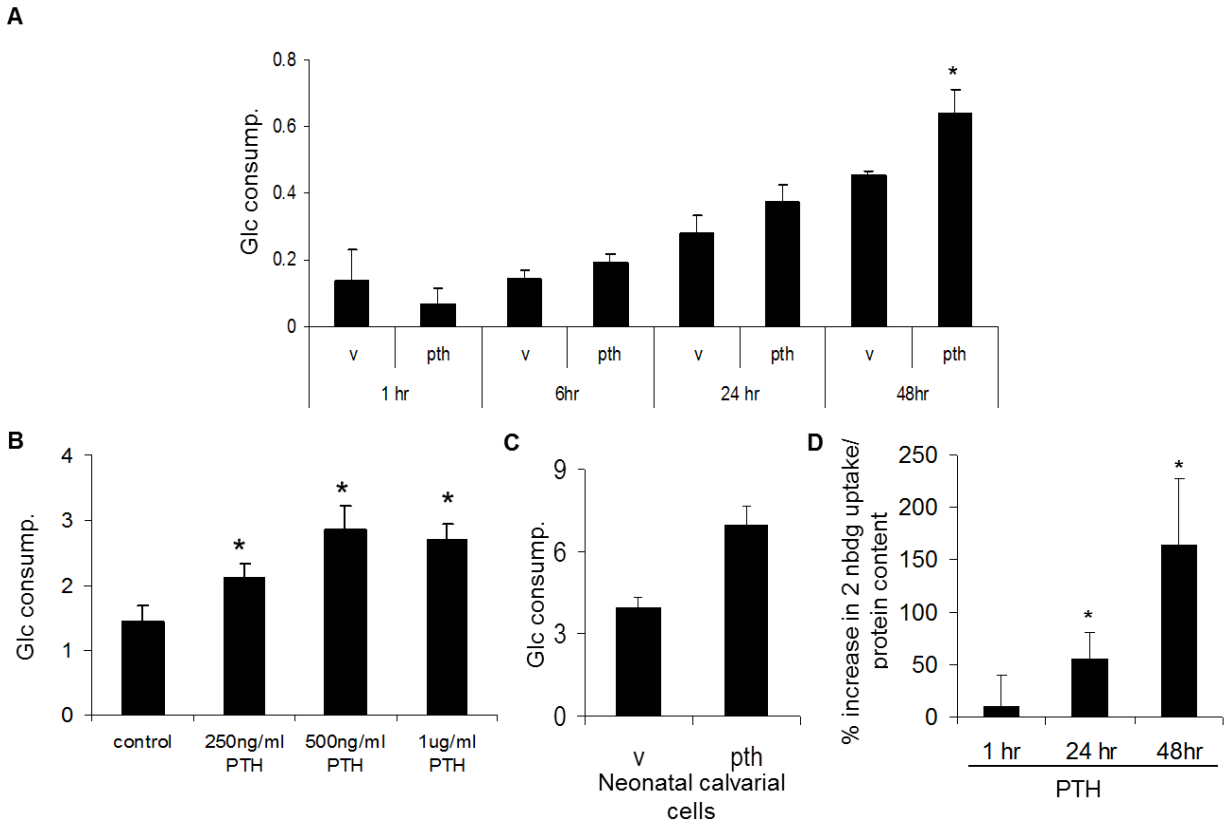

(A) Increase in glucose consumption (mg) by PTH compared to vehicle (V) for indicated times in MC3T3-E1 cells.

(B) Concentration dependent increase in glucose consumption in response to PTH (mg glucose/mg protein) after 48 hours.

(C) Glucose consumption (mg glucose/mg protein) in neonatal calvarial cells after 24 hours.

(D) Glucose uptake using 2-NBDG following PTH treatment for indicated times, shown as % increase [(PTH-v)/v*100]

Figure 2. PTH Increases both Oxygen Consumption and Glycolysis

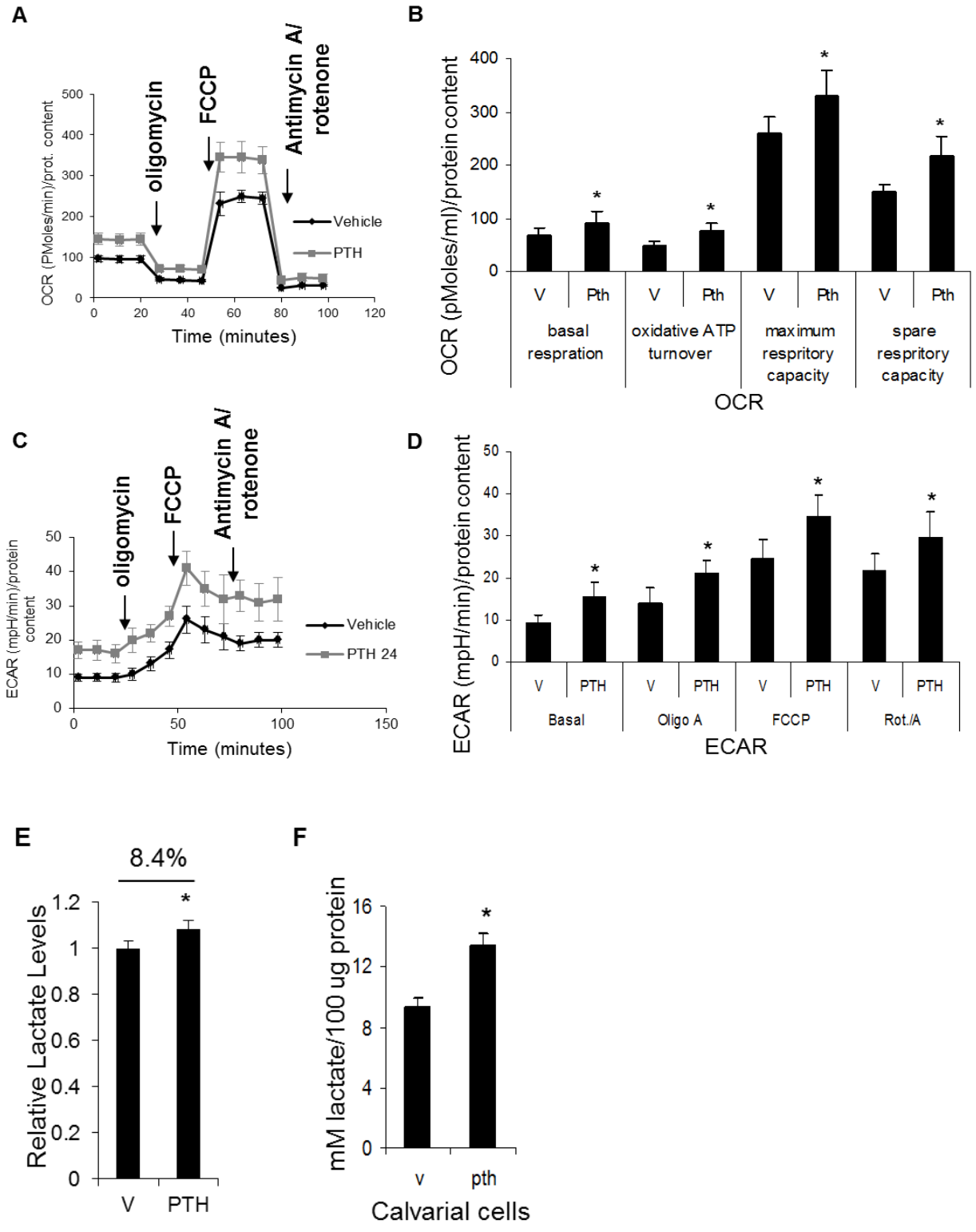

Figure 2. PTH Increases both Oxygen Consumption and Glycolysis

(A) Oxygen consumption rate (OCR) and after 24 hours of PTH or vehicle (V) treatment.

(B) Basal respiration, oxidative ATP turnover, maximum respiratory capacity and spare capacity after 24 hours of PTH or vehicle (V) treatment.

(C-D) Extracellular acidification rate (ECAR) after 24 hours of PTH or vehicle (V) treatment under basal condition or following Oligomycin, FCCP or Rotenone/Antimycin A injection.

(E) Relative lactate level in the medium after 48 hours of vehicle (V) or PTH treatment.

(F) Lactate concentration (mM lactate/ 100 μg protein) in medium after 24 hours PTH treatment in neonatal calvarial cells.

Figure 3. PTH Increases Glycolytic Enzymes both *in vitro* and *in vivo*

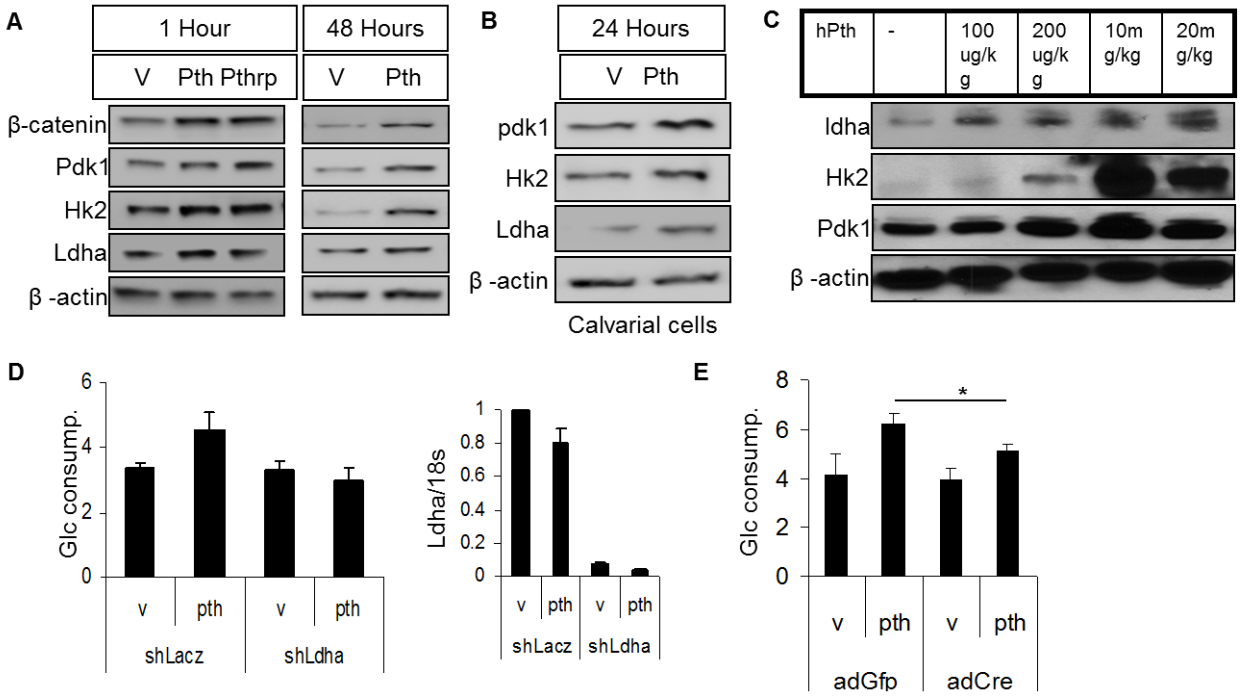

(A) 1 hour PTH (250 ng/ml) or PTHrP (250 ng/ml) treatment; 48 hours of PTH treatment.

B) 24 hours of PTH treatment in calvarial cells.

(C) Bone extracts from BL6 mice prepared 6 hours after PTH injection.

(D, E) Glucose consumption in response to PTH after LDHA knockdown using shRNA in MC3T3 cells (D) or deleting LDHA from calvarial cells prepared from Ldha $^{f/f}$ mice (E).

Figure 4. PTH Suppresses Glucose Oxidation in TCA cycle but Stimulates PPP

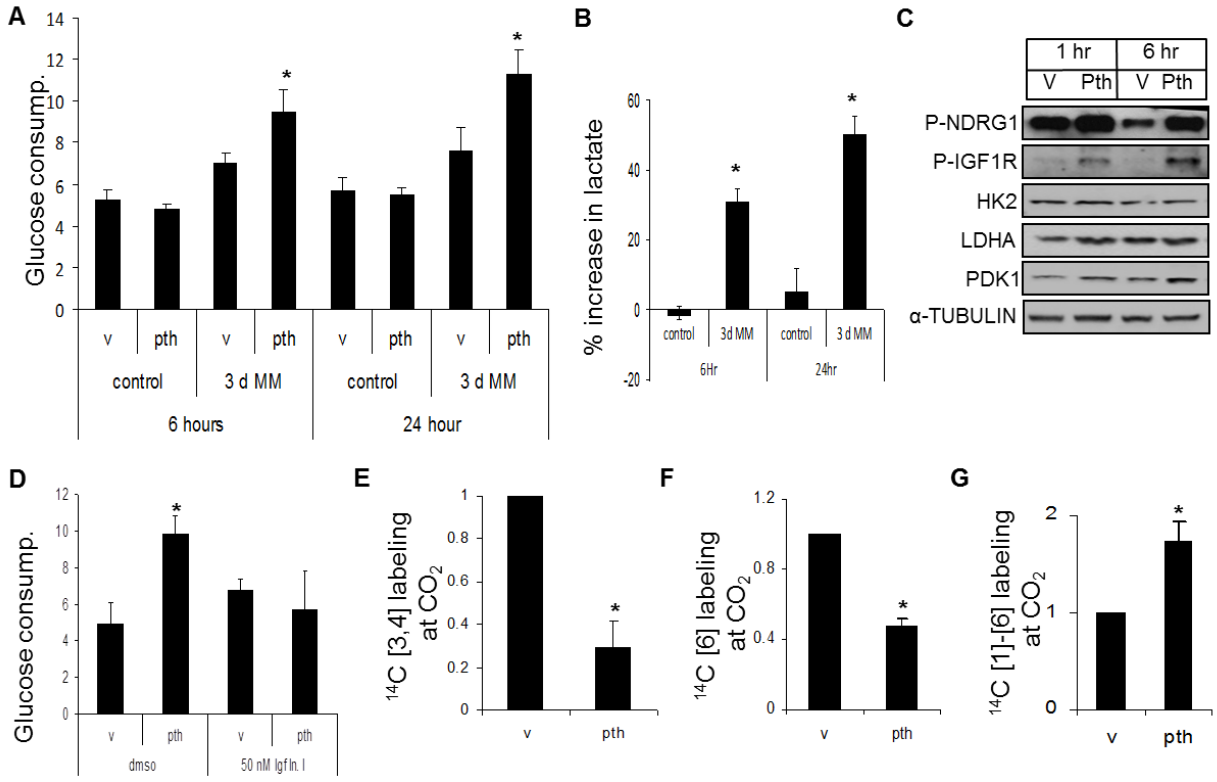

(A, B) MC3T3 cells differentiated for 3 days in osteogenic medium before PTH treatment for 6 or 24 hours and assayed for glucose consumption (mg glucose/mg protein) (A) and lactate production (PTH-Vehicle/Vehicle*100) (B).

(C) Activation of IGF and SGK signaling after 1 and 6 hours of PTH treatment following 3 days osteogenic medium treatment in MC3T3 cells.

(D) Effect of IGF1R Inhibitor I (50ng/ml) on glucose consumption (mg glucose/mg protein) in differentiated MC3T3 cells.

(E-F-G) Differentiated MC3T3 cells are treated with 500ng/ml PTH along with [$^{14}C_{3,4}$]-Glucose, [$^{14}C_1$]-Glucose or [$^{14}C_6$]-Glucose for 24 hours. Labeling index for trapped CO_2 from [$^{14}C_{3,4}$]-Glucose (E) [$^{14}C_6$]-Glucose (F), [$^{14}C_1$]-Glucose- [$^{14}C_6$]-Glucose (G) are shown.

Figure 5. PTH Increase Glucose Consumption through IGF Signaling Independent of WNT Pathway

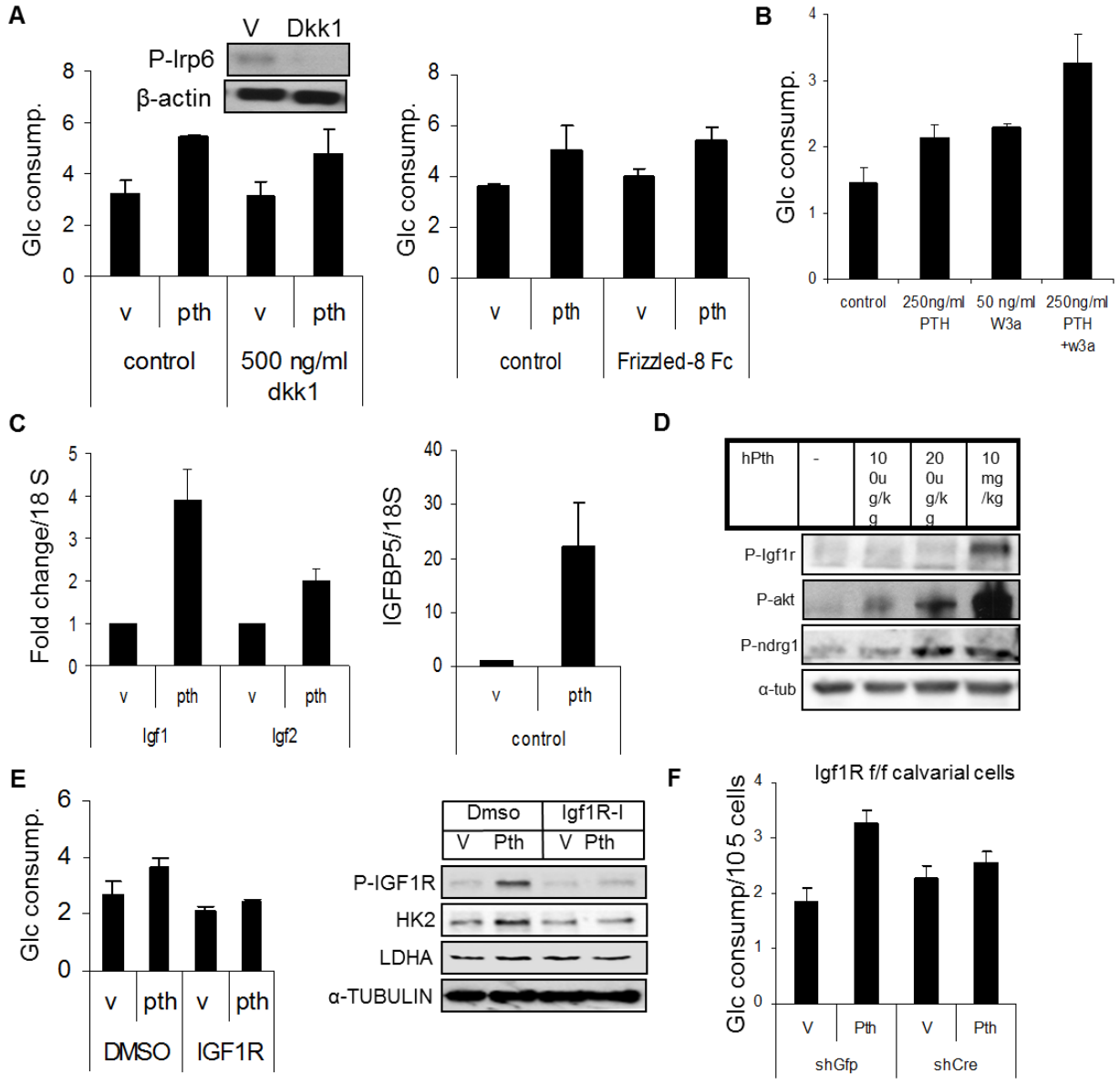

Figure 5 (CONT). PTH Increase Glucose Consumption through IGF Signaling Independent of WNT Pathway

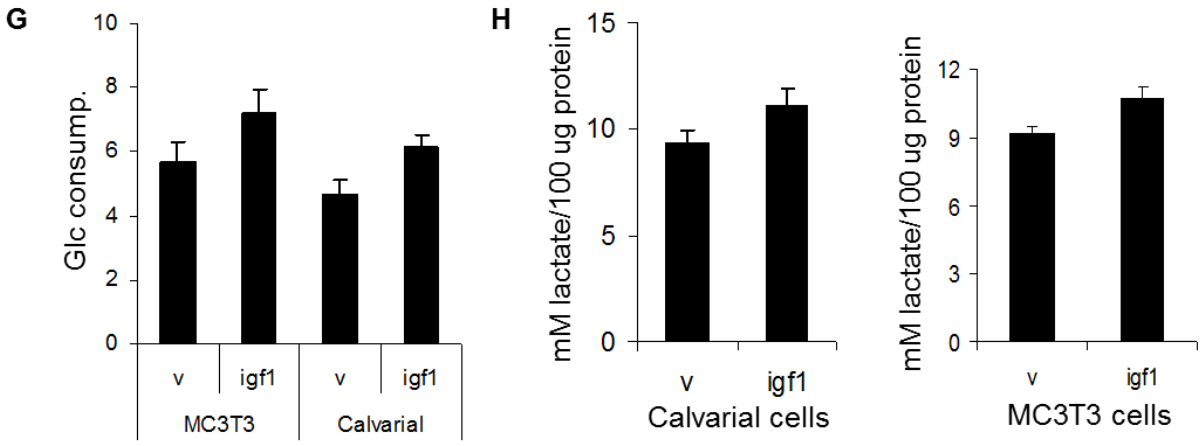

(A) Glucose consumption (mg glucose/mg protein) after 48 hours of PTH treatment in the presence of 500ng/ml DKK1 or 500 ng/ml Frizzled-8 Fc Chimera.

(B) Glucose consumption after 48 hours of PTH and WNT3A (50ng/ml) treatments individually or together.

(C) mRNA levels of Igf1, Igf2 and Igfbp5 normalized to 18S relative to controls following 6 hours of PTH treatment in MC3T3 cells.

(D) Bone extracts prepared 6 hours after IP PTH injection in males.

(E) The effect of inhibiting IGF1R by using 100 nM Linsitinib (IGF1R IN. 1) on glucose consumption (mg glucose/mg protein) and glycolytic enzymes.

(F) Effect of genetic removal of Igf1R from calvarial cells on glucose consumption by adenoviral infection of shGFP or shCRE.

(G-H) Effect of IGF1 (500ng/ml) on (G) glucose consumption (mg glucose/mg protein) or lactate production (mM lactate/ 100µg protein) (H) in MC3T3 cells or in calvarial cells.

Figure 6. PTH Regulates Glucose Metabolism through a PI3K-SGK1 Dependent Signaling Cascade

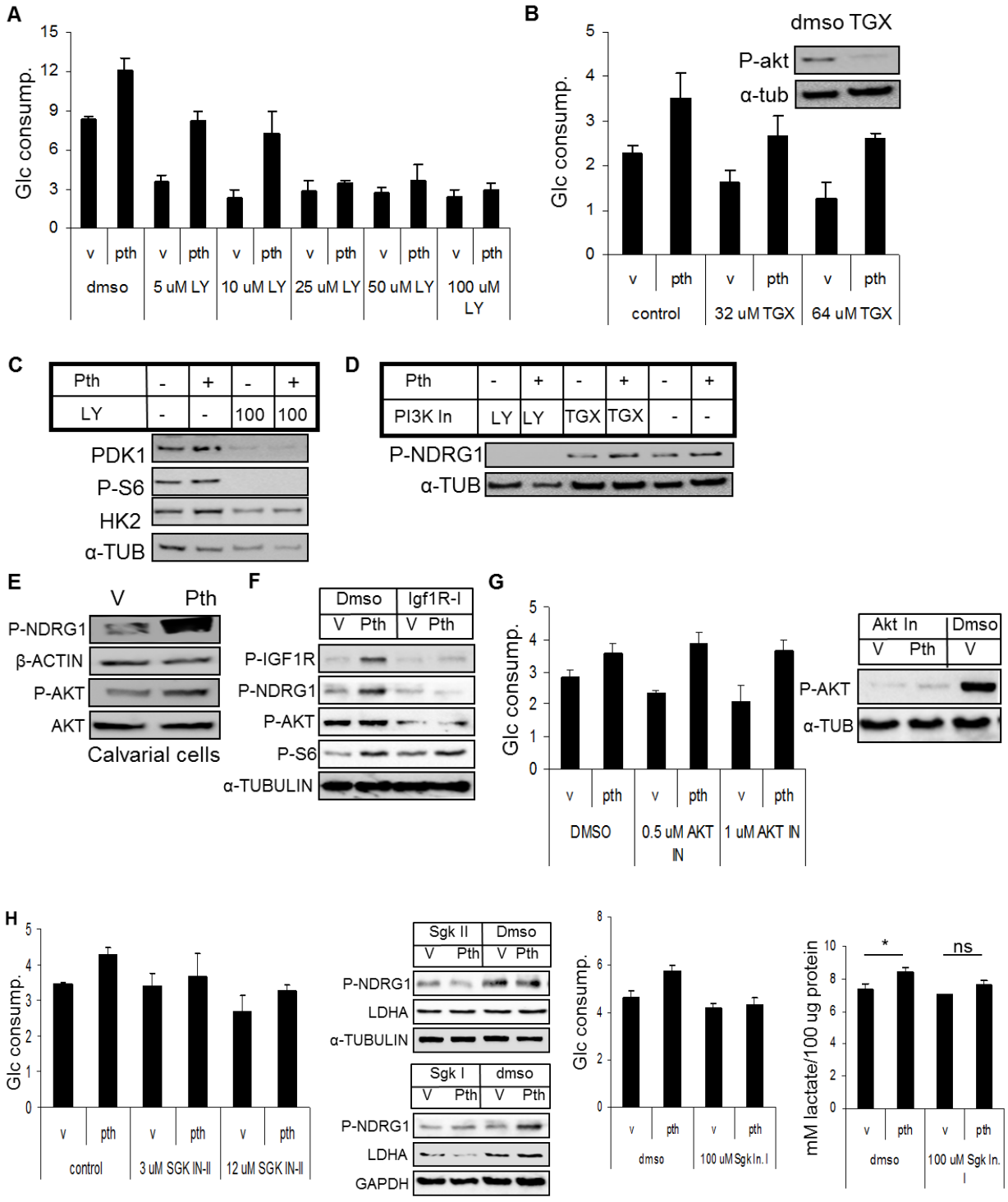

Figure 6 (CONT). PTH Regulates Glucose Metabolism through a PI3K-SGK1 Dependent Signaling Cascade

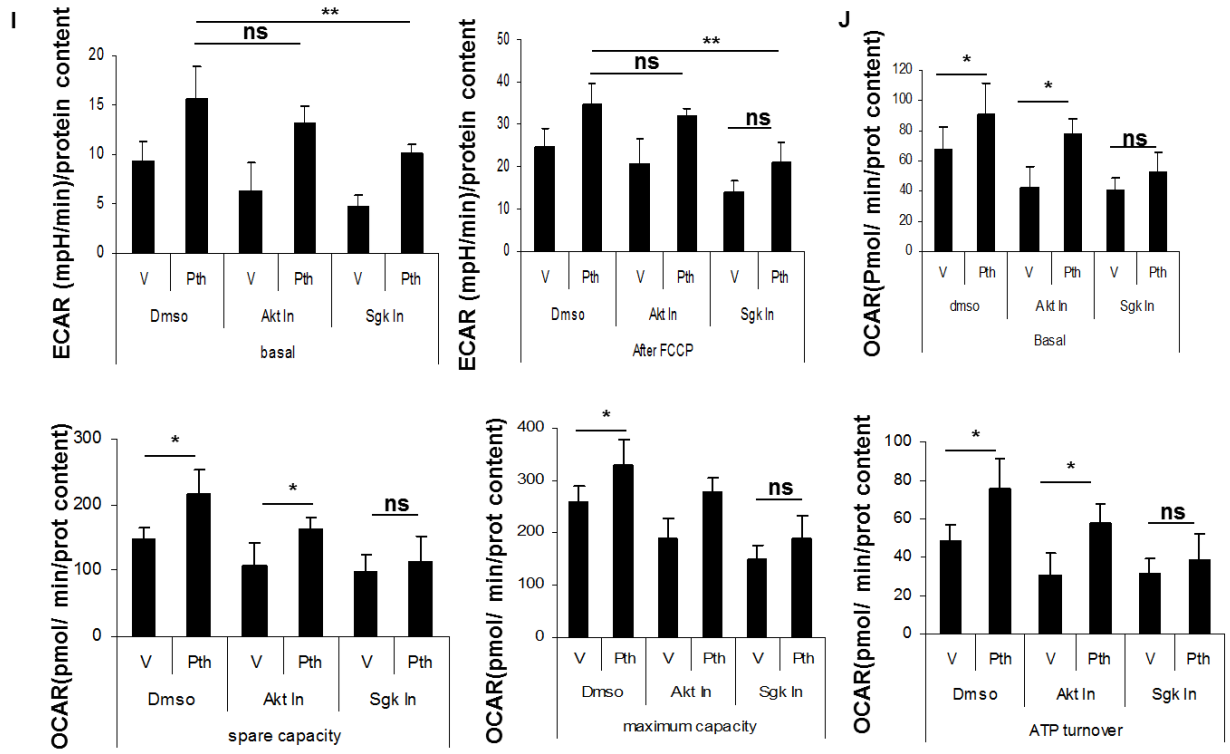

Figure 6. PTH Regulates Glucose Metabolism through a PI3K-SGK1 Dependent Signaling Cascade

(A-B) Effect of the pan-PI3K inhibitor LY294002 (A) or p110β-specific PI3K inhibitor TGX-221 (B) on glucose consumption.

(C) Effect of 100μM LY294002 on glycolytic enzymes.

(D) Effect of 100μM LY294002 and 64 μM TGX-221 on SGK1 activation examined by NDRG1 phosphorylation.

(E) Phosphorylation of AKT (s473) and the SGK1 target NDRG1 by 24 hours PTH treatment in calvarial cells.

(F) Effect of IGF1R inhibitor (100nM IGF1R In. I) on downstream PTH targets. MC3T3 cells are treated with vehicle or PTH for 48 hours either with or without IGF1R inhibitor I.

(G) Glucose consumption in the presence of 0.5 μM AKT inhibitor MK2206 along with PTH treatment.

(H) Effect of inhibition of SGK1 by either GSK 650394 (SGK inhibitor I) or EMD638683 (SGK inhibitor II) on PTH-induced glucose consumption, LDHA and lactate production.

(I-J) Effect of 2 μM SGK In. I or 0.5 μM Akt inhibitor MK2206 on PTH-stimulated ECAR (I) and OCR (J).

Figure 7. cAMP Dependent Pathway is more Important Regulating PTH-induced Glucose Metabolism

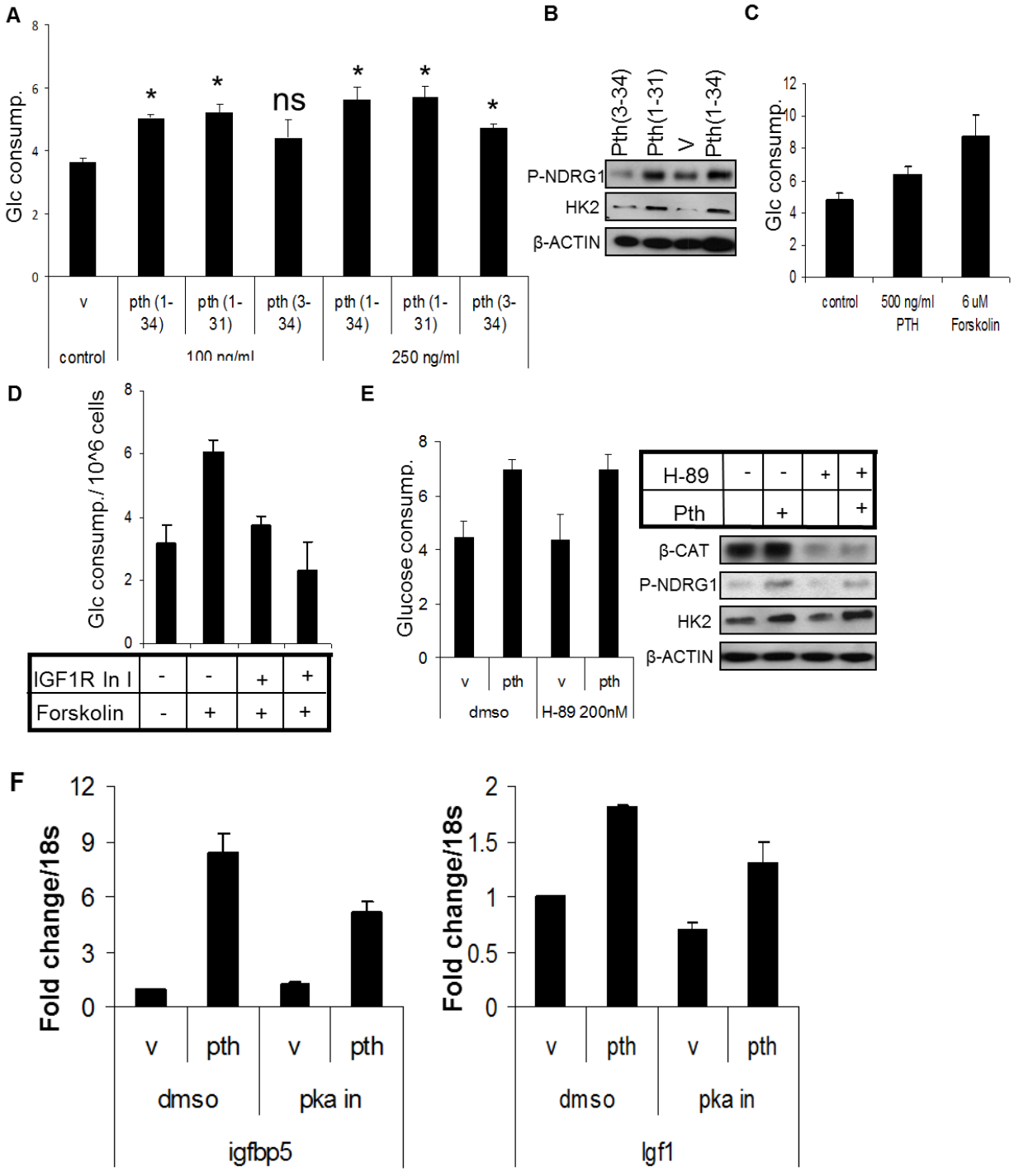

Figure 7. cAMP Dependent Pathway is more Important Regulating PTH-induced Glucose Metabolism

(A, B) Glucose consumption (A), activation of SGK1 pathway and upregulation of HK2 (B) in response to PTH (1-34), PTH (1-31) and PTH (3-34) at indicated concentrations.

(C) Effect of 6 μM Forskolin on glucose consumption (mg glucose/mg protein).

(D) Effect of IGF1R In. I on Forskolin induced glucose consumption (mg glucose/mg protein).

(E) Effect of 200 nM H-89 on SGK1 activation, HK2 and β-catenin upregulation and glucose consumption in response to 48 hours of PTH treatment.

(F) Effect of 10 μM H-89 on Igfbp5 and Igf1 mRNA upregulation by PTH.

Figure 8. Glucose Flux through Aerobic Glycolysis is Important for the Anabolic Effect of iPTH *in vivo*

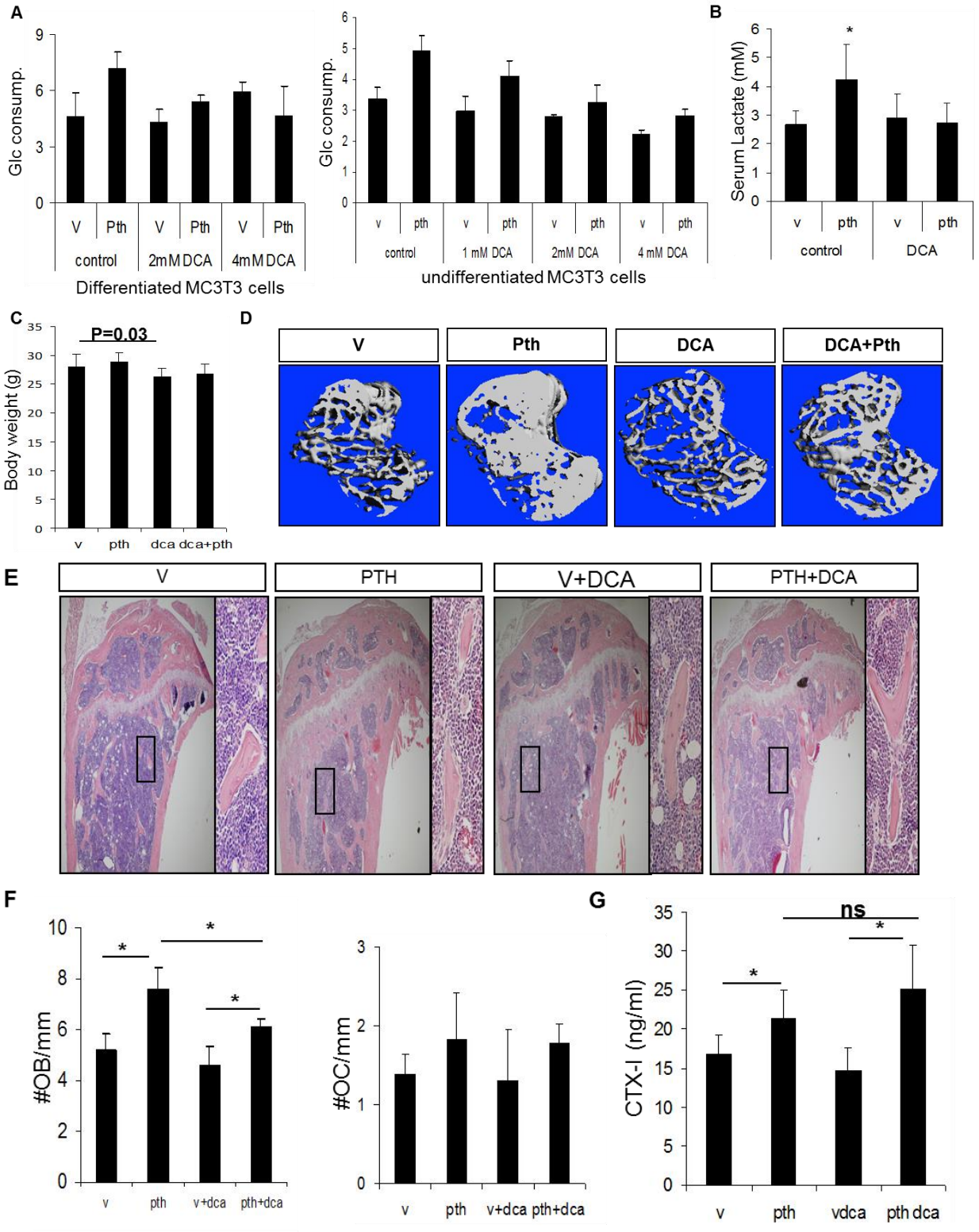

Figure 8 (CONT). Glucose Flux through Aerobic Glycolysis is Important for the Anabolic Effect of iPTH *in vivo*

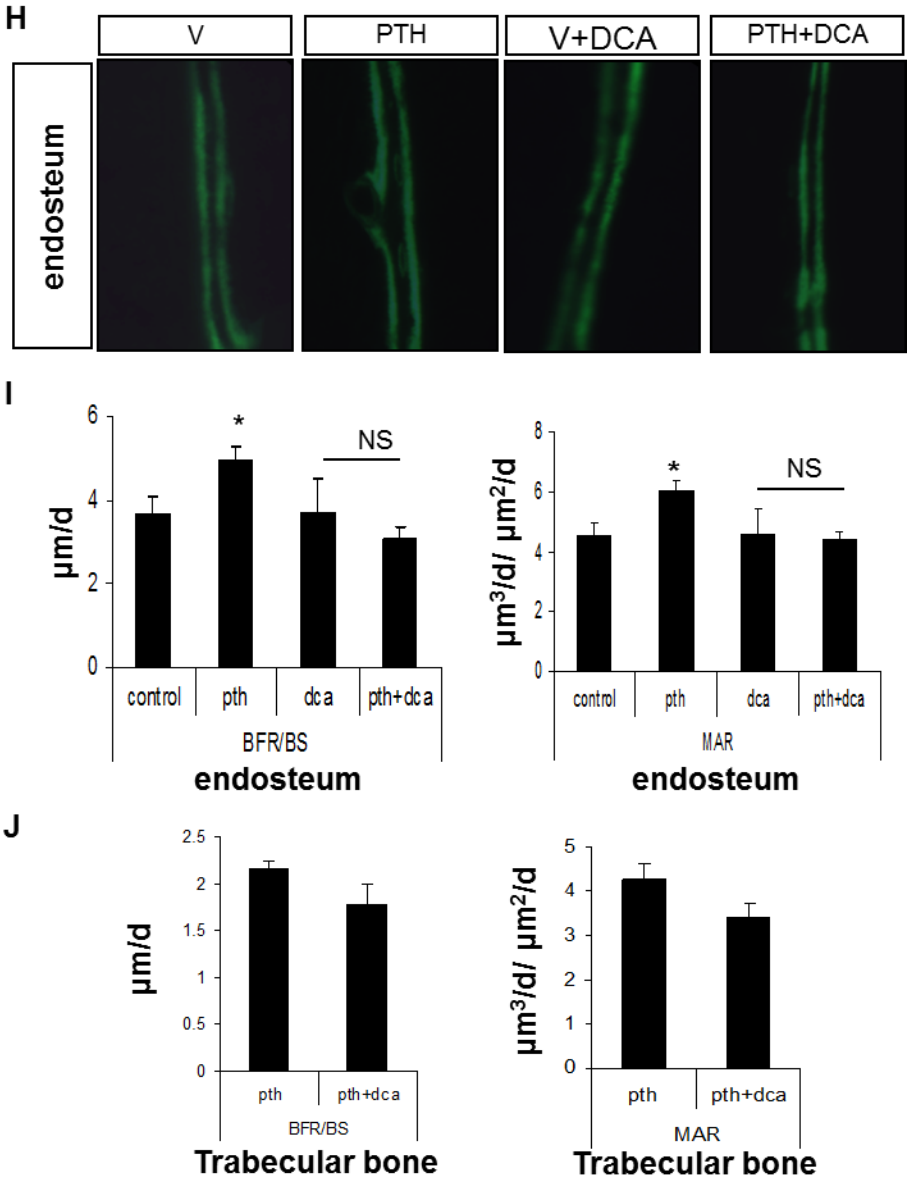

Figure 8. Glucose Flux through Aerobic Glycolysis is Important for the Anabolic Effect of iPTH *in vivo*

(A) Effect of DCA treatment in glucose consumption in both differentiated and undifferentiated MC3T3 cells in response to 48 hours of PTH treatment.

(B) Serum lactate levels (mM) in 4 months of BL6 mice administered vehicle (V), iPTH, V+ DCA or iPTH+DCA for 1 month.

(C) Effect of iPTH and DCA on body weight (gr) at the end of 1 month administration.

(D) μCT 3D reconstruction of 35 tibial trabecular sections right under the growth plate.

(E) 10X and 40X images from H&E stained sections from the proximal tibias.

(F) Histomorphometric parameters of osteoblasts and osteoclasts on tibial sections. #OB/mm: number of osteoblasts normalized to trabecular bone perimeter; #Oc/mm: osteoclast number normalized to trabecular bone perimeter. Analysis is done using Bioquan II.

(G) Serum CTX-I (ng/ml) levels.

(H) Representative images of calcein double labeling in tibias of vehicle (V), iPTH, V+ DCA and iPTH+DCA treated animals from endosteum.

(I-J) Dynamic histomorphometry parameters from endosteal and trabecular region of tibias. MAR: mineral apposite rate; BFR/BS: bone formation rate.

7. Supplemental Figures

Figure S1. PTHrP Increases Glucose Consumption

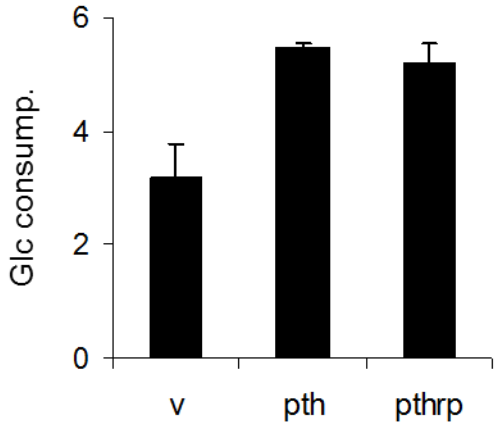

Increase in glucose consumption (mg glucose/mg protein) by PTHrP (250ng/ml) after 48 hours treatment in MC3T3-E1 cells.

Figure S2. Protein Concentration after 48 hours PTH Treatment

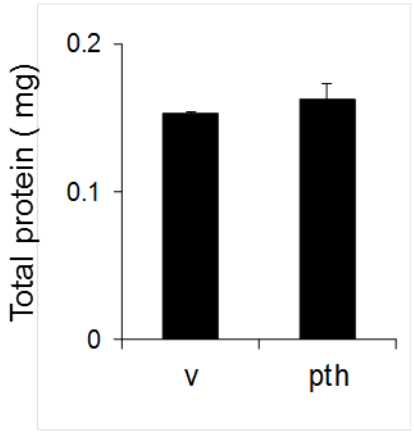

Protein concentration (mg) after 48 hours PTH treatment in MC3T3-E1 cells.

Figure S3. PTH Increases Glucose Consumption in the Absence of Serum

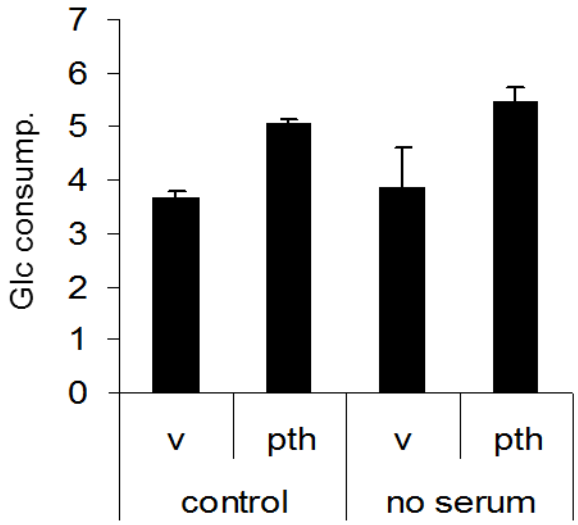

Increase in glucose consumption (mg glucose/mg protein) by PTH after 48 hours in the presence and absence of serum.

Figure S4. Bone Extracts Prepared 6 or 12 hours after PTH Injections

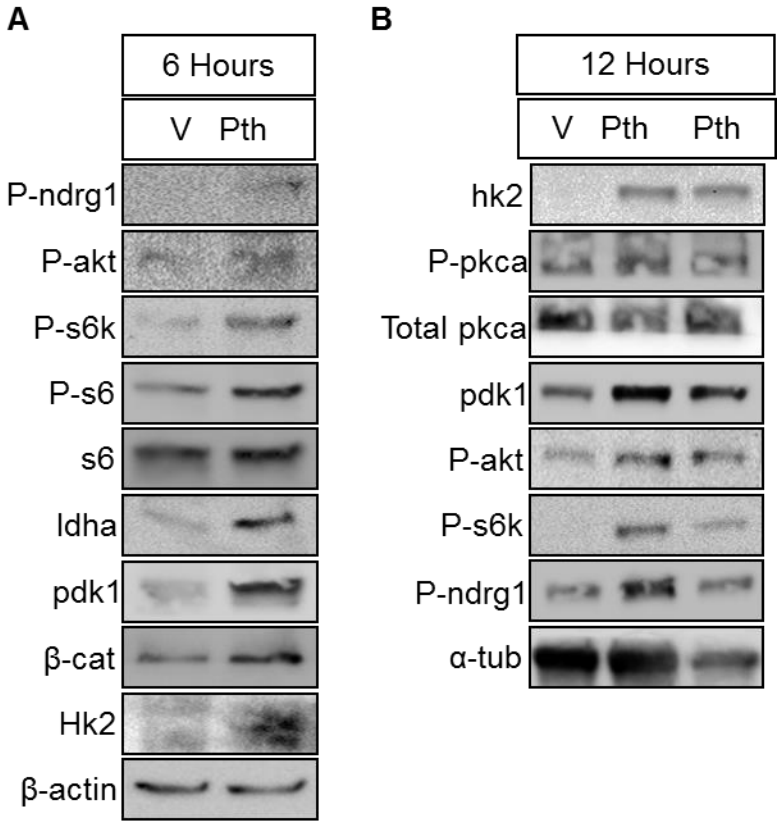

Male BL6 mice were injected with PTH (200 μg/kg) and bones are harvested at the indicated hours. Bone extracts prepared from tibias and femurs.

Figure S5. 3 Days Osteogenic Medium Treatment (Min M) Increased AP mRNA levels

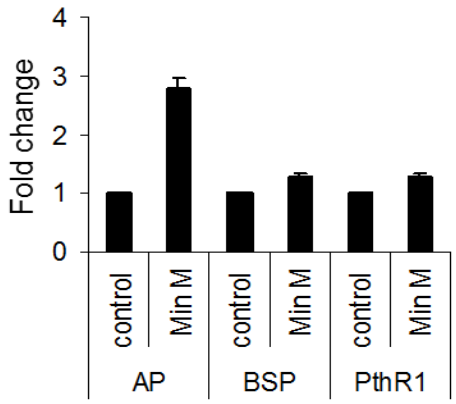

The effect of osteogenic medium treatment in MC3T3 cells. Expression of osteoblast markers was determined by qPCR. Fold changes between treated and control cells were calculated after normalization to 18S RNA.

Figure S6. Representative Illustration of the Experimental Set-up for the CO_2 trap

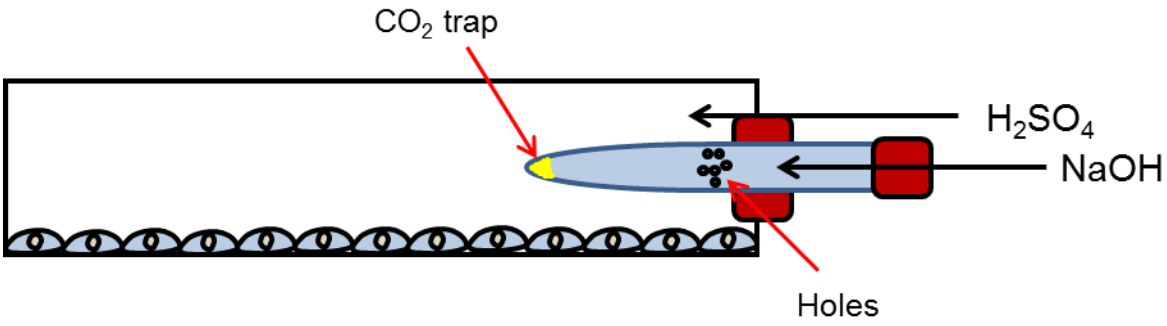

Cells are treated with PTH along with the radioactively labeled glucose in a sealed flask. There is a tube with the holes inserted into the flask. At the end of the control or PTH treatment along with radioactively labeled glucose, H_2SO_4 is injected into the flask; NaOH is injected into the tube.

Figure S7. Schematic Representation of the fates of Carbons 1, 3/4 and 6 on Glucose

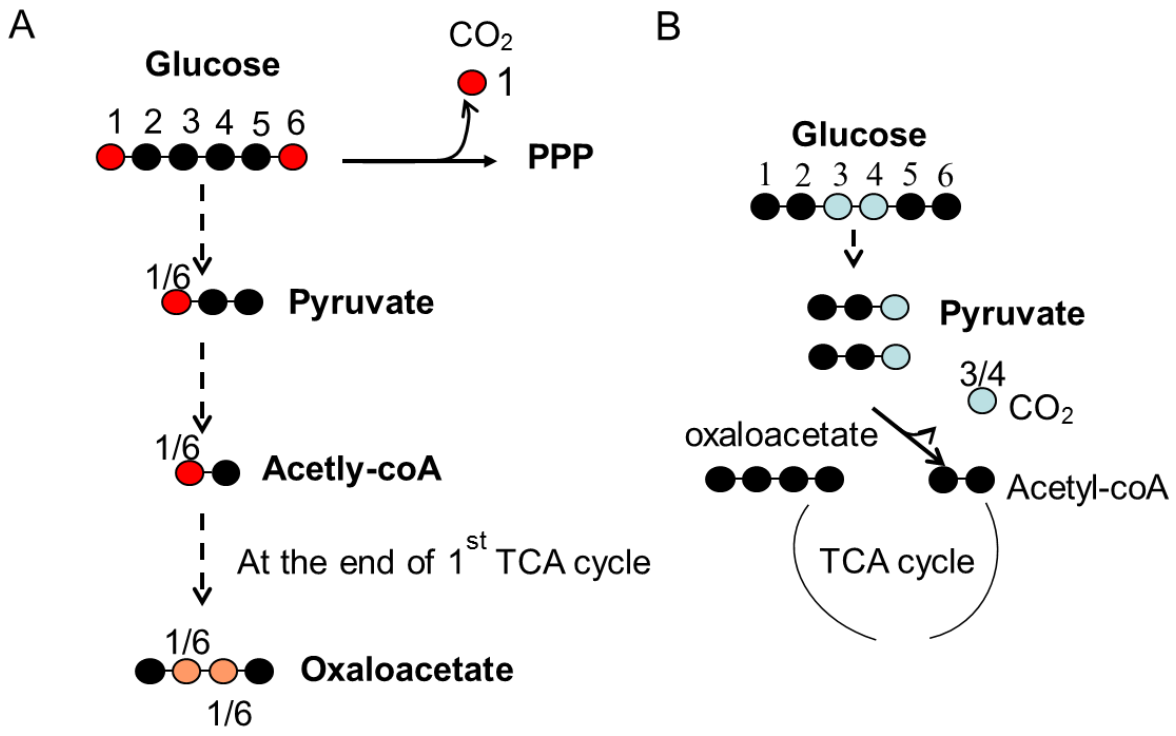

(A) Carbon 1 (red circle) of glucose is released as CO_2 at the step where glucose-6-phosphate is diverted to PPP. Carbon 1 also gets integrated in one of the central carbons in oxaloacetate after the first cycle. It later gets released after 3rd round of TCA cycle. Carbon 6 (red) is only released after the 3rd round of TCA cycle.

(B) Carbons 3 and 4 (blue) are only released when pyruvate is oxidized to acetyl-coA.

Figure S8. PTH increase Glucose Consumption and Lactate Production

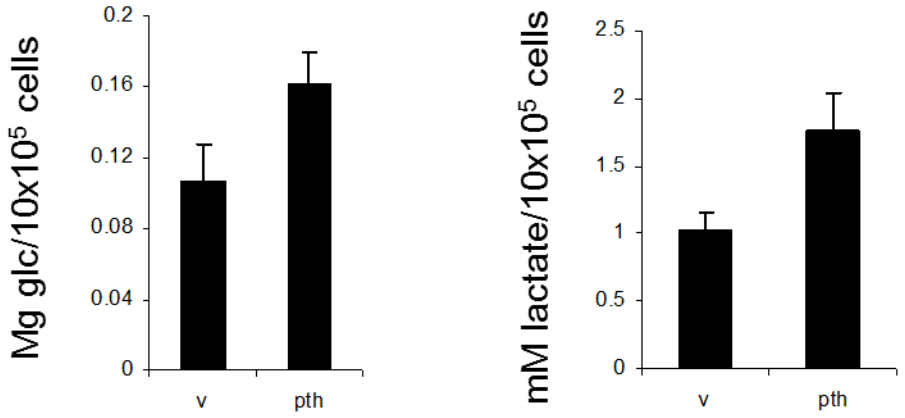

Differentiated MC3T3 cells are treated with PTH along with glucose ^{14}C [3, 4] for CO_2 trap experiments. In the same experiment glucose uptake and lactate production were significantly upregulated.

Figure S9. Effect of IGF1R Inhibitor-II on Glucose Consumption

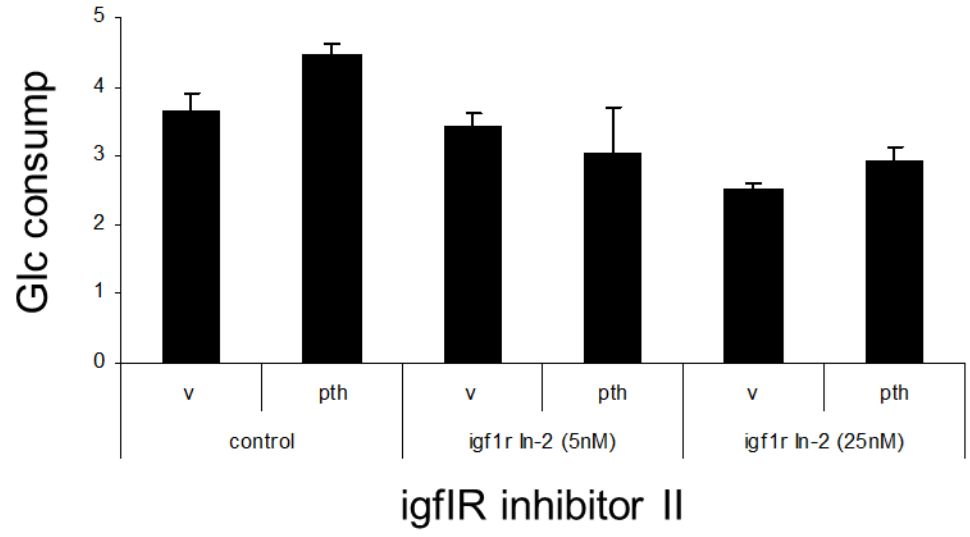

IGF1R inhibitor II (Picropodophyllotoxin) blocked glucose consumption in response to 48 hours of PTH treatment.

Figure S10. Effect of H-89 on Glucose Consumption

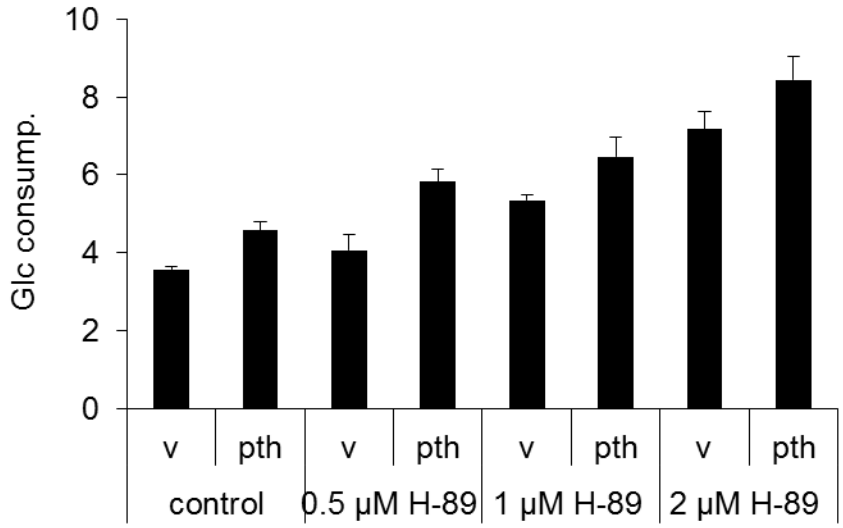

Glucose consumption (mg glucose/mg protein) from MC3T3 cells treated with PTH and different concentrations of PKA inhibitor H-89 for 48 hours.

Figure S11. PLC/PKC Pathway is not a Major Player for PTH Induced Glucose Consumption

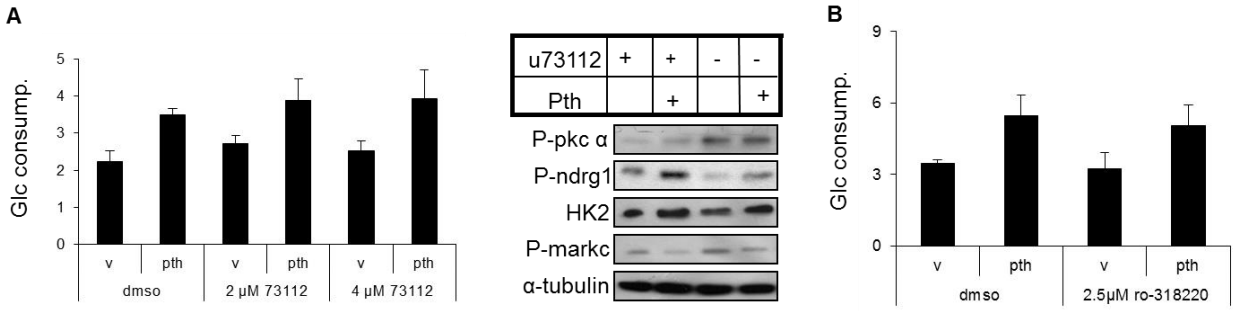

(A) Glucose consumption and western blot analysis after 48 hours of PTH treatment with or without 4 μM PLC inhibitor u73112.

(B) Glucose consumption after 48 hours of PTH treatment with 2.5 μM PKC inhibitor ro-318220.

Figure S12. MAPK/ERK Pathway is not involved in PTH Induced Glucose Utilization

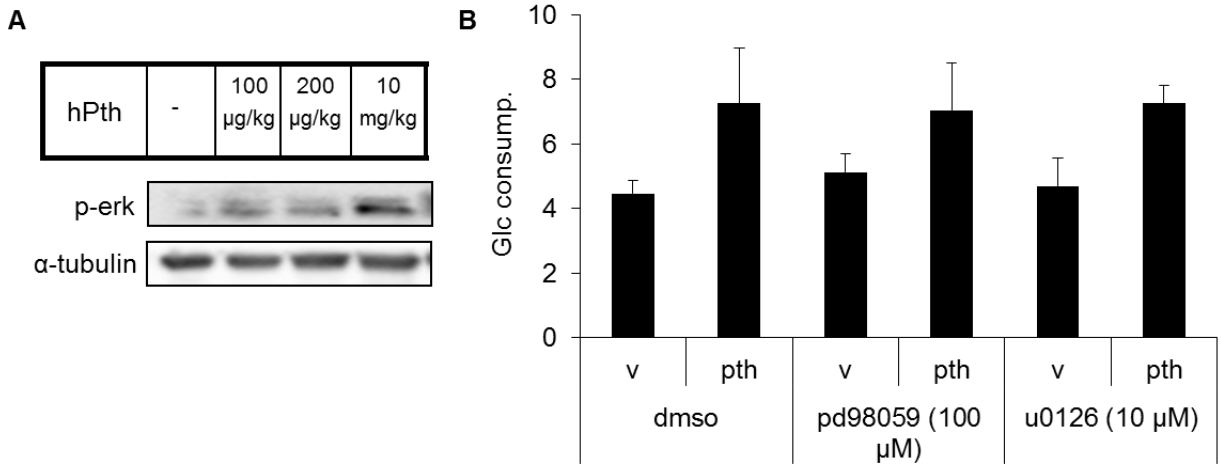

(A) Western blots of p-ERK in bone protein extracts from PTH or vehicle injected mice after 6 hours.

(B) Effect of Erk inhibitors PD98059 and U0126 on glucose consumption.

Figure S13. Proposed Model for the PTH Action on Glucose Metabolism

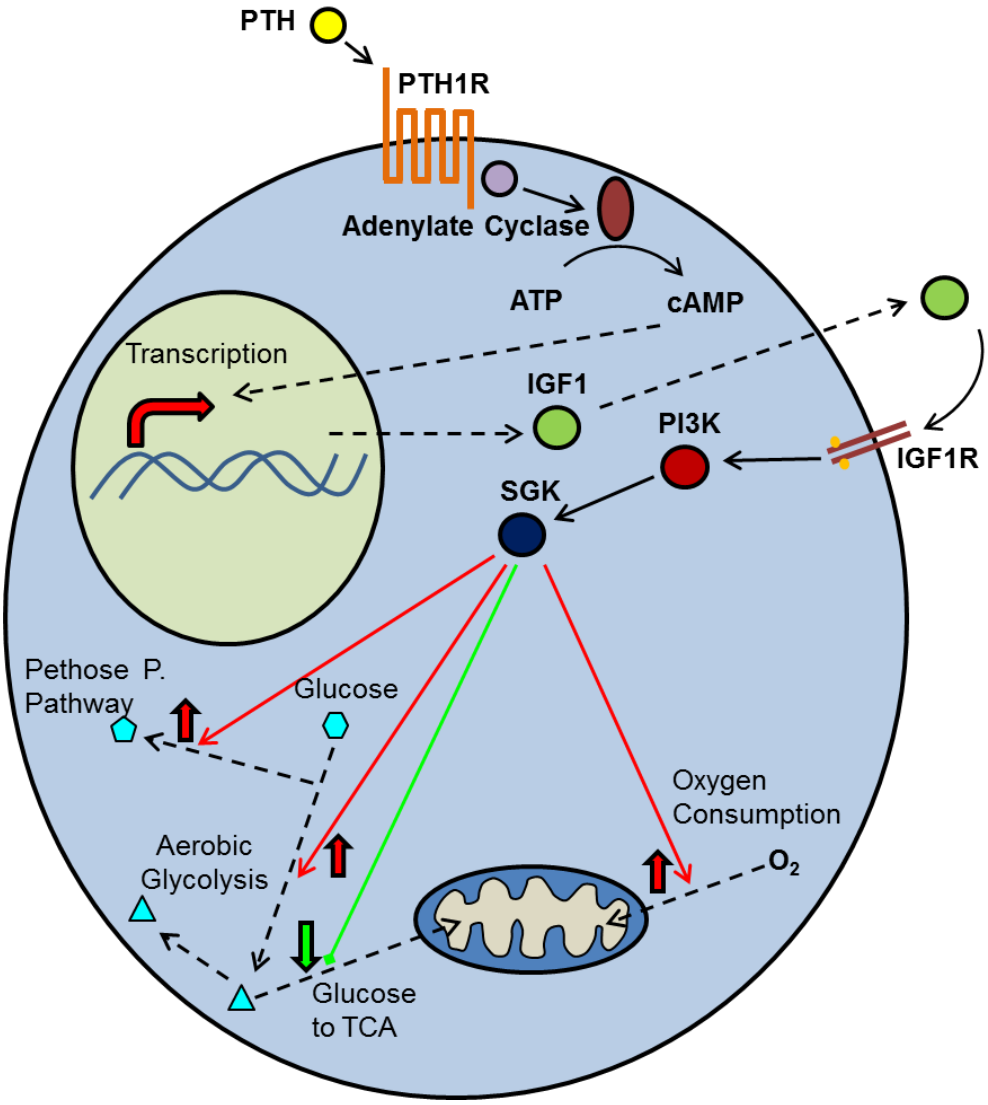

PTH binds to its receptor, PTH1R that leads to activation of adenylate cyclase that produces cAMP. By increasing cAMP, PTH stimulates the transcription of IGF1. IGF1 then activates PI3K, which then activates SGK1. By signaling through cAMP/IGF/P13K/SGK1, PTH increases glucose consumption, increases glucose oxidation in PPP, increases lactate-production and reduces contribution of glucose to TCA cycle.

Figure S14. Temporal Activation of Downstream Targets in Response to PTH

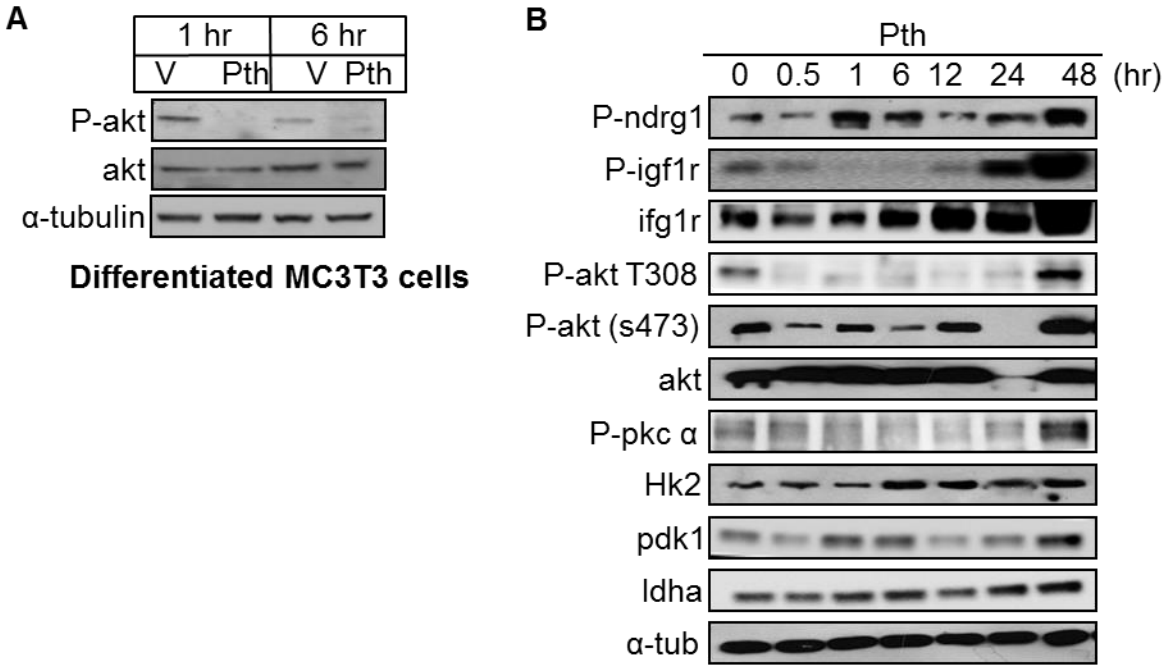

(A) Western blots from 1 or 6 hours vehicle (V) or PTH treatment in differentiated MC3T3 cells. (B) Western blots from MC3T3 cells treated with PTH for different time intervals and harvested at the same time.

8. Tables

Table 1. μCT Results of Proximal Tibia from indicated treatment groups.

Group	BV/TV	Tb N*	Tb Th*	Tb Sp*
	% t-test	1/mm t-test	mm t-test	mm t-test
V	27.16+/-3.8 0004	5.17 +/- 0.5 p1:0.056	0.07+/-0.0062 p1:0.0214	0.2+- 0.034 p1:0.064
PTH	37.52+/-0.065 p2:0.0076	5.59+/-0.36 p2:0.0076	0.081+/-0.0077 p2: 0.094	0.17+/-0.016 p2:0.043
DCA	24.88+/-0.078 p3:0.042	5.23+/-0.4 p3:0.78	0.067+/-0.01 p3:0.1654	0.19+/-0.017 p3:0.050
PTH +DCA	30.12+/-0.037 P4:0.16	4.9+/- 0.38 P4:0.067	0.075+/-0.0045 P4:0.122	0.19+/- 0.17 P4:0.39

BV: bone volume; TV; total volume; Tb. N*: trabecular number; Tb. Th*: trabecular thickness; Tb. Sp*: trabecular spacing; data obtained from 35 of 16-mm slices right below growth plate, n = 10 for each group. P1: p between V vs PTH; P2: p between PTH vs PTH+DCA; P3: p between V vs DCA; P4: p between DCA vs PTH+DCA. V: vehicle

Table 2. μCT Result of Cortical Bone at Tibial Midshaft from indicated treatment groups.

Group	BV	TV	BV/TV	Cortical Th*
	Mm t-test	1/mm t-test	mm t-test	mm t-test
V	0.74 +/-9.133	1.1 +/- 0.19	0.65+/-0.015	0.25+- 0.009
PTH	0.80 +/-0.078 p1:0.48	1.13+/-0.0087 p1:0.798	0.70+/-0.0052 p1: 0.0086	0.27+/-0.006 p1:0.09
DCA	0.71 +/-0.13	1.057+/-0.185	0.67+/-0.019	0.26+/-0.02
PTH +DCA	0.78 +/-0.14 p2:0.29	1.17+/-0.19 p2:0.19	0.65+/-0.029 P2:0.12	0.26+/- 0.017 P2:0.99

BV: bone volume; TV; total volume; Cortical. Th*: cortical thickness; data obtained from 50 of 16-mm slices at midshaft, n = 5 for each group. P1: p between V vs PTH; P2: p between DCA vs PTH+DCA.

References

Anastasilakis, A., Goulis, D.G., Koukoulis, G., Kita, M., Slavakis, A., and Avramidis, A. (2007). Acute and chronic effect of teriparatide on glucose metabolism in women with established osteoporosis. Exp Clin Endocrinol Diabetes *115*, 108-111.

Arlot, M., Meunier, P.J., Boivin, G., Haddock, L., Tamayo, J., Correa-Rotter, R., Jasqui, S., Donley, D.W., Dalsky, G.P., Martin, J.S.*, et al.* (2005). Differential effects of teriparatide and alendronate on bone remodeling in postmenopausal women assessed by histomorphometric parameters. J Bone Miner Res *20*, 1244-1253.

Armamento-Villareal, R., Ziambaras, K., Abbasi-Jarhomi, S.H., Dimarogonas, A., Halstead, L., Fausto, A., Avioli, L.V., and Civitelli, R. (1997). An intact N terminus is required for the anabolic action of parathyroid hormone on adult female rats. J Bone Miner Res *12*, 384-392.

Bellido, T., Ali, A.A., Plotkin, L.I., Fu, Q., Gubrij, I., Roberson, P.K., Weinstein, R.S., O'Brien, C.A., Manolagas, S.C., and Jilka, R.L. (2003). Proteasomal degradation of Runx2 shortens parathyroid hormone-induced anti-apoptotic signaling in osteoblasts. A putative explanation for why intermittent administration is needed for bone anabolism. J Biol Chem *278*, 50259-50272.

Bikle, D.D., Sakata, T., Leary, C., Elalieh, H., Ginzinger, D., Rosen, C.J., Beamer, W., Majumdar, S., and Halloran, B.P. (2002). Insulin-like growth factor I is required for the anabolic actions of parathyroid hormone on mouse bone. J Bone Miner Res *17*, 1570-1578.

Borle, A.B., Nichols, N., and Nichols, G., Jr. (1960). Metabolic studies of bone in vitro. II. The metabolic patterns of accretion and resorption. J Biol Chem *235*, 1211-1214.

Canalis, E., Centrella, M., Burch, W., and McCarthy, T.L. (1989). Insulin-like growth factor I mediates selective anabolic effects of parathyroid hormone in bone cultures. J Clin Invest *83*, 60-65.

Dobnig, H., Sipos, A., Jiang, Y., Fahrleitner-Pammer, A., Ste-Marie, L.G., Gallagher, J.C., Pavo, I., Wang, J., and Eriksen, E.F. (2005). Early changes in biochemical markers of bone formation correlate with improvements in bone structure during teriparatide therapy. J Clin Endocrinol Metab *90*, 3970-3977.

Dobnig, H., and Turner, R.T. (1995). Evidence that intermittent treatment with parathyroid hormone increases bone formation in adult rats by activation of bone lining cells. Endocrinology *136*, 3632-3638.

Dobnig, H., and Turner, R.T. (1997). The effects of programmed administration of human parathyroid hormone fragment (1-34) on bone histomorphometry and serum chemistry in rats. Endocrinology *138*, 4607-4612.

Esen, E., Chen, J., Karner, C.M., Okunade, A.L., Patterson, B.W., and Long, F. (2013). WNT-LRP5 signaling induces Warburg effect through mTORC2 activation during osteoblast differentiation. Cell Metab *17*, 745-755.

Ferrari, S.L., Pierroz, D.D., Glatt, V., Goddard, D.S., Bianchi, E.N., Lin, F.T., Manen, D., and Bouxsein, M.L. (2005). Bone response to intermittent parathyroid hormone is altered in mice null for {beta}-Arrestin2. Endocrinology *146*, 1854-1862.

Frolik, C.A., Black, E.C., Cain, R.L., Satterwhite, J.H., Brown-Augsburger, P.L., Sato, M., and Hock, J.M. (2003). Anabolic and catabolic bone effects of human parathyroid hormone (1-34) are predicted by duration of hormone exposure. Bone *33*, 372-379.

Garcia-Martinez, J.M., and Alessi, D.R. (2008). mTOR complex 2 (mTORC2) controls hydrophobic motif phosphorylation and activation of serum- and glucocorticoid-induced protein kinase 1 (SGK1). Biochem J *416*, 375-385.

Gesty-Palmer, D., Chen, M., Reiter, E., Ahn, S., Nelson, C.D., Wang, S., Eckhardt, A.E., Cowan, C.L., Spurney, R.F., Luttrell, L.M.*, et al.* (2006). Distinct beta-arrestin- and G protein-dependent pathways for parathyroid hormone receptor-stimulated ERK1/2 activation. J Biol Chem *281*, 10856-10864.

Gesty-Palmer, D., Flannery, P., Yuan, L., Corsino, L., Spurney, R., Lefkowitz, R.J., and Luttrell, L.M. (2009). A beta-arrestin-biased agonist of the parathyroid hormone receptor (PTH1R) promotes bone formation independent of G protein activation. Sci Transl Med *1*, 1ra1.

Hodsman, A.B., Bauer, D.C., Dempster, D.W., Dian, L., Hanley, D.A., Harris, S.T., Kendler, D.L., McClung, M.R., Miller, P.D., Olszynski, W.P.*, et al.* (2005). Parathyroid hormone and teriparatide for the treatment of osteoporosis: a review of the evidence and suggested guidelines for its use. Endocr Rev *26*, 688-703.

Hodsman, A.B., and Steer, B.M. (1993). Early histomorphometric changes in response to parathyroid hormone therapy in osteoporosis: evidence for de novo bone formation on quiescent cancellous surfaces. Bone *14*, 523-527.

Horwitz, M.J., Tedesco, M.B., Gundberg, C., Garcia-Ocana, A., and Stewart, A.F. (2003). Short-term, high-dose parathyroid hormone-related protein as a skeletal anabolic agent for the treatment of postmenopausal osteoporosis. J Clin Endocrinol Metab *88*, 569-575.

Huang, J.C., Sakata, T., Pfleger, L.L., Bencsik, M., Halloran, B.P., Bikle, D.D., and Nissenson, R.A. (2004). PTH differentially regulates expression of RANKL and OPG. J Bone Miner Res *19*, 235-244.

Ishizuya, T., Yokose, S., Hori, M., Noda, T., Suda, T., Yoshiki, S., and Yamaguchi, A. (1997). Parathyroid hormone exerts disparate effects on osteoblast differentiation depending on exposure time in rat osteoblastic cells. J Clin Invest *99*, 2961-2970.

Jilka, R.L. (2007). Molecular and cellular mechanisms of the anabolic effect of intermittent PTH. Bone *40*, 1434-1446.

Jilka, R.L., O'Brien, C.A., Ali, A.A., Roberson, P.K., Weinstein, R.S., and Manolagas, S.C. (2009). Intermittent PTH stimulates periosteal bone formation by actions on post-mitotic preosteoblasts. Bone *44*, 275-286.

Keller, H., and Kneissel, M. (2005). SOST is a target gene for PTH in bone. Bone *37*, 148-158.
Kim, S.W., Pajevic, P.D., Selig, M., Barry, K.J., Yang, J.Y., Shin, C.S., Baek, W.Y., Kim, J.E., and Kronenberg, H.M. (2012). Intermittent parathyroid hormone administration converts quiescent lining cells to active osteoblasts. J Bone Miner Res *27*, 2075-2084.

Kousteni, S., and Bilezikian, J.P. (2008). The cell biology of parathyroid hormone in osteoblasts. Curr Osteoporos Rep *6*, 72-76.

Kraenzlin, M.E., and Meier, C. (2011). Parathyroid hormone analogues in the treatment of osteoporosis. Nat Rev Endocrinol *7*, 647-656.

Kramer, I., Loots, G.G., Studer, A., Keller, H., and Kneissel, M. (2010). Parathyroid hormone (PTH)-induced bone gain is blunted in SOST overexpressing and deficient mice. J Bone Miner Res *25*, 178-189.

Kulkarni, N.H., Halladay, D.L., Miles, R.R., Gilbert, L.M., Frolik, C.A., Galvin, R.J., Martin, T.J., Gillespie, M.T., and Onyia, J.E. (2005). Effects of parathyroid hormone on Wnt signaling pathway in bone. J Cell Biochem *95*, 1178-1190.

Li, X., Liu, H., Qin, L., Tamasi, J., Bergenstock, M., Shapses, S., Feyen, J.H., Notterman, D.A., and Partridge, N.C. (2007). Determination of dual effects of parathyroid hormone on skeletal gene expression in vivo by microarray and network analysis. J Biol Chem *282*, 33086-33097.

Lindsay, R., Cosman, F., Zhou, H., Bostrom, M.P., Shen, V.W., Cruz, J.D., Nieves, J.W., and Dempster, D.W. (2006). A novel tetracycline labeling schedule for longitudinal evaluation of the short-term effects of anabolic therapy with a single iliac crest bone biopsy: early actions of teriparatide. J Bone Miner Res *21*, 366-373.

Linkhart, T.A., and Mohan, S. (1989). Parathyroid hormone stimulates release of insulin-like growth factor-I (IGF-I) and IGF-II from neonatal mouse calvaria in organ culture. Endocrinology *125*, 1484-1491.

Ma, Y.L., Zeng, Q., Donley, D.W., Ste-Marie, L.G., Gallagher, J.C., Dalsky, G.P., Marcus, R., and Eriksen, E.F. (2006). Teriparatide increases bone formation in modeling and remodeling osteons and enhances IGF-II immunoreactivity in postmenopausal women with osteoporosis. J Bone Miner Res *21*, 855-864.

Martin, T.J., and Sims, N.A. (2005). Osteoclast-derived activity in the coupling of bone formation to resorption. Trends Mol Med *11*, 76-81.

McCarthy, T.L., Centrella, M., and Canalis, E. (1989). Parathyroid hormone enhances the transcript and polypeptide levels of insulin-like growth factor I in osteoblast-enriched cultures from fetal rat bone. Endocrinology *124*, 1247-1253.

McCarthy, T.L., Centrella, M., and Canalis, E. (1990). Cyclic AMP induces insulin-like growth factor I synthesis in osteoblast-enriched cultures. J Biol Chem *265*, 15353-15356.

McCauley, L.K., Koh, A.J., Beecher, C.A., Cui, Y., Rosol, T.J., and Franceschi, R.T. (1996). PTH/PTHrP receptor is temporally regulated during osteoblast differentiation and is associated with collagen synthesis. J Cell Biochem *61*, 638-647.

Miyakoshi, N., Kasukawa, Y., Linkhart, T.A., Baylink, D.J., and Mohan, S. (2001). Evidence that anabolic effects of PTH on bone require IGF-I in growing mice. Endocrinology *142*, 4349-4356.

Neuman, W.F., Neuman, M.W., and Brommage, R. (1978). Aerobic glycolysis in bone: lactate production and gradients in calvaria. Am J Physiol *234*, C41-50.

Park, J., Leong, M.L., Buse, P., Maiyar, A.C., Firestone, G.L., and Hemmings, B.A. (1999). Serum and glucocorticoid-inducible kinase (SGK) is a target of the PI 3-kinase-stimulated signaling pathway. Embo J *18*, 3024-3033.

Pettway, G.J., Schneider, A., Koh, A.J., Widjaja, E., Morris, M.D., Meganck, J.A., Goldstein, S.A., and McCauley, L.K. (2005). Anabolic actions of PTH (1-34): use of a novel tissue engineering model to investigate temporal effects on bone. Bone *36*, 959-970.

Potts, J.T. (2005). Parathyroid hormone: past and present. J Endocrinol *187*, 311-325.

Qin, L., Qiu, P., Wang, L., Li, X., Swarthout, J.T., Soteropoulos, P., Tolias, P., and Partridge, N.C. (2003). Gene expression profiles and transcription factors involved in parathyroid hormone signaling in osteoblasts revealed by microarray and bioinformatics. J Biol Chem *278*, 19723-19731.

Rodan, G.A., Rodan, S.B., and Marks, S.C., Jr. (1978). Parathyroid hormone stimulation of adenylate cyclase activity and lactic acid accumulation in calvaria of osteopetrotic (ia) rats. Endocrinology *102*, 1501-1505.

Romero, G., Sneddon, W.B., Yang, Y., Wheeler, D., Blair, H.C., and Friedman, P.A. (2010). Parathyroid hormone receptor directly interacts with dishevelled to regulate beta-Catenin signaling and osteoclastogenesis. J Biol Chem *285*, 14756-14763.

Schiller, P.C., D'Ippolito, G., Roos, B.A., and Howard, G.A. (1999). Anabolic or catabolic responses of MC3T3-E1 osteoblastic cells to parathyroid hormone depend on time and duration of treatment. J Bone Miner Res *14*, 1504-1512.

Suzuki, A., Ozono, K., Kubota, T., Kondou, H., Tachikawa, K., and Michigami, T. (2008). PTH/cAMP/PKA signaling facilitates canonical Wnt signaling via inactivation of glycogen synthase kinase-3beta in osteoblastic Saos-2 cells. J Cell Biochem *104*, 304-317.

Taylor, W.H. (1991). The prevalence of diabetes mellitus in patients with primary hyperparathyroidism and among their relatives. Diabet Med *8*, 683-687.

Tessier, M., and Woodgett, J.R. (2006). Serum and glucocorticoid-regulated protein kinases: variations on a theme. J Cell Biochem *98*, 1391-1407.

Tian, Y., Xu, Y., Fu, Q., and He, M. (2011). Parathyroid hormone regulates osteoblast differentiation in a Wnt/beta-catenin-dependent manner. Mol Cell Biochem *355*, 211-216.

Tobimatsu, T., Kaji, H., Sowa, H., Naito, J., Canaff, L., Hendy, G.N., Sugimoto, T., and Chihara, K. (2006). Parathyroid hormone increases beta-catenin levels through Smad3 in mouse osteoblastic cells. Endocrinology *147*, 2583-2590.

Valdemarsson, S., Lindblom, P., and Bergenfelz, A. (1998). Metabolic abnormalities related to cardiovascular risk in primary hyperparathyroidism: effects of surgical treatment. J Intern Med *244*, 241-249.

Verheijen, M.H., and Defize, L.H. (1995). Parathyroid hormone inhibits mitogen-activated protein kinase activation in osteosarcoma cells via a protein kinase A-dependent pathway. Endocrinology *136*, 3331-3337.

Wan, M., Yang, C., Li, J., Wu, X., Yuan, H., Ma, H., He, X., Nie, S., Chang, C., and Cao, X. (2008). Parathyroid hormone signaling through low-density lipoprotein-related protein 6. Genes Dev *22*, 2968-2979.

Wang, Y., Nishida, S., Boudignon, B.M., Burghardt, A., Elalieh, H.Z., Hamilton, M.M., Majumdar, S., Halloran, B.P., Clemens, T.L., and Bikle, D.D. (2007). IGF-I receptor is required for the anabolic actions of parathyroid hormone on bone. J Bone Miner Res *22*, 1329-1337.

Watson, P., Lazowski, D., Han, V., Fraher, L., Steer, B., and Hodsman, A. (1995). Parathyroid hormone restores bone mass and enhances osteoblast insulin-like growth factor I gene expression in ovariectomized rats. Bone *16*, 357-365.

Werner, S., Hjern, B., and Sjoberg, H.E. (1974). Primary hyperparathyroidism. Analysis of findings in a series of 129 patients. Acta Chir Scand *140*, 618-625.

Whitfield, J.F., Morley, P., Willick, G.E., Ross, V., Barbier, J.R., Isaacs, R.J., and Ohannessian-Barry, L. (1996). Stimulation of the growth of femoral trabecular bone in ovariectomized rats by the novel parathyroid hormone fragment, hPTH-(1-31)NH2 (Ostabolin). Calcif Tissue Int *58*, 81-87.

Yang, D., Singh, R., Divieti, P., Guo, J., Bouxsein, M.L., and Bringhurst, F.R. (2007). Contributions of parathyroid hormone (PTH)/PTH-related peptide receptor signaling pathways to the anabolic effect of PTH on bone. Bone *40*, 1453-1461.

Yao, G.Q., Wu, J.J., Troiano, N., and Insogna, K. (2011). Targeted overexpression of Dkk1 in osteoblasts reduces bone mass but does not impair the anabolic response to intermittent PTH treatment in mice. J Bone Miner Metab *29*, 141-148.

Zoidis, E., Ghirlanda-Keller, C., and Schmid, C. (2011). Stimulation of glucose transport in osteoblastic cells by parathyroid hormone and insulin-like growth factor I. Mol Cell Biochem *348*, 33-42.

CHAPTER 5

Conclusions & Future Directions

Many investigators have studied the metabolic characteristics of bone in 1960s by analyzing bone slices and using crude isolation methods. Those studies demonstrated that bone cells consume a large amount of glucose, producing lactate as the major end product, but consume oxygen at very low levels even in aerobic conditions (Borle et al., 1960a; Cohn and Forscher, 1962; Peck et al., 1964). The earlier studies also found that bone cells secrete citrate bone (Dixon and Perkins, 1952). However, the identity of lactate and citrate-producing cells in the bone was not defined clearly. PTH was shown to enhance both lactate and citrate production in bone slices and calvarial cells (Borle et al., 1960b; Laskin and Engel, 1960). Initially, it was proposed that increased lactic acid and citrate production could trigger Ca^{2+} mobilization from bone. Upon the disproval of this hypothesis, metabolic features of bone have lost attention from investigators. It was only recently demonstrated that citrate binds to hydroxyapatite and is important for the mechanical properties of the bone (Hu et al., 2010; Kenny et al., 1959; Taylor, 1960). However, the field still lacks any in-depth studies in several areas: 1) a global view of cellular metabolism in bone cells; 2) the importance of increased aerobic glycolysis for bone formation; 3) the mechanism underlying metabolic changes in bone cells; 4) other hormones and growth factors, in addition to PTH, that can regulate cellular metabolism.

In this thesis study, I further characterized the alterations of cellular metabolism during osteoblast differentiation and tested the functional importance of these alterations. More specifically, I first showed that both WNT and PTH stimulated glucose utilization and lactate-producing glycolysis. Moreover, contribution of glucose to TCA cycle was decreased in both conditions. PTH and WNT utilized different intracellular signaling cascades for these metabolic alterations. Second, I demonstrated that decreased glucose entry to TCA cycle was important for

both WNT and PTH stimulated bone formation *in vivo.* Finally, I showed that genetic deletion of LDHA from osteoblast-lineage cells suppressed normal postnatal bone accrual due to reduced osteoblast number and function. Overall, this thesis indicates that osteoblast differentiation concurs with changes in cellular metabolism in response to anabolic signals, and that such metabolic changes are necessary for the differentiation process.

Both WNT3A and PTH alter cellular metabolism, but their effects are not identical. For instance, WNT3A suppresses glucose flux to PPP, whereas PTH enhances it. WNT3A does not change oxygen consumption rate, but PTH enhances it. However, these differences could be due to the different cellular contexts as WNT3a was tested in the mesenchymal progenitor ST2 cells whereas PTH in the preosteoblast MC3T3 cells. Regardless of the differences, pharmacological enhancement of glucose contribution to TCA cycle attenuated bone formation stimulated by either PTH or WNT. Hence, I propose that repressed glucose oxidation in TCA cycle is a key metabolic alteration. Moreover, the drastic effect of LDHA ablation on osteoblast number and function suggests that lactate-producing glycolysis is indispensable for osteoblast differentiation and activity. Examining if PTH or WNT can still induce bone formation in LDHA knockout animals will provide more insights on the importance of pyruvate-to-lactate conversion for bone anabolism. Overall, switching glucose usage from TCA cycle to lactate production is a critical event for bone formation.

PTH and WNT employ different mechanisms to increase glucose consumption. WNT induced metabolic changes through direct activation of mTORC2-AKT signaling, whereas PTH reprogrammed metabolism indirectly through IGF signaling that was independent of AKT, but dependent on SGK1. SGK1 and AKT are closely related members of the AGC kinase family with both overlapping and non-overlapping functions (Palmada et al., 2006; Wang et al., 1999).

Since PTH targets more committed cells in the osteoblast lineage compared to WNT, there might be stage-specific intracellular cascades for altering cellular metabolism. In the future, either genetic or pharmacological inhibition of AKT or SGK in the presence of WNT or PTH hyperactivation *in vivo* will provide insights about the functional relevance of either kinase in bone anabolism.

Both WNT and PTH stimulate critical enzymes involved in glucose metabolism. For this stimulation, WNT signals through LRP5-Rac1-mTORC2-AKT, whereas PTH functions through cAMP-IGF1-SGK1 signaling. However, how the metabolic enzymes are regulated by AKT or SGK1 is not known. Some of the enzymes that we studied have post-translational modifications. For example, PDK1 (Tessier and Woodgett, 2006), Hexokinase II (Tatsumi et al., 2007) and LDHA (Fan et al., 2011) are all phosphorylated at tyrosine residues. However, both AKT and SGK1 are serine/threonine kinases with no known downstream tyrosine-kinase targets. In addition to phosphorylation, LDHA can undergo acetylation that leads to its degradation (Zhao et al., 2013). Since both WNT3A and PTH reduce the glucose derived pyruvate oxidation to acetyl-coA, there might be less overall protein acetylation but this possibility has not been explored. In brief, post-translation modifications downstream of AKT and SGK might be a mechanism for the changes of the enzyme levels.

It is still not understood why directing glucose from TCA cycle to lactate-producing glycolysis is important for osteoblast biology. Below I discuss how altering cellular metabolism can potentially affect cell function and fate in four different sections.

1. Metabolites as Substrates for Post-translational Modification

Altered cytosolic metabolites can affect protein function via post-translational modifications. For instance, acetyl-coA provides acetyl group for protein acetylation, which can both activate or repress protein function. As discussed above, reduced pyruvate oxidation to acetyl-coA via WNT and PTH can result a reduced pool of substrate available for the acetyltransferases. Therefore, it is important to assess total acetyl-coA levels after PTH and WNT3A treatments.

TCA cycle intermediate, α-ketoglutarate (α-KG), is used as a co-substrate for dioxygenases including prolyl hydroxylase enzymes (PHDs). PHDs catalyze the post-translational modification mediating the degradation of Hypoxia-inducible factor alpha (HIFα) and can be inhibited by succinate or fumarate (King et al., 2006). Stabilization of HIF1α regulates bone formation. Thus, via effects on TCA cycle, PTH and WNT3A can change the cytosolic α-KG pool required for dioxygenases, which can be critical for osteoblast differentiation and function.

Metabolites can also be used as co-substrates for epigenetic modifications. For instance, α-KG is required for the JmjC domain-containing histone demethylases and the TET (ten-eleven translocation) family of DNA hydroxylases (Tahiliani et al., 2009; Tsukada et al., 2006). Knocking down JmJc3 *in vitro* suppressed osteoblast differentiation through increasing H3K27me3 on the Runx2 and Osx promoters (Yang et al., 2013). Thus, alterations of cytoplasmic metabolites via PTH or WNT3A can possibly control gene expression via epigenetic changes.

HBP intermediates were reduced after WNT3A treatment, although it is not clear at present whether Wnt3a suppressed glucose entry to HBP. Although HBP consumes the lowest

percentage of glucose in the cell, it generates substrates for glycosylation. Many proteins including some transcription factors undergo glycosylation that regulates their function (Comer and Hart, 2000; Wells et al., 2001). By generating substrates for glycosylation, HBP can affect the activity of critical transcription factors. With the availability of more specific antibodies detecting glycosylated proteins, the effect of PTH and WNT3A on protein glycosylation and its effect on osteoblasts can be examined.

2. Lactate as a Signaling Molecule and pH Regulator

WNT and PTH increase lactate level in the serum in mice and in the culture medium *in vitro*, indicating that not only the production but also the secretion of lactate is increased. Lactate is capable of entering cells via monocarboxylate transporters (MCT) and can work as a signaling compound (Philp et al., 2005). Addition of lactate to cultured fibroblasts significantly increases their collagen (Klein et al., 2001) and upregulates vascular endothelial growth factor (VEGF) synthesis (Constant et al., 2000). Detailed examination of MCT expression in different cell types in bone together with functional studies of MCT can test whether lactate is a signaling molecule in bone. Moreover, lactate secreted out of the cell can modify the pH of the bone matrix. The acidity of the microenvironment might be important for osteoblast differentiation. Investigation of the osteoblast microenvironment *in vivo* with pH sensitive probes is important to examine this possibility. Overall, secreted lactate may affect osteoblast differentiation either via direct signaling or indirectly through changing the microenvironment.

3. Redirection of Carbon Source in Osteoblasts

Osteoblasts are known to secrete citrate that binds to hydroxyapatite nanocrystals and is important for the mechanical properties of bone. Citrate producing cells usually rely on glycolysis to compensate for ATP loss due to exit of carbons from TCA cycle, and to generate more pyruvate available for acetyl-CoA production. The best-characterized citrate-secreting cells are the prostate gland cells, in which exit of citrate out of the TCA cycle is partially due to the inhibition of aconitase via increased zinc metabolism. Interestingly, zinc is abundant in bone (Alhava et al., 1977) and mice lacking a zinc transporter, ZNT5, manifest poor growth and decreased bone density due to impairment of osteoblast maturation (Inoue et al., 2002). Moreover, during *in vitro* osteoblast differentiation from human mesenchymal stem cell, zinc accumulation as well as ZIP1 zinc transporter expression is upregulated. Overexpressing ZIP1 enhances the osteogenic differentiation (Tang et al., 2006). The primary role of the zinc in bone is to enhance ALP activity, but it has never been investigated whether increased zinc uptake is also important for enhancing citrate production (Tsuzuike et al., 1993) in osteoblast. In summary, osteoblasts might go through changes in Zn metabolism analogous to that in prostate cells in response to anabolic stimulation. Detailed investigation is required to determine whether citrate-production is coupled with lactate-producing glycolysis during bone anabolism.

Suppressed glucose utilization in response to WNT3A in ST2 cells is coupled with increased glutamine entry to TCA cycle. It was reported that glutamine (Brown et al., 2011) and glutamate (Lin et al., 2008) are necessary for bone matrix mineralization and osteoblast differentiation, respectively. Therefore, glutamine is another necessary carbon and energy source for osteoblasts.

The previous literature and our findings support a model that osteoblasts reprogram the carbon and energy source during differentiation in response to anabolic signals. In a nutshell,

glucose is mainly used for lactate-producing glycolysis with a small contribution to TCA cycle whereas citrate exits the cycle to be secreted out of the cell. Since osteoblast differentiation requires high amounts of ATP due to the energy cost of protein synthesis, other energy sources such as extracellular glutamine appears to be necessary for generating ATP. Detailed tracer experiments are required to examine the source of secreted citrate, and to find other potential energy sources for TCA metabolism. Moreover, how different anabolic signals alter carbon and energy sources and whether such alterations are functionally relevant, need to be further investigated.

4. NAD/NADH Redox Balance for Osteoblast Differentiation

In this thesis, I have not examined the cellular NAD^+/NADH changes in response to PTH or WNT3A. However, intracellular NAD^+ levels can be critical for osteoblast differentiation. The expression of Nampt, the NAD^+ biosynthetic enzyme, increases during osteogenic differentiation in preosteoblast MC3T3-E1 cells (Li et al., 2013). NAD^+ dependent lysine deacetylase, Sirt1, accelerates osteoblast differentiation from MSCs *in vitro* (Backesjo et al., 2006), while preventing adipocyte differentiation (Picard et al., 2004). It is noteworthy that NAD^+ is regenerated via the reaction catalyzed by LDHA in the cytoplasm. It is possible that anabolic signals increase cytosolic NAD^+ pool via aerobic glycolysis that will in turn enhance osteoblast differentiation.

Bisphosphonates (BPs) are often used for treating bone diseases such as osteoporosis, Paget's disease and fibrous dysplasia. BPs inhibit bone resorption, hence preserving bone mass. Although the therapeutic effects of BPs are believed to depend on osteoclasts, there is increasing evidence that osteoblasts might be a target as well. It is noteworthy that BPs have direct effect on

cellular metabolism. Several decades ago, BPs were demonstrated to inhibit glucose uptake and lactate production and enhance citrate oxidation in calvarial cells (Fast et al., 1978). Further investigation is required to understand the role of metabolic alterations in the action of BPs, as metabolic regulation might be an integral part of the negative effect of BPs on osteoblasts. If confirmed, such effects may help to explain the long-standing clinical observation that BPs suppresses bone formation.

This thesis reveals that osteoblast differentiation concurs with a unique metabolic switch in response to two anabolic signals, WNT and PTH. This metabolic switch is a required feature of differentiation. Understanding how metabolism influence gene expression will bring new insights to our understanding of osteoblast differentiation. A recent study shows that differentiating osteoblasts increase both glycolysis and oxidative phosphorylation; mature osteoblasts rely mostly on glycolysis, indicating stage-specific metabolic needs (Guntur et al., 2014). Metabolomics together with flux analysis can be used to reveal how different developmental signals affect metabolic pathways in a stage dependent manner. Moreover, investigating metabolic control of osteoblast differentiation might help to understand the link between osteoporosis and diabetes.

References

Alhava, E.M., Olkkonen, H., Puittinen, J., and Nokso-Koivisto, V.M. (1977). Zinc content of human cancellous bone. Acta Orthop Scand *48*, 1-4.

Backesjo, C.M., Li, Y., Lindgren, U., and Haldosen, L.A. (2006). Activation of Sirt1 decreases adipocyte formation during osteoblast differentiation of mesenchymal stem cells. J Bone Miner Res *21*, 993-1002.

Borle, A.B., Nichols, N., and Nichols, G., Jr. (1960a). Metabolic studies of bone in vitro. I. Normal bone. J Biol Chem *235*, 1206-1210.

Borle, A.B., Nichols, N., and Nichols, G., Jr. (1960b). Metabolic studies of bone in vitro. II. The metabolic patterns of accretion and resorption. J Biol Chem *235*, 1211-1214.

Brown, P.M., Hutchison, J.D., and Crockett, J.C. (2011). Absence of glutamine supplementation prevents differentiation of murine calvarial osteoblasts to a mineralizing phenotype. Calcified tissue international *89*, 472-482.

Cohn, D.V., and Forscher, B.K. (1962). Aerobic metabolism of glucose by bone. J Biol Chem *237*, 615-618.

Comer, F.I., and Hart, G.W. (2000). O-Glycosylation of nuclear and cytosolic proteins. Dynamic interplay between O-GlcNAc and O-phosphate. J Biol Chem *275*, 29179-29182.

Constant, J.S., Feng, J.J., Zabel, D.D., Yuan, H., Suh, D.Y., Scheuenstuhl, H., Hunt, T.K., and Hussain, M.Z. (2000). Lactate elicits vascular endothelial growth factor from macrophages: a possible alternative to hypoxia. Wound Repair Regen *8*, 353-360.

Dixon, T.F., and Perkins, H.R. (1952). Citric acid and bone metabolism. Biochem J *52*, 260-265.

Fan, J., Hitosugi, T., Chung, T.W., Xie, J., Ge, Q., Gu, T.L., Polakiewicz, R.D., Chen, G.Z., Boggon, T.J., Lonial, S*., et al.* (2011). Tyrosine phosphorylation of lactate dehydrogenase A is important for NADH/NAD(+) redox homeostasis in cancer cells. Mol Cell Biol *31*, 4938-4950.

Fast, D.K., Felix, R., Dowse, C., Neuman, W.F., and Fleisch, H. (1978). The effects of diphosphonates on the growth and glycolysis of connective-tissue cells in culture. Biochem J *172*, 97-107.

Guntur, A.R., Le, P.T., Farber, C.R., and Rosen, C.J. (2014). Bioenergetics during calvarial osteoblast differentiation reflect strain differences in bone mass. Endocrinology, en20131974.

Hu, Y.Y., Rawal, A., and Schmidt-Rohr, K. (2010). Strongly bound citrate stabilizes the apatite nanocrystals in bone. Proc Natl Acad Sci U S A *107*, 22425-22429.

Inoue, K., Matsuda, K., Itoh, M., Kawaguchi, H., Tomoike, H., Aoyagi, T., Nagai, R., Hori, M., Nakamura, Y., and Tanaka, T. (2002). Osteopenia and male-specific sudden cardiac death in mice lacking a zinc transporter gene, Znt5. Hum Mol Genet *11*, 1775-1784.

Kenny, A.D., Draskoczy, P.R., and Goldhaber, P. (1959). Citric acid production by resorbing bone in tissue culture. Am J Physiol *197*, 502-504.

King, A., Selak, M.A., and Gottlieb, E. (2006). Succinate dehydrogenase and fumarate hydratase: linking mitochondrial dysfunction and cancer. Oncogene *25*, 4675-4682.

Klein, M.B., Pham, H., Yalamanchi, N., and Chang, J. (2001). Flexor tendon wound healing in vitro: the effect of lactate on tendon cell proliferation and collagen production. J Hand Surg Am *26*, 847-854.

Laskin, D.M., and Engel, M.B. (1960). Relations between the metabolism and structure of bone. Ann N Y Acad Sci *85*, 421-430.

Li, Y., He, J., He, X., and Lindgren, U. (2013). Nampt expression increases during osteogenic differentiation of multi- and omnipotent progenitors. Biochem Biophys Res Commun *434*, 117-123.

Lin, T.H., Yang, R.S., Tang, C.H., Wu, M.Y., and Fu, W.M. (2008). Regulation of the maturation of osteoblasts and osteoclastogenesis by glutamate. Eur J Pharmacol *589*, 37-44.

Palmada, M., Boehmer, C., Akel, A., Rajamanickam, J., Jeyaraj, S., Keller, K., and Lang, F. (2006). SGK1 kinase upregulates GLUT1 activity and plasma membrane expression. Diabetes *55*, 421-427.

Peck, W.A., Birge, S.J., Jr., and Fedak, S.A. (1964). Bone Cells: Biochemical and Biological Studies after Enzymatic Isolation. Science *146*, 1476-1477.

Philp, A., Macdonald, A.L., and Watt, P.W. (2005). Lactate--a signal coordinating cell and systemic function. J Exp Biol *208*, 4561-4575.

Picard, F., Kurtev, M., Chung, N., Topark-Ngarm, A., Senawong, T., Machado De Oliveira, R., Leid, M., McBurney, M.W., and Guarente, L. (2004). Sirt1 promotes fat mobilization in white adipocytes by repressing PPAR-gamma. Nature *429*, 771-776.

Tahiliani, M., Koh, K.P., Shen, Y., Pastor, W.A., Bandukwala, H., Brudno, Y., Agarwal, S., Iyer, L.M., Liu, D.R., Aravind, L.*, et al.* (2009). Conversion of 5-methylcytosine to 5-hydroxymethylcytosine in mammalian DNA by MLL partner TET1. Science *324*, 930-935.

Tang, Z., Sahu, S.N., Khadeer, M.A., Bai, G., Franklin, R.B., and Gupta, A. (2006). Overexpression of the ZIP1 zinc transporter induces an osteogenic phenotype in mesenchymal stem cells. Bone *38*, 181-198.

Tatsumi, S., Ishii, K., Amizuka, N., Li, M., Kobayashi, T., Kohno, K., Ito, M., Takeshita, S., and Ikeda, K. (2007). Targeted ablation of osteocytes induces osteoporosis with defective mechanotransduction. Cell Metab *5*, 464-475.

Taylor, T.G. (1960). The nature of bone citrate. Biochim Biophys Acta *39*, 148-149.

Tessier, M., and Woodgett, J.R. (2006). Serum and glucocorticoid-regulated protein kinases: variations on a theme. J Cell Biochem *98*, 1391-1407.

Tsukada, Y., Fang, J., Erdjument-Bromage, H., Warren, M.E., Borchers, C.H., Tempst, P., and Zhang, Y. (2006). Histone demethylation by a family of JmjC domain-containing proteins. Nature *439*, 811-816.

Tsuzuike, N., Segawa, Y., Tagashira, E., and Yamaguchi, M. (1993). Beta-alanyl-L-histidinato zinc enhances various bone-regulating factors' effects on bone alkaline phosphatase activity in tissue culture. Pharmacology *47*, 66-72.

Wang, Q., Somwar, R., Bilan, P.J., Liu, Z., Jin, J., Woodgett, J.R., and Klip, A. (1999). Protein kinase B/Akt participates in GLUT4 translocation by insulin in L6 myoblasts. Mol Cell Biol *19*, 4008-4018.

Wells, L., Vosseller, K., and Hart, G.W. (2001). Glycosylation of nucleocytoplasmic proteins: signal transduction and O-GlcNAc. Science *291*, 2376-2378.

Yang, D., Okamura, H., Nakashima, Y., and Haneji, T. (2013). Histone demethylase Jmjd3 regulates osteoblast differentiation via transcription factors Runx2 and osterix. J Biol Chem *288*, 33530-33541.

Zhao, D., Zou, S.W., Liu, Y., Zhou, X., Mo, Y., Wang, P., Xu, Y.H., Dong, B., Xiong, Y., Lei, Q.Y.*, et al.* (2013). Lysine-5 acetylation negatively regulates lactate dehydrogenase A and is decreased in pancreatic cancer. Cancer Cell *23*, 464-476.